Functional and Structural Analysis of the Retinoschisin-Na/K-ATPase Complex- Unraveling the Pathomechanism of X-linked Juvenile Retinoschisis

DISSERTATION ZUR ERLANGUNG DES DOKTORGRADES DER NATURWISSENSCHAFTEN (DR. RER. NAT.)

DER FAKULTÄT FÜR BIOLOGIE UND VORKLINISCHE MEDIZIN DER UNIVERSITÄT REGENSBURG

vorgelegt von

Verena Schmid

aus

Regensburg

im Jahr

2022

Functional and Structural Analysis of the Retinoschisin-Na/K-ATPase Complex-

Unraveling the Pathomechanism of X-linked Juvenile Retinoschisis

DISSERTATION ZUR ERLANGUNG DES DOKTORGRADES DER NATURWISSENSCHAFTEN (DR. RER. NAT.)

DER FAKULTÄT FÜR BIOLOGIE UND VORKLINISCHE MEDIZIN DER UNIVERSITÄT REGENSBURG

vorgelegt von

Verena Schmid

aus

Regensburg

im Jahr

2022

Das Promotionsgesuch wurde eingereicht am**:**

11.02.22

Die Arbeit wurde angeleitet von:

Prof. Dr. Bernhard H.F. Weber

_____

Verena Schmid

Parts of this work have already been published in peer-reviewed journals in an open access format

Plössl K, Straub K, **Schmid V**, Strunz F, Wild J, Merkl R, Weber BHF, and Friedrich U. 2019. “Identification of the Retinoschisin-Binding Site on the Retinal Na/K-ATPase.” *PloS One* 14(5):e0216320 doi: 10.1371/JOURNAL.PONE.0216320 (**IF_{2019} = 2.740**)

Schmid V, Plössl K, Schmid C, Bernklau S, Weber BHF, and Friedrich U. 2020. “Retinoschisin and Cardiac Glycoside Crosstalk at the Retinal Na/K-ATPase.” *Investigative Ophthalmology & Visual Science* 61(5):1. doi: 10.1167/iovs.61.5.1. (**IF_{2020} = 4.045**)

Schmid V, Wurzel A, Wetzel CH, Plössl K, Bruckmann A, Weber BHF, and Friedrich U. 2022 “Retinoschisin and novel Na/K-ATPase interaction partners Kv2.1 and Kv8.2 define a growing protein complex at the inner segments of mammalian photoreceptors” *Cellular and Molecular Life Sciences* 25;79(8):448 doi: 10.1007/s00018-022-04409-9. (**IF_{2020} = 9.261**)

Table of Contents

Zusammenfassung

Pathologische Mutationen im *RS1*-Gen auf Xp 22.13 verursachen die X-chromosomale juvenile Retinoschisis (XLRS) (Sauer et al. 1997), eine erbliche Netzhautdystrophie, die bei jugendlichen oder heranwachsenden Männern auftritt (Pagenstecher et al. 1913). Ein Kennzeichen von XLRS ist die Spaltung der inneren Netzhautschichten (Schisis) und Defekte in der Signalweiterleitung von den Photorezeptoren zu den Bipolarzellen (Khan et al. 2001). Das *RS1*-Gen kodiert für das retina-spezifische Protein Retinoschisin, welches direkt mit der ATP1B2-Untereinheit der retinalen Na/K-ATPase in den inneren Segmenten der Photorezeptoren interagiert (Molday et al. 2007; Plössl et al. 2017a). Die retinale Na/K-ATPase, bestehend aus den beiden Untereinheiten ATP1A3 und ATP1B2, verankert Retinoschisin an der Plasmamembran von Photorezeptoren (Friedrich et al. 2011). Ziel dieser Arbeit war es, die strukturellen und funktionellen Merkmale des Retinoschisin-Na/K-ATPase-Komplexes zu analysieren, um so einen Beitrag zur weiteren Aufklärung der initialen Ereignisse der XLRS-Pathologie zu leisten.

Das erste Projekt befasste sich mit der Fragestellung zur ATP1B2-Retinoschisin Interaktionsfläche sowie zur Diffusion des Komplexes innerhalb der Plasmamembran. Bei der Analyse der Bindung von Retinoschisin an die deglykosylierte retinale Na/K-ATPase in Gegenwart verschiedener Zucker oder an mutiertes ATP1B2 zeigte sich, dass die Bindung von Retinoschisin an die retinale Na/K-ATPase durch hohe Zuckerkonzentrationen abgeschwächt wird, aber dennoch unabhängig von ATP1B2-gebundenen Zuckerketten erfolgt. Im Gegensatz dazu wurde gezeigt, dass Retinoschisin direkt mit der ATP1B2-Untereinheit interagiert. Zudem wurde festgestellt, dass die Anwesenheit eines polaren Restes an der Aminosäure 240 eine Schlüsselrolle bei der Interaktion mit Retinoschisin spielt. Fluoreszenz-Korrelation spektrometrische Analysen an Hek293 Zellen, die die retinalen Na/K-ATPase-Untereinheiten ATP1A3 und ATP1B2 heterolog exprimieren, zeigten keinen Effekt von Retinoschisin auf die laterale Diffusion der Na/K-ATPase.
In einem zweiten Projekt wurde das Zusammenspiel von Retinoschisin und Herzglykosiden, die an die ATP1A3-Untereinheit der Na/K-ATPase binden, untersucht. Retinoschisin-Bindungsversuche zeigten eine Verdrängung von Retinoschisin gegenüber der retinalen Na/K-ATPase durch die beiden Herzglykoside Ouabain und Digoxin. Enzymatische Assays zur Quantifizierung der Herzglykosid-sensitiven Na/K-ATPase Pumpaktivität sowie Analysen zur Messung der Retinoschisin-abhängigen Bindung von Tritium-markiertem Ouabain an die Na/K-ATPase zeigten keinen Einfluss von Retinoschisin auf die Bindung von Herzglykosiden an die retinale Na/K-ATPase. Die immunhistochemische Färbung von Netzhautexplantaten Retinoschisin-defizienter Mäuse, die mit rekombinantem Retinoschisin oder Herzglykosiden

behandelt wurden, zeigte, dass bei Anwesenheit von Herzglykosiden die Fähigkeit von Retinoschisin, vor der Degeneration der Photorezeptoren zu schützen, beeinträchtigt ist.
Ziel des dritten Projektes der Dissertation war es, etwaige weitere Interaktionspartner des Retinoschisin-Na/K-ATPase-Komplexes zu identifizieren. Western Blot Analysen einer Ko-Immunpräzipitation von Schweineretina-Lysaten mit ATP1A3 zeigten, dass keiner der bekannten Interaktionspartner anderer α-Untereinheiten der Na/K-ATPasen (z.B. SRC, RAS, PI3K, NCX und PLC für ATP1A1) an die retinale Na/K-ATPase bindet. Die immunhistochemische Färbung von Retinoschisin-defizienten Mäusen zeigte eine Fehllokalisierung des aus der Literatur bekannten retinalen Na/K-ATPase-Interaktionspartners AnkB ab dem postnatalen Tag (P) 18, ähnlich zur Fehllokalisierung der retinalen Na/K-ATPase. Ein ungerichteter Ansatz, bei dem eine massenspektrometrische Analyse der ATP1A3 Ko-Immunpräzipitationsprodukte aus Schweineretina-Lysaten durchgeführt wurde, identifizierte mehr als 200 mögliche Interaktionspartner der retinalen Na/K-ATPase. Drei Kandidaten, ANXA2 und die beiden Kv-Kanal Untereinheiten Kv2.1 und Kv8.2, wurden weiteren Untersuchungen unterzogen. Während eine Ko-Immunpräzipitation aus murinen Netzhaut-Lysaten eine direkte Interaktion der retinalen Na/K-ATPase mit AnxA2 nicht bestätigte, wurde die Interaktion mit Kv2.1 und Kv8.2 bestätigt. Bei der immunhistochemischen Färbung von retinalen Kryoschnitten wurde eine zunehmende Fehllokalisierung von AnxA2, Kv2.1 und Kv8.2 während der postnatalen Entwicklung der Retinoschisin-defizienten Mausretina festgestellt. Insbesondere Kv2.1 zeigte bereits bei P7 eine Fehlverteilung, während eine fehlerhafte Lokalisation für AnxA2, ähnlich wie bei AnkB und der retinalen Na/K-ATPase, bei P18, nach Schisis und Photorezeptorapoptose, auftrat. Bei weiteren Untersuchungen von Kv2.1 und Kv8.2 in Retinoschisin-defizienten Mäusen wurde mittels Western Blot Analyse eine Verringerung ihrer Proteinkonzentrationen, ebenfalls vor P14, insbesondere bei P10, nachgewiesen, während jeweils keine Auswirkung auf die Genexpression nachzuweisen war. Schließlich wurde die Kv-Kanalaktivität in Y-79 Zellen gemessen. Patch-Clamp Analysen und Live-Cell Calcium Imaging zeigten keine Auswirkungen von Retinoschisin auf den Kv-Kanal-vermittelten Kalium-Ionenfluss oder die Calcium-Homöostase.

Zusammenfassend geben die durchgeführten experimentellen Arbeiten neue Einblicke in die funktionelle und strukturelle Zusammensetzung des Retinoschisin-Na/K-ATPase-Komplexes und deuten auf die Bildung eines makromolekularen Komplexes in den inneren Segmenten der Photorezeptoren u.a. mit den Kanaluntereinheiten Kv2.1 und Kv8.2 hin. Damit liefern diese Befunde neue Erkenntnisse für die initialen pathologischen Prozesse der XLRS und könnten somit die Entwicklung neuer therapeutischer Optionen für diese derzeit unbehandelbare Krankheit fördern.

Summary

Pathologic mutations in the *RS1* gene on Xp 22.13 cause X-linked juvenile retinoschisis (XLRS) (Sauer et al. 1997), a hereditary retinal dystrophy manifesting in juvenile or adolescent males (Pagenstecher et al. 1913). A hallmark of XLRS is the splitting of the inner retinal layers (schisis) and defects in signal transmission of photoreceptor to bipolar cells (Khan et al. 2001). The *RS1* gene encodes the retina-specific protein retinoschisin known to directly interact with the ATP1B2 subunit of the retinal Na/K-ATPase at photoreceptor inner segments (Molday et al. 2007; Plössl et al. 2017a). The retinal Na/K-ATPase, consisting of the two subunits ATP1A3 and ATP1B2, was shown to anchor retinoschisin at the plasma membrane of photoreceptors (Friedrich et al. 2011). This work aimed to analyze structural and functional features of the retinoschisin-Na/K-ATPase complex to provide further insights into the initial steps in XLRS pathology.

The first project addressed the question of the ATP1B2-retinoschisin interphase as well as the diffusion of the complex in the membrane. Testing retinoschisin binding to deglycosylated retinal Na/K-ATPase, under the presence of different sugars, or to mutant ATP1B2, the binding of retinoschisin to the retinal Na/K-ATPase was shown to be attenuated by high sugar concentrations but nevertheless independent of ATP1B2-attached glycoside chains. Instead, retinoschisin binding was shown to be achieved by direct interaction with the ATP1B2 subunit. In specific, the presence of a polar residue at amino acid 240 was determined to play a key role in the interaction with retinoschisin. Fluorescence correlation spectroscopy analyses using Hek293 cells heterologously expressing the retinal Na/K-ATPase subunits ATP1A3 and ATP1B2 revealed no effect of retinoschisin on the lateral diffusion of the Na/K-ATPase.
In a second project, the interplay of retinoschisin and cardiac glycosides, which bind to the ATP1A3 subunit of the Na/K-ATPase, was investigated. Retinoschisin binding assays revealed a displacement of retinoschisin from the retinal Na/K-ATPase by both cardiac glycosides ouabain and digoxin. Enzymatic assays, which quantified cardiac glycoside-sensitive Na/K-ATPase pump activity, and analyses measuring retinoschisin-dependent binding of tritium-labeled ouabain to the Na/K-ATPase showed no effect of retinoschisin on the binding of cardiac glycosides to the retinal Na/K-ATPase. Immunolabeling of retinal explants of retinoschisin-deficient mice incubated with recombinant retinoschisin or cardiac glycosides showed that the presence of cardiac glycosides disturbed the capacity of retinoschisin to protect against photoreceptor degeneration.
The third project of the thesis aimed to identify possible additional interaction partners of the retinoschisin-Na/K-ATPase complex. Western blot analyses of a co-immunoprecipitation of porcine retinal lysates with ATP1A3 showed that none of the known interaction partners of other α-subunits of Na/K-ATPases (e.g., SRC, RAS, PI3K, NCX, and PLC for ATP1A1) binds

to the retinal Na/K-ATPase. Immunolabeling of retinoschisin-deficient murine retinae showed mislocalization from the literature known retinal Na/K-ATPase interaction partner AnkB starting at postnatal day (P)18 similar to the mislocalization of the retinal Na/K-ATPase. An undirected approach using mass spectrometric analysis of ATP1A3 co-immunoprecipitation products from porcine retinal lysates identified more than 200 possible interaction partners of retinal Na/K-ATPase. Three candidates, ANXA2, and both Kv channel subunits Kv2.1 and Kv8.2, were subjected to further analyses. While co-immunoprecipitation from murine retinal lysates did not corroborate a direct interaction of the retinal Na/K-ATPase with AnxA2, the interaction with Kv2.1 and Kv8.2 was confirmed. In immunolabeling of retinal cryosections, an increasing mislocalization of AnxA2, Kv2.1 and Kv8.2 was detected during postnatal development of the retinoschisin-deficient mouse retina. Notably, Kv2.1 showed maldistribution already at P7, while an incorrect localization for AnxA2, similar to AnkB and the retinal Na/K-ATPase, emerged at P18, after schisis and photoreceptor apoptosis. In further investigations of Kv2.1 and Kv8.2 in retinoschisin-deficient mice, a reduction in their protein levels, also before P14, in specific at P10, was demonstrated *via* western blot analysis, while in each case no effect on gene expression was observed. Finally, Kv channel activity was measured with Y-79 cells. Patch-clamp analyses and live-cell calcium imaging revealed no effect of retinoschisin on the Kv channel mediated potassium ion current or calcium homeostasis.

Taken together, the performed experimental work provides new insights into the functional and structural composition of the retinoschisin Na/K-ATPase complex and suggests the formation of a macromolecular complex in photoreceptor inner segments with other proteins like the channel subunits like Kv2.1 and Kv8.2. These findings provide new insights into the initial pathological processes of XLRS and could thus promote the development of new therapeutic options for this currently untreatable disease.

1 Introduction

1.1 X-linked juvenile Retinoschisis (XLRS)

1.1.1 Clinical features of XLRS

X-linked juvenile Retinoschisis (XLRS, OMIM #312700) is an inherited macular dystrophy caused by pathologic mutations in the retinoschisin (*RS1*) gene on chromosome Xp22.13. The disease entity was described initially in 1898 by the Austrian ophthalmologist Josef Haas in two affected brothers (7 and 11 years of age) who presented with cystic cavities within the retina (Haas 1898). Due to an X-chromosomal recessive transmission, which was initially suggested by Pagensteiner in 1913 (Pagenstecher 1913), mostly males are affected with an estimated prevalence between 1/5.000-1/25.000 (George et al. 1995; Tantri et al. 2004). In general, female heterozygous carriers of an *RS1* mutation remain asymptomatic, while female homozygous carriers of *RS1* mutations, observed rarely in consanguineous families, develop clinical features of XLRS (Saleheen et al. 2008; Staffieri et al. 2015).

1- month and 3-month-old male infants have been described with XLRS symptoms, suggesting a congenital onset of the disease (George et al. 1995; Prasad et al. 2006; Lee et al. 2009). Still, XLRS is mostly diagnosed in elementary school due to unusual reading difficulties. Eyesight is highly variable with best-corrected visual acuity from 20/20 to 20/600 (Forsius 1973; George et al. 1996). The penetrance of the disease is almost 100%, whereas the phenotypic disease expression can be highly variable within families harboring the same mutation (Vijayasarathy et al. 2021). A characteristic hallmark of XLRS is the spoke-wheel like pattern in the macula associated with peripheral schisis in about 50% of patients. Schisis develops as a splitting of the retinal layers, especially in the area of the inner nuclear layer and the outer plexiform layer leading to a disruption of the layered organization in the retina (Gerth et al. 2008; Yu et al. 2010). The schisis cavities can be visualized *via* optic coherence tomography (OCT) as shown in **Figure 1A**.

The splitting of the retinal layers leads to defective signal transduction from photoreceptor to bipolar cells, which can be diagnosed by electroretinography (ERG) (Khan et al. 2001). The so-called “negative” ERG waveform is characteristic for XLRS patients. It reveals a reduced amplitude of the b-wave, which indicates depolarization of ON bipolar cells due to signal transduction from photoreceptor cells to bipolar cells, while simultaneously the amplitude of the a-wave, which indicates the hyperpolarization of photoreceptors in response to a light stimulus, remains largely unaffected (**Figure 1B**) (George et al. 1995; Alexander et al. 2001; Tantri et al. 2004).

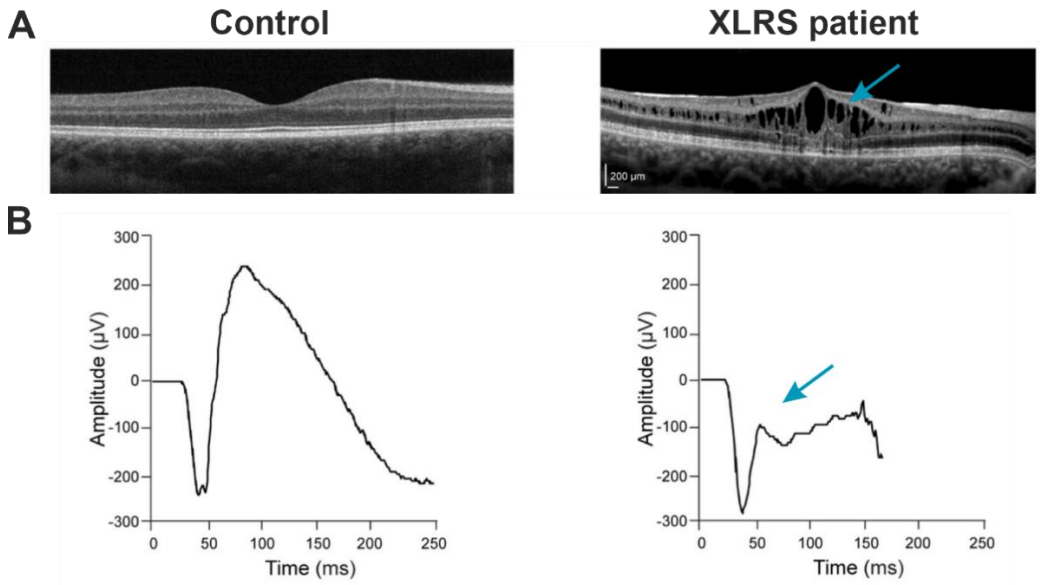

Figure 1: Clinical and electrodiagnostic features of X-linked juvenile retinoschisis

A: Optical coherence tomography scan of a control individuum (left panel) and a 17-year old X-linked juvenile retinoschisis (XLRS) patient (right panel) with large schisis cavities in the inner retinal layers labeled by a blue arrow. **B**: Representative electroretinogram of a dark-adapted response of a control individuum with normal a- and b-wave (left panel) as well as a 17-year old XLRS patient (right panel) with a normal a-wave and a XLRS-associated b-wave reduction labeled by a blue arrow (Images modified from Vijayasarathy et al. 2021).

In most XLRS patients, only small or minimal progression of the disease is documented: A longitudinal study (follow-up mean length: 19.78) of Roesch and colleagues revealed that a significant loss in visual acuity occurred only in 21.2% eyes of 43 patients during childhood or adolescence and in 17.1% eyes of 59 patients in the postadolescent period (Roesch et al. 1998). In another follow-up study with a mean length of 7.4 years from Wood and colleagues evaluating XLRS disease stability or progression in children, long-term stability was observed in 83% of affected eyes while only 17% showed disease conversion or progression to more severe symptoms (Wood et al. 2019). Nevertheless, these studies and a study of Fahim in 2017 revealed that patients with foveal and peripheral schisis have an increased risk for further complications like vitreous hemorrhage and retinal detachment at young age (Fahim et al. 2017; Wood et al. 2019). Moreover, at the age of around 30, mild retinal pigmentary changes may occur, and by age 50 to 60, a mild reduction in visual acuity due to macular atrophy is often experienced by the patient (Apushkin et al. 2005).

1.1.2 *RS1* gene and its protein retinoschisin

In 1983, the *RS1* gene was first mapped near the Xg blood group markers on the X chromosome (Wieacker et al. 1983) while in 1997, Sauer and colleagues positionally identified the gene and showed that mutations therein are causative for XLRS (Sauer et al. 1997). The human *RS1* gene with a genomic dimension of 32.43 kb consists of six exons and five introns and it is highly expressed in the retina of photoreceptor and bipolar cells (Sauer et al. 1997; Takada et al. 2006). Minimal expression of *RS1* mRNA is also detected in the pineal gland

(Takada et al. 2006). The retinoschisin protein is composed of 224 amino acids (aa) and it consists of four domains: A 23-aa N-terminal signal peptide, the 39-aa retinoschisin domain, a 157-aa discoidin domain, and a 5-aa C-terminal segment (**Figure 2A**) (Wu and Molday 2003; Molday et al. 2007). The N-terminal signal sequence ensures transport to the endoplasmic reticulum (ER) and secretion of the protein of the cell by interacting with the signal recognition particle (SRP). The retinoschisin domain has no sequence homology to other proteins deposited in the databases (Molday et al., 2007), and it is essential for folding and oligomerization of the protein (Sauer et al. 1997; Wu and Molday 2003; Wu et al. 2005). In contrast, discoidin domains were found in many eucaryotic and procaryotic membrane proteins like the blood coagulation factors V and VIII (Kiedzierska et al. 2007; Villoutreix and Miteva 2016). The discoidin domain accounts for 75% of the retinoschisin protein and is considered the essential functional and structural subunit (Wu and Molday 2003). In 2005, octamerization of retinoschisin enabled by the formation of intra- (between Cys63 and Cys219, or between Cys110 and Cys142) and intermolecular (between Cys59 and Cys223) disulfide bonds was demonstrated *via* non-denaturing SDS-polyacrylamide gel electrophoresis (SDS-PAGE) (Wu et al. 2005). In 2016, the assembly of retinoschisin monomers into a double octameric ring was visualized *via* cryo-electron microscopy. The resulting hexadecamer is organized in a back-to back cogwheel-like structure with the discoidin domains facing outward and the retinoschisin domains and C-terminal segments localized in the center (**Figure 2B**) (Bush et al. 2016; Ramsay et al. 2016; Tolun et al. 2016). Cryo-electron microscopy studies also revealed the formation of branched networks by the retinoschisin hexadecamers (Heymann et al. 2019).

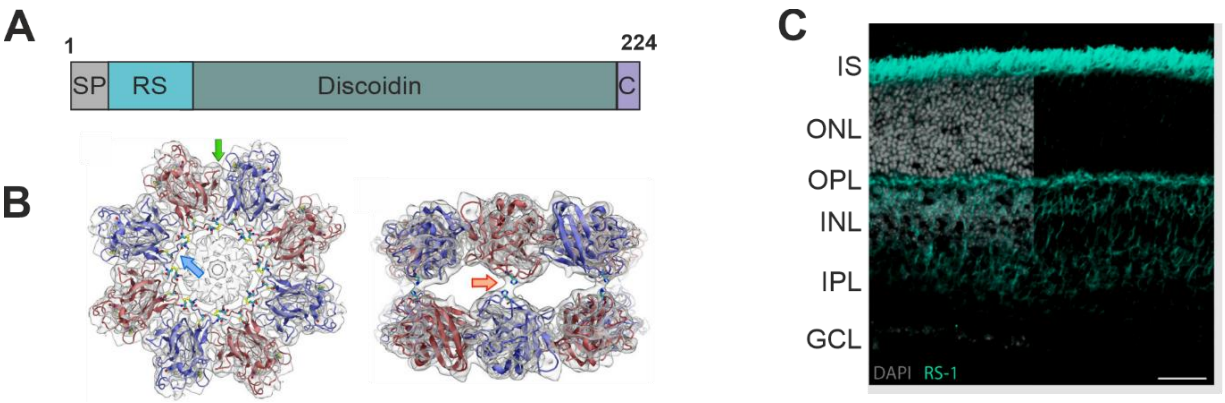

Figure 2: Structure and retinal localization of the protein retinoschisin

A: Linear representation of the 224-amino acid (aa) retinoschisin protein showing a 23-aa N-terminal signal peptide (SP), the 39-aa retinoschisin domain (RS), a 157-aa discoidin domain, and a 5-aa C-terminal segment (C), **B:** Top and side views of the retinoschisin hexadecamer. Blue arrow: Rod-like density connecting neighboring subunits between the discoidin and retinoschisin domains; green arrow: Subunit-subunit boundary; red arrow: Connections between the octameric rings (modified from Tolun et al. 2016). **C:** Confocal fluorescence images of a retinal cryosection of a wildtype mouse at postnatal day 60 stained with antibodies against retinoschisin (RS-1, turquoise) and with 4',6-Diamidino-2-phenylindol (DAPI) (gray, depicting nuclei); Scale bar: 100 µm; IS, inner segments; ONL/INL, outer/inner nuclear layer; OPL/IPL, outer/inner plexiform layer; GCL, ganglion cell layer (modified from Vijayasarathy et al. 2021)

The protein retinoschisin is mainly localized in rod and cone photoreceptor inner segments and bipolar cells (Grayson et al. 2000; Molday et al. 2001; Reid et al. 2003). A minor expression was also detected in pinealocytes of the pineal gland (Takada et al. 2006). In the retina, the secreted retinoschisin has been detected by immunohistochemical studies in the inner segments of the photoreceptors as well as in the inner and outer plexiform layers (Friedrich et al. 2011; Molday et al. 2001; Vijayasarathy et al. 2021) (**Figure 2C**).

1.1.3 XLRS-associated mutations

Over 200 disease causing mutations have been described in the *RS1* gene so far (Leiden Open Variation Database, https://www.lovd.nl/). Around 40% of these are true null alleles including splice site, nonsense, or frameshift mutations while the remaining mutations are missense mutations that lead to an aa exchange in the translated protein. Missense mutations localized in the N-terminal signal sequence (e.g., L12H) exhibit a greatly reduced protein expression and a defective protein localization. Since these mutations affect the α-helical conformation of the signal peptide, no cleavage of the SRP occurs leading to a cytoplasmic mislocalization with subsequent degradation (Wu and Molday 2003; Wang et al. 2006). Most of the missense mutations (85%) are localized within the discoidin domain of retinoschisin and several studies have shown that these mutations result in defective folding of the protein (Wang et al. 2002; Wu et al. 2003). For example, mutations of a cysteine residue in the discoidin domain (e.g., C142W) can lead to the formation of unphysiological disulfide bridges and thus to an altered protein structure (Wu et al., 2003). Mutations that do not affect cysteine residues (e.g., P203L) also may cause misfolding by disrupting hydrophobic or electrostatic interactions (Wu and Molday 2003). These misfolded proteins are retained and degraded in the ER.

Only a few mutated retinoschisin species are still secreted, e.g., missense mutants C59S, C223S, F108C, R182C, R141H, and H207Q (Wang et al. 2002, 2006; Wu and Molday 2003; Wu et al. 2005; Dyka et al. 2008; Ramsay et al. 2016; Plössl et al. 2018). The missense mutants C59S and C223S exhibit loss of the cysteine residues responsible for octamerization and are secreted as dimers (Wang et al. 2002, 2006; Wu and Molday 2003). R141H and H207Q are secreted as double octamers, whereas F108C and R182C do not show double-octamerization but rather aggregation (Dyka et al. 2008; Ramsay et al. 2016; Plössl et al. 2018). Interestingly, *in vitro* investigations suggest a loss of function of all secreted retinoschisin mutants (Plössl et al. 2018), in line with the autosomal-recessive mode of inheritance of XLRS.

1.1.4 Mouse models to study XLRS

Several retinoschisin-knockout or knockin mouse models have been established so far to study XLRS disease pathomechanism and therapeutic approaches (Weber et al. 2002; Zeng et al.

2004; Jablonski et al. 2005; Chen et al. 2018; Liu et al. 2019). Among these, three are knockout lines (Weber et al. 2002; Zeng et al. 2004; Liu et al. 2019), one mouse model has a splice-site mutation (retinoschisisn-44TNJ; Jablonski et al. 2005) and three are knockin models (Chen et al. 2018; Liu et al. 2019). In all of which the murine ortholog of the human *RS1* gene, namely *Rs1h*, was disrupted using various genetic tools. For this study, the retinoschisin-knockout mouse was generated *via* targeted disruption of exon 3 by Weber and colleagues (Weber et al. 2002). In addition to the retinoschisin-deficient mice, Liu and colleagues generated two mouse models harboring XLRS patient specific missense mutations in *Rs1h* (Liu et al. 2019), specifically RS1_C59S and RS1_R141C. Finally, Chen and colleagues generated a mouse line harboring the nonsense mutation RS1_P65* (Chen et al. 2018). Comparable to the "negative ERG", typically recorded in XLRS patients, the ERG of the retinoschisin-knockout mice reveal a reduction in the b-wave as well (**Figure 3A**, Weber et al. 2002; Zeng et al. 2004; Jablonski et al. 2005; Liu et al. 2019). The ERGs of mice with a missense mutation in the retinoschisin gene also show a b-wave reduction although less pronounced. In addition, all retinoschisin-knockout and -knockin mice share structural alterations of the retina comparable to human XLRS, including the formation of schisis cavities with a disruption of the inner retinal layers starting around postnatal days (P) 14 (**Figure 3B**, Weber et al. 2002; Zeng et al. 2004; Jablonski et al. 2005; Chen et al. 2018; Liu et al. 2019). Furthermore, photoreceptor degeneration due to apoptotic events peaking around P18 was reported (Gehrig et al. 2006).

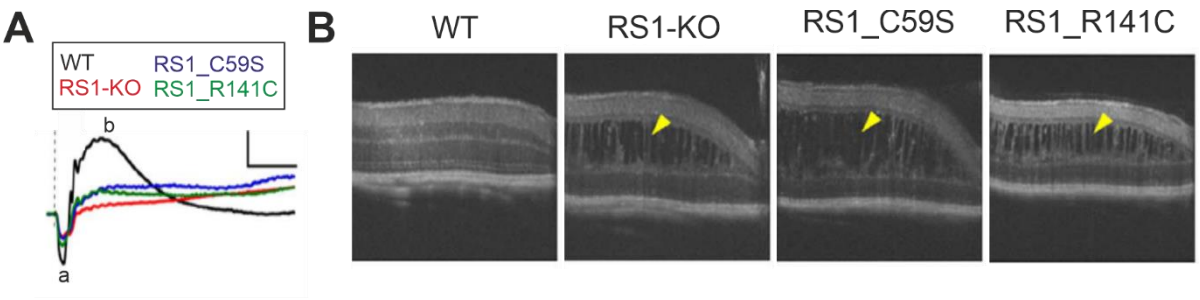

Figure 3: Schisis formation and negative electroretinography of retinoschisin-knockout and mutant mice

A: Representative dark-adapted retinography obtained from wildtype (WT), retinoschisin-knockout (KO), retinoschisin mutant C59S (RS1_C59S), and R141C (RS1_R141C) mice aged postnatal day (P) 24. Scale bars indicate 500 µV and 100 ms. **B**: Representative spectral domain optic coherence tomography images of the retina of wildtype (WT), retinoschisin-knockout (KO), retinoschisin mutant C59S (RS1_C59S), and R141C (RS1_R141C) mice aged P18. All images were obtained from the temporal region of the right eye and include the edge of the outer nuclear layer on the right. Yellow arrowheads indicate schisis (Figure modified from Liu et al., 2019)

1.1.5 Retinoschisin and its putative interaction partners

In recent years, several potential interaction partners of retinoschisin have been reported, but replication of these studies or physiological relevance is still lacking. Kotova and colleagues (2010) observed an interaction between retinoschisin and a phosphatidylserine containing lipid bilayer *via* atomic force microscopy (Kotova et al. 2010). This interaction was not confirmed by other works (Dyka et al. 2008; Friedrich et al. 2011). Since phosphatidylserines are intracellular

proteins and retinoschisin is a secreted extracellular protein, the physiological relevance of an interaction between retinoschisin and phosphatidylserine remains questionable. Using affinity columns and immunohistochemistry in porcine retinae, an interaction of retinoschisin with extracellular matrix and cytoplasmic proteins β2-laminin and αB-crystallin was suggested (Steiner-Champliaud et al. 2006). The authors postulated, that interactions with αB-crystallin should most likely be intracellular, while the association with β2-laminin probably arises at the level of the extracellular scaffold involved in stabilizing synapses. In addition, retinoschisin was proposed to be an interaction partner of the L-type voltage-gated calcium channels (LTCC) (Shi et al. 2009; 2017), namely Cav1.3, which regulates the calcium ion flow (Morgans et al. 2005), and Cav1.4, which is responsible for neurotransmitter release in retinal photoreceptors (Barnes and Kelly 2002). Shi and colleagues reported that retinoschisin is important for LTCC anchorage in the plasma membrane and enhances its currents, channel conductance, and voltage-dependent activation (Shi et al. 2009; 2017). Thus, they suggested that XLRS-associated retinoschisin-deficiency leads to a reduction of plasma membrane located LTCC, which consequently should cause failure in the formation of synaptic connections, ultimately resulting in retinal degeneration (Shi et al. 2017). Furthermore, the sugar molecules galactose-agarose and to a lesser extent lactose-agarose were found to interact with retinoschisin (Dyka et al. 2008). So far, however, no physiological relevance was suggested for the interaction of retinoschisin with sugar motifs. Finally, in 2007 Molday and colleagues identified the retina-specific Na/K-ATPase consisting of two subunits, the catalytic ATP1A3 (α3) and the stabilizing ATP1B2 (β2), to interact with retinoschisin at the retinal plasma membrane (Molday et al. 2007). This study also observed co-localization of retinoschisin and the Na/K-ATPase in cryosections from mouse retina (Molday et al. 2007).

1.2 The Na/K-ATPase

1.2.1 Structure of the Na/K-ATPase

The Na/K-ATPase is an intrinsic plasma membrane protein of the P-type ATPase family. The Na/K-ATPases have the transport of cations across the plasma membrane through ATP hydrolysis in common (Skou and Hoffman 1998). Their minimal functional unit is composed of an alpha (α, ATP1A) subunit and a beta (β, ATP1B) subunit. The auxiliary Phe-X-Tyr-Asp protein (FXYD) subunit can also be part of the complex (Geering 2008; Clausen et al. 2017).

The α-subunit contains the major transmembrane (TM) region consisting of ten TM helices, and it harbors the ion binding sites (Reinhard et al. 2013). In addition, three major cytoplasmatic domains are present including the actuator, the nucleotide binding, and the phosphorylation domain. During the catalytic cycle and ATP hydrolysis, the nucleotide binding domain serves as the kinase, the phosphorylation domain as the substrate, and the actuator

domain as the phosphatase (Clausen et al. 2017). There are four different human Na/K-ATPase α-isoforms (ATP1A1 – ATP1A4) with highly conserved primary peptide sequences. The ATP1A1, ATP1A2, and ATP1A3 subunits share about 87% sequence identity, and about 78% with the sperm-specific ATP1A4 isoform (Shamraj and Lingrel 1994).

The β-subunit consists of a single TM helix and an extracellular domain, which is highly glycosylated. In humans, three β-isoforms (ATP1B1 - ATP1B3) exist with different sequence identities. ATP1B1 and ATP1B2 share 39%, ATP1B1 and ATP1B3 36%, and ATP1B2 and ATP1B3 47% sequence identity. Thus, in contrast to the α-subunit, the sequence identities between the β-subunits are fairly low (Reinhard et al. 2013). The FXYD subunit contains a single TM helix and an extracytoplasmic N-terminus (Geering 2006). Humans express seven FXYD proteins (FXYD1-FXYD7) (Clausen et al. 2017).

1.2.2 Tissue-specific expression of Na/K-ATPase isoforms

In higher vertebrates, the α- and ß-isoforms as well as the FXYD proteins show a tissue-specific expression.

In humans, the ATP1A1 isoform is ubiquitously expressed, while the ATP1A2 isoform is predominantly expressed in muscle (heart and skeletal) and brain tissue (in glia cells and astrocytes) (Clausen et al. 2017). The ATP1A3 isoform is present predominantly in neuronal tissue and human heart (Clausen et al. 2017), but with gender-specific differences (the ratio of ATP1A3 to ATP1A1 is higher in men than in women) (Gaborit et al. 2010). In contrast, the ATP1A4 isoform is considered a sperm-specific Na/K-ATPase (Clausen et al. 2017). The ATP1B1 isoform is the predominant isoform in brain, heart, colon, and kidney, the ATP1B2 isoform in neuronal tissue. Expression of ATP1B3 has been found in lung, liver, and testis (Clausen et al. 2017). FXYD1 is highly expressed in the heart, skeletal muscle, and brain, FXYD2 and 4 in kidney, FXYD5 in lung, kidney, spleen and FXYD6 and 7 in the brain (Lubarski et al. 2005; Geering 2006; Clausen et al. 2017; Yap et al. 2021). FXYD3 and also 5 show high expression in some cancer cells, but their role has not yet been clarified (Nam et al. 2007).

In the adult retina, the highest concentration of the Na/K-ATPases can be observed in the inner segments of photoreceptors with ATP1A3 and ATP1B2 as the predominant isoforms, and thus the enzyme complex composed of ATP1A3 and ATP1B2 is consequently referred to as the “retinal Na/K-ATPase” (Schneider and Kraig 1990; Wetzel et al.1999). Wetzel and colleagues (1999) analyzed the expression of the Na/K-ATPase isoforms within the different cell types of the murine retina. The ATP1A1 isoform was detected in Müller glia and horizontal cells, ATP1A2 in Müller glia, and ATP1A3 predominantly in photoreceptors. All α-isoforms were found in retinal neurons. Expression of ATP1B1 was specific to the horizontal, amacrine, and

ganglion cells, while ATP1B2 was specifically localized to photoreceptors, bipolar cells, and Müller glia.

1.2.3 Function of the Na/K-ATPase

In 1969, Robert Post first described the Na/K-ATPase as an active ion pump, transporting Na^+ and K^+ ions across the plasma membrane (Post et al. 1969). He later showed that the ion pumping mechanism is linked to a cycle of conformational changes of the Na/K-ATPase, which is important for its ability to convert ATP hydrolysis and the transport of ions across the plasma membrane (Post et al. 1969; Cui and Xie 2017). As the α-subunit contains the ATP binding site, it is also referred to as the catalytic subunit. The α-subunit mediates hydrolysis of one ATP molecule and leads to phosphorylation of the Asp369 residue which provides the conformation change from E1 (also referred to as the Na^+-bound state) and E2 (also referred to as the K^+-bound state) and allows the transport of three Na^+ and two K^+ ions at a baseline rate of 60–80 phosphorylation-dephosphorylation cycles per second. This two-stage change from E1 to E2 can be described using the Albers-Post reaction cycle (**Figure 4**) (Albers 1967; Post et al. 1972) and it also allows the binding of many ligands to the Na/K-ATPase in a conformational state-dependent manner (Cui and Xie 2017).

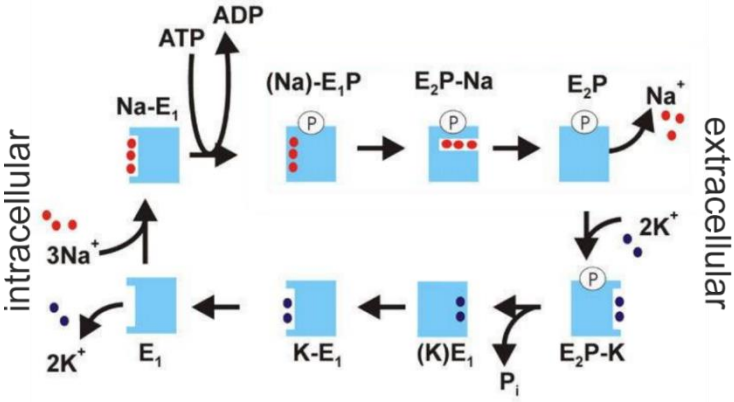

Figure 4: Schematic representation of the Albers-Post reaction cycle

The reaction cycle of the Na/K-ATPase (light blue) is described by the Albers-Post scheme, where the enzyme can assume two principle conformational states, E_1 and E_2. In E_1, three Na^+ ions (red) bind cytoplasmically for subsequent ion transport across the membrane, while two K^+ ions (dark blue) bind to extracellular sites when the protein is in the E_2 conformation for transport into the cell. (Figure modified from Dempski et al., 2005)

The dynamic regulation of ionic concentration is essential for maintaining cellular homeostasis, as it regulates the cellular membrane potential, the cell volume, and osmolarity, as well as the excitability of neuronal cells (Therien and Blostein 2000; Geering 2008; Cui and Xie 2017). In addition to its pump-function, the Na/K-ATPase and especially the α-subunit is thought to be a protein-docking station as it is engaged in the assembly of macromolecular complexes for an increasing number of proteins, thus enabling the formation of specific lateral plasma membrane signaling microdomains (Reinhard et al. 2013; Cui and Xie 2017). Specifically, the ATP1A1-containing Na/K-ATPase regulates the membrane-associated tyrosine kinase SRC activity through a conformation-dependent interaction with SRC, whereas both ATP1A2 and ATP1A3 showed no interaction with SRC (Xie et al. 2015; Madan et al. 2017). It is

hypothesized, that upon cardiac binding to the α-subunit of the Na/K-ATPase, SRC is released from the N-domain, resulting in SRC activation and communication of the Na/K-ATPase-SRC complex with other intracellular signal transducers such as phospholipase C (PLC), rat sarcoma (RAS), or the inositol 1,4,5-trisphosphate (IP3) receptor. This assembly of the so-called "signalosome complex" induces several signaling pathways such as the mitogen-activated protein (MAP) kinase signaling, phosphatidylinositol 3-kinase (PI3K)Akt signaling, and Ca^{2+} signaling (Reinhard et al. 2013; Cui and Xie 2017).

The α-subunit of the Na/K-ATPases also interacts with other membrane proteins, ion channels, or transporters. In cardiomyocytes, the ATP1A2-containing Na/K-ATPase builds a macromolecular protein complex together with the adaptor protein ankyrinB (ANKB) and the Na/Ca exchanger (NCX) (Mohler et al. 2005). In this complex, ANKB together with the Na/K-ATPase controls NCX activity by reducing the intracellular Na^+ levels at the cytosolic site of NCX. A study by Skogestad and colleagues (2020) showed that disruption of the Na/K-ATPase and ANKB has severe effects on ion homeostasis. An interaction between the scaffolding protein caveolin-1 (CAV1), the ATP1A2-containing Na/K-ATPase, and ANKB in so-called caveolae was described as well. Here, a disruption of the CAV1 and ANKB interaction sites leads to alterations in the Na/K-ATPase membrane diffusion (Junghans et al. 2017). In the brain, the α1-3 subunits were detected as interaction partner of the glutamate aspartate transporter (GLAST) and the glutamate transporter 1 (GLT-1) (Rose et al. 2009), both playing an important role in the glutamate uptake (Kanner 2006). The binding of the cardiac glycoside ouabain to the Na/K-ATPase revealed a Na/K-ATPase dependent activity regulation of the glutamate transporter and *vice versa* the glutamate transporters might also be able to modulate the Na/K-ATPase activity (Gegelashvili et al. 2007). In addition, a coupling of the ATP1A3-containing Na/K-ATPase and the dopamine system was identified in photoreceptors and in the spines of striatal neurons. In a study by Nishi and colleagues, it was shown that the dopamine receptor D1 inhibits the pump (Nishi et al. 1999). Moreover, the ATP1A1 and ATP1A2 subunits revealed an interaction with the water channel protein aquaporin-4 (Illarionova et al. 2010), and ATP1A1 with the AMPA glutamatergic receptor (Zhang et al. 2009).

The β-subunit of the Na/K-ATPase exerts a scaffolding function important for stabilizing and membrane targeting of the Na/K-ATPase (Reinhard et al. 2013). Another role of the β-subunit is the modulation of the functional properties of the Na/K-ATPase, including cation binding affinity and the occlusion of potassium ions (Tidow et al. 2010; Toyoshima et al. 2011). The β-subunit of the Na/K-ATPase also acts as a cell adhesion molecule regulating tight junction formation and thus it is involved in intracellular adhesion (Krupinski and Beitel 2009). In mammalian epithelial cells, the basolateral ATP1B1 subunit of the Na/K-ATPase acts as an

adhesion molecule and in some cell types the Na/K-ATPase can interact with the protein phosphatase in tight junctions (Krupinski and Beitel 2009). The ATP1B2 subunit of the Na/K-ATPase is also known as the adhesion molecule on glia (AMOG), as it mediates the glial-astrocyte interactions and can promote neurite outgrowth (Gloor et al. 1990).

FXYD proteins are not required for the functional expression of the Na/K-ATPase, but they can modulate the activity of the Na/K-ATPase pump by decreasing the substrate affinities or the V_{max} of the pump, allowing a dynamic response to changing physiological conditions (Geering 2006; Yap et al. 2021).

1.2.4 Cardiac glycosides – ligands of the Na/K-ATPase

Cardiac glycosides are important regulators of the Na/K-ATPase (Therien and Blostein 2000). They are conjugates of a glycone and an aglycone part (**Figure 5A**). Glucose, fructose, glucuronide, rutinose, and rhamnose are glycone motifs, and the aglycone part is a steroidal nucleus (Patel 2016). Cardiac glycosides such as digoxin and ouabain were first found as secondary metabolites in plants, and bufalin and marinobufagenin in amphibians and later in other animals as well as in human (Schoner and Scheiner-Bobis 2007). Ouabain has been isolated from human blood (Hamlyn et al. 1991; Mathews et al. 1991), from bovine adrenal glands (Schneider et al. 1998), bovine hypothalamus (Kawamura et al. 1999), and in the supernatant of rat pheochromocytoma cells (Nishimura et al. 2001). Digoxin and marinobufagenin were found in the human urine (Goto et al. 1990; Bagrov et al. 1998).

Cardiac glycosides show an interaction with the catalytic α-subunit through a high-affinity cardiac glycoside binding site formed by TM 1-6, which creates a pocket exposed to the extracellular side and overlaps with the extracellular ion exchange pathway (Yatime et al. 2011; Laursen et al. 2013). Once cardiac glycosides bind to the Na/K-ATPase, the E2P-state (**Figure 5B**) is stabilized leading to the activation of numerous downstream signal transduction pathways (Silva and Soares-da-Silva 2012). Thus, cardiac glycosides in the human body have a high impact on the regulation of many important physiological and pathophysiological states (Schoner and Scheiner-Bobis 2007; Prassas and Diamandis 2008). Cardiac glycosides are postulated to regulate gene expression, orientation of cell polarity, protein trafficking, and proliferation (Prassas and Diamandis 2008).

Cardiac glycosides inhibit the Na/K-ATPase pump function in cardiomyocytes and thus are used as a common therapy for certain heart diseases. The inhibition of the Na/K-ATPase activity prevents the Na^+ exit from the cell which leads to an increase of intracellular Ca^{2+} levels through functional coupling to NCX. Higher cytoplasmic calcium enhances Ca^{2+} uptake into the

sarcoplasmic reticulum by the SERCA2 transporter, which improves the contractility of cardiac muscle and causes positive inotropy (Patel 2016; Cui and Xie 2017).

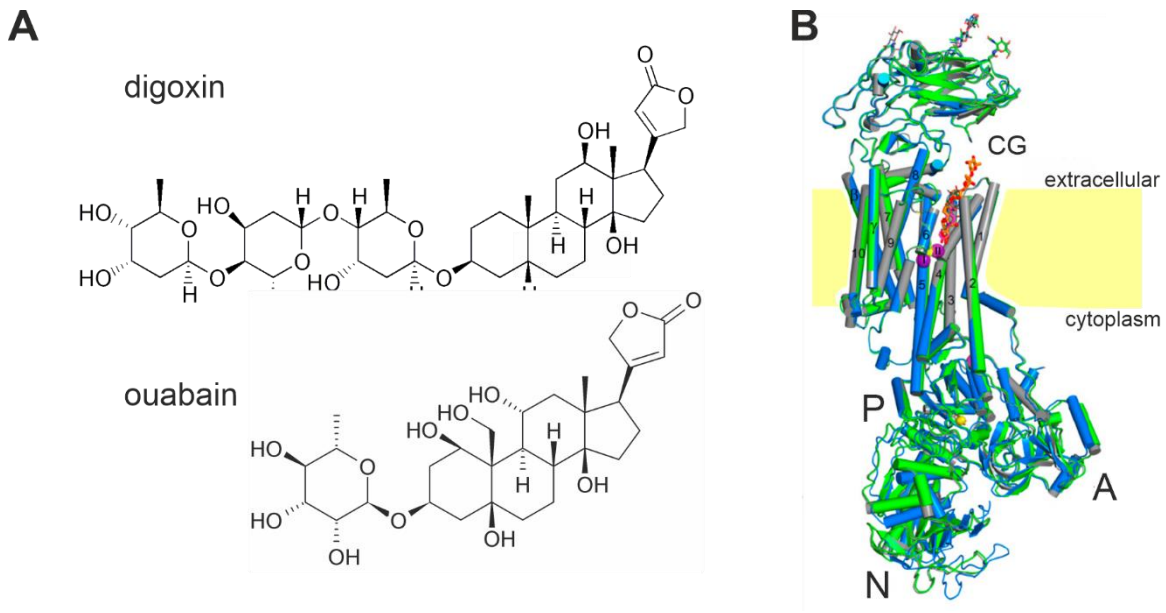

Figure 5: Cardiac glycoside binding to the retinal Na/K-ATPase

A: Structural representation of the cardiac glycosides (CG) digoxin, and ouabain (Wikimedia). **B:** Schematic representation of the Na/K-ATPase (ATP1A1-ATP1B1) E2P–CG complex consisting of the α-subunit with three major cytoplasmatic domains: the actuator (A), the nucleotide binding (N), and the phosphorylation domain (P), as well as the β-subunit, and CG complexes. The phosphoenzyme stabilized by bufalin, digoxin, and ouabain is depicted in blue, green, and gray cartoons, respectively, and the bufalin, digoxin, and ouabain molecules are represented by magenta, orange, and dark gray sticks, respectively. The K^+ and Mg^{2+} ions are represented by purple and yellow spheres, respectively. (Figure modified from Laursen et al. 2015)

Of note, cardiac glycosides can increase the output force of the heart and its rate of contractions, but it was reported that too high Ca^{2+} levels due to high dosage of cardiac glycosides can lead to severe side effects like electrical instability, ventricular tachycardia, and fibrillation (Laurita and Rosenbaum 2008; Patel 2016). Moreover, patients administered cardiac glycosides also often experience vision impairment as a side effect of treatment (Duncker 1981; Haustein 1982; Lawrenson et al. 2002; Fraunfelder et al. 2014; Renard et al. 2015). A study of 30 elderly hospitalized patients receiving the cardiac glycoside digoxin in a regular therapeutic dose revealed a high incidence of impaired color vision (Lawrenson et al. 2002). Other reported visual side effects of digoxin are xanthopsia, the illusion of objects exhibiting abnormal colors, decreased visual acuity, central scotomas, or visual field reduction, photopsia most pronounced in daylight, photophobia, blurry or snowy vision. Moreover, ERG measurements often reveal evidence of cone dysfunction, suggesting the retina is the site of toxicity, perhaps at the level of Na/K-ATPase pumps in photoreceptor cells (Renard et al. 2015; Liu et al 2019).

1.2.5 Interaction between retinoschisin and the retinal Na/K-ATPase

Retinoschisin was shown to directly interact with the ATP1B2 subunit of the Na/K-ATPase, whereas the ATP1A3 subunit had no specific role in this interaction (Plössl et al. 2017b). Moreover, a recent study of the Institute of Human Genetics in Regensburg revealed a hydrophobic patch of ATP1B2 *via in-silico* analyzes. These patches were further examined using functional assays and showed that one patch and specifically the associated aa at position 240 are crucial for retinoschisin binding to the ATP1B2 subunit (Plössl et al. 2019). Moreover, another study of the Institute investigated the interaction site of retinoschisin, and it was suggested that a substructure of the retinoschisin octamer the so-called “spike 3” and its vicinity plays a fundamental role in mediating the specific interaction of retinoschisin with its ligand. (Plössl et al. 2018).

The influence of recombinant retinoschisin on functional processes of the Na/K-ATPase was investigated by using two model systems; the human retinoblastoma cell line Y-79 and retinoschisin-deficient murine retinal explants, both capable to bind extracellularly added recombinant retinoschisin due to an endogenous expression of the Na/K-ATPase subunits ATPA3 and ATP1B2. These studies revealed no effect of retinoschisin binding to the Na/K-ATPase on ATP hydrolysis or ion transport. In contrast, retinoschisin negatively influenced the Na/K-ATPase regulated signaling cascades like the MAPK/ERK signaling or the Ca^{2+} signaling, whereas no effect was observed on PI3K/Akt signaling pathways (Plössl et al. 2017a; b). Retinoschisin was also shown to regulate the localization of the retina-specific Na/K-ATPase in the retinal plasma membrane (Friedrich et al. 2011).

1.3 Aim of the study

Several studies have shown that the retinal Na/K-ATPase is an important interaction partner of retinoschisin in the plasma membrane of photoreceptors (Molday et al. 2007; Friedrich et al. 2011). In addition, intensive research was performed to understand the consequences of retinoschisin-deficiency on retinal integrity. Nevertheless, the initial processes in XLRS pathology and the function of the retinoschisin-Na/K-ATPase complex in the retina have not been fully elucidated. Therefore, the present study focused on the functional and structural characterization of the retinoschisin-Na/K-ATPase complex and its ligands or possible interaction partners.

The first project focused on defining the physical interaction surface between retinoschisin and the retinal Na/K-ATPase. This led to further studies delineating the impact of ATP1B2 glycoside residues and specifically of ATP1B2 residue T240 on the binding of retinoschisin. In addition, the effect of retinoschisin binding to the retinal Na/K-ATPase was analyzed for the possibility of an effect known as lateral membrane diffusion. The second project aimed at understanding

the interplay between retinoschisin and the cardiac glycosides digoxin and ouabain at the retinal Na/K-ATPase and its consequences on the regulation of Na/K-ATPase activity and retinal integrity. The goal of the third project sought to delineate further the retinoschisin-Na/K-ATPase complex at the photoreceptor inner segments. The immediate aim was to identify further interaction partners of the complex and to clarify the consequences of retinoschisin-deficiency on the respective constituents of this complex.

Together, the three subprojects were targeted to better understand the pathomechanism of XLRS. Such a refined understanding is likely to ultimately provide novel research-based approaches for innovative therapeutic options for this blinding disease.

2 Material

2.1 Cell lines

Table 1: Listed are cell lines used in this work, their organism of origin, their tissue of origin, and their source

Cell Line	Organism of Origin	Tissue of Origin	Source
Hek293	*Homo sapiens*	Embryonic kidney	ATCC; LGC Standards GmbH, Wesel, Germany
Hek293 + RS1	*Homo sapiens*	Embryonic kidney, Hek293 cells stably transfected with retinoschisin expression vector	Institute of Human Genetics, University of Regensburg, Germany
Y-79	*Homo sapiens*	Retinoblastoma	ATCC; LGC Standards GmbH, Wesel, Germany

2.2 Animal models

Table 2: Listed are animal models used in this work and their source

Animal model	Source
Atp1b2-knockout (EM00023)	European Mouse Mutant Archive, Munich, Germany
C57BL/6	The Jackson Laboratory, Bar Harbor, ME, USA
Rs1h-knockout ($Rs1^{tm1Web}$)	Bernhard HF Weber, Institute of Human Genetics, University of Regensburg, Germany
Sus Scrofa	Metzgerei Kurth, Regensburg, Germany

2.3 *Escherichia Coli* strain

Table 3: Listed is the *Escherichia Coli* strain used in this work and its source

Escherichia Coli (*E-Coli*) Strain	Source
E. coli strain DH5α	Life Technologies, Carlsbad, CA, USA

2.4 Primers used for cycle sequencing

Table 4: Listed are oligonucleotides used in this work, their 5'-3' sequence, and their purpose.

Primer name	5'-3' Sequence	Purpose
M13_F	CGC CAG GGT TTT CCC AGT CAC GAC	Vector primer for pGEM®-T
M13_R	AGC GGA TAA CAA TTT CAC ACA GGA	
T7_F	TAA TAC GAC TCA CTA TAG GG	Vector primer for pCDNA3.1
BGH_R	TAG AAG GCA CAG TCG AGG	
pTLN1_F	GAA TAC AAG CTT GCT TGT TCT	Vector primer for pTLN1
pTLN1_R	CGA ATC TCTGAG GTA AGC CC	
pCEP_new_F	GGA CTT TCC AAA ATG TCG TAA TAA	Vector primer for pCEP4
pCEP_new_R	CAA ATA AAG CAA TAG CAT CAC AAA T	
hATP1A3Seq1F	ATG GGG GAC AAG AAA GAT GA	Primer for sequencing of *ATP1A3* and *ATP1B2*
hATP1A3Seq2F	CCC AGA GTG GGT CAA GTT TT	
hATP1A3Seq3F	GTG GAG ATC AAG GGT GGA GA	
hATP1A3Seq4F	GCA CTT CAT CCA GCT CAT CA	

hATP1A3Seq5F	GAC AGG GAC CCT CAC TCA GA	
hATP1A3Seq6F	TAC CAG CTC TCC ATC CAT GA	
hATP1A3Seq7F	CCT TCGACT GTG ATG ACG TG	
hATP1A3Seq8F	AGC AAATCG ACG AGATCC TG	
hATP1A3Seq9F	CCT ACA CCC TGA CCA GCA AT	
hATP1A3Seq10F	TTG GAA TGA TCC AGG CTC TC	
hATP1A3Seq1R	ATG CCA GGT ACA GGT TGTC	
hATP1A3Seq2R	GTC AGG GAG GAG TTG TCC A	
hATP1A3Seq4R	CAG GTG TGC GAA CTC TTG TC	
ATP1A3-Ex4_R	AGAGGGGTCGTCCTCGGTGC	
pCDNA3-E/G/C/Y/F	TTCAGGGTCAGCTTGCCGTA	
hATP1B2-ex1-2-F	CTGGCCACACCGGGCTTGATG	
RT_human_mAtp1b2_R1	CTGGTCCCAGCTTTCAGTGT	
RT_human_mAtp1b2_R2	CAGGGGCTGTGTGTAGTTCA	
ATP1B2-F	ACATCGACCTCATGTACTTCC	
GFP-RT-F	GAAGCGCGATCACATGGT	
hATP1B2Seq1R	TTT GGG CTT GGA TA GAG TCG	
hATP1B2Seq2R	ATG ACG AAG TTG CCG AGA TT	
hATP1B2Seq3F	TCC ACC CAC TAT GGT TAC AGC	
hATP1B2_T240S_F	CGTGAACTACTCACAGCCCCTGG	Site directed mutagenesis of *ATP1B2* (T240S)
hATP1B2_T240S_R	TGGAACTTTTTGCCATAGTAGGG	
hATP1B2_T240A_F	CGTGAACTACGCACAGCCCCTGG	Site directed mutagenesis of *ATP1B2* (T240A)
hATP1B2_T240A_R	TGGAACTTTTTGCCATAGTAGGGG	

F: forward, R: reverse; all oligonucleotides were purchased from Metabion, Planegg, Germany.

2.5 KiCqStart® probe assays used for RNA expression analysis

Table 5: Listed are KiCqStart® probe assays used in this work, their 5'-3' sequence, and their purpose.

Probe name	Sense-Primer	Anti-sense Primer	5'-3'- Probe Sequence
ATP1A3 NM_001290469.1	TCCTACTTTGTCATCCTGGC	TCTGCTCATAAGTCCACTGC	CGGAAACCTGGTGGGCATCCGGC
ATP1B2 NM_013415.5	GAGTCGGGAGTTTTCTAG	AAGGGCATCTCATTCATAA	TCACTCAGCGACAGAGGACTTG
KCNB1 NM_008420	CCCTACTACGTCACCATC	GGAAGATCTGGACCACAC	ACAGAATCCAACAAGAGCGTGC
KCNV2 NM_183179.1	ATCTTCTCCTTCTCTGCAGC	GGTACATGTCTCCATAGCCC	TGGTGGTGGGCCGCGGTAAGCA
Sncg (NM_011430.3)	CTGAAAACATCGTGGTCACC	CTTGCTCTTTGGCTTCTTGG	CGGGGTGGTGCGCAAGGAGGACT

All oligonucleotides were purchased from Sigma-Aldrich, St. Louis, MO, USA.

2.6 Plasmids and expression constructs

Table 6: Listed are plasmids and expression constructs used in this work, their purpose, and their source.

Plasmid name	Purpose	Source
pCDNA3.1	Expression vector	Thermo Fisher Scientific, Waltham, MA, USA
pCDNA3_ATP1A3-GFP_ATP1B2	Bicistronic expression of GFP-tagged ATP1A3 and ATP1B2	Generated during this project
pCDNA3_Kv2.1	Expression of Kv2.1	Institute of Human Genetics, University of Regensburg

pCDNA3_Kv8.2	Expression of Kv8.2	Institute of Human Genetics, University of Regensburg
pCEP_ATP1A3	Expression of ATP1A3	Institute of Human Genetics, University of Regensburg
pCEP_ATP1A3_ATP1B2	Bicistronic expression of ATP1A3 and ATP1B2	Institute of Human Genetics, University of Regensburg
pCEP_ATP1A3_OI	Expression of ATP1A3 (ouabain insensitive)	Institute of Human Genetics, University of Regensburg
pCEP_ATP1A3_OI_GFP	Expression of GFP-tagged ATP1A3 (ouabain insensitive)	Institute of Human Genetics, University of Regensburg
pCEP_ATP1B2	Expression of ATP1B2	Institute of Human Genetics, University of Regensburg
pCEP_ATP1B2_T240A	Expression of ATP1B2 mutant T240A	Generated during this project
pCEP_ATP1B2_T240L	Expression of ATP1B2 mutant T240L	Institute of Human Genetics, University of Regensburg
pCEP_ATP1B2_T240S	Expression of ATP1B2 mutant T240S	Generated during this project
pCEP_RS1	Expression of RS1	Institute of Human Genetics, University of Regensburg
pCEP_RS1_C59S	Expression of RS1 mutant C59S	Institute of Human Genetics, University of Regensburg
pCDNA3_RS1_C59S_Myc	Expression of Myc-tagged RS1_C59S	Institute of Human Genetics, University of Regensburg
pCDNA3_RS1_Myc	Expression of Myc-tagged RS1	Institute of Human Genetics, University of Regensburg
pCEP4	Expression vector	Thermo Fisher Scientific, Waltham, MA, USA
pGEM®-T	Vector for Cloning	Promega Corporation, Madison, WI, USA
pTLN1_ATP1B2	Vector for Cloning	Institute of Human Genetics, University of Regensburg

2.7 Primary antibodies

Table 7: Listed are primary antibodies used in this work, their species, their dilution, and their source

Antibody	Species	Dilution	Source
AnkyrinB (2.2)	mouse	IHC: 1:50 WB: 1:500	Invitrogen, Thermo Fisher Scientific, Waltham, MA, USA
AnnexinA2 (610068)	mouse	IHC: 1:500 WB: 1:5000	BioSciences, Franklin Lakes, NJ, USA
ATP1A1 (#55187-1-AP)	rabbit	WB: 1:10000	Proteintech, Rosemont, IL, USA
ATP1A3 (#MA3-915)	mouse	IHC: 1:100 - 1:1000 WB: 1:10000 FACS: 1:50	Thermo Fisher Scientific, Waltham, MA, USA
ATP1A3 (#ab2826)	mouse	IHC: 1:1000 WB: 1:10000 ICC: 1:1000	Abcam, Cambridge, UK

ATP1B2 (#PA5-26279)	rabbit	IHC: 1:250 ICC: 1 :500 WB: 1:2000 FACS: 1:50	Thermo Fisher Scientific, Waltham, MA, USA
ATP1B2 (#22338-1-AP)	rabbit	IHC: 1:50	Proteintech, Rosemont, IL, USA
GFP (#sc-390394)	rabbit	WB: 1:5000	Santa Cruz Biotechnology, Inc., Dallas, TX, USA
6*His-tag (#66005-1-Ig)	mouse	-	Proteintech, Rosemont, IL, USA
Kv2.1 (#75-014)	mouse	IHC: 1:400 -1:800 WB: 1:1000	UC Davis/NIH NeuroMab Facility, Davis, CA, USA
Kv8.2 (#75-435)	mouse	IHC: 1:50 -1:800 WB: 1:1000	UC Davis/NIH NeuroMab Facility, Davis, CA, USA
Myc-Tag (9B11) (#2276)	mouse	WB: 1:1000	Cell Signaling Technologies, Danvers, MA, USA
NCX (#ab177952)	rabbit	WB: 1:4000	Abcam, Cambridge, UK
PI3K (#4228)	rabbit	WB: 1:1000	Cell Signaling Technologies, Danvers, MA, USA
PLC (#5690)	rabbit	WB: 1:250	Cell Signaling Technologies, Danvers, MA, USA
RAS (#3965)	rabbit	WB: 1:1000	Cell Signaling Technology, Danvers, MA, USA
RS1	rabbit	IHC: 1:1000 ICC: 1:3000 WB: 1:10000	Professor Dr. Robert Molday, University of British Columbia, Canada
SNCG #H00006623-M01	mouse	WB: 1:5000	Abnova, Taipeh, Tawain
SRC (#2123)	rabbit	WB: 1:1000	Cell Signaling Technologies, Danvers, MA, USA
ß-Actin (#A2228)	mouse	WB: 1:10000	Sigma-Aldrich, St. Louis, MO, USA

IHC: Immunohistochemistry, ICC: Immunocytochemistry, WB: Western Blot, FACS: Fluorescence Activated Cell Sorting, indicated in brackets (#) are manufacturer's product identification numbers where available

2.8 Secondary antibodies

Table 8: Listed are secondary antibodies used in this work, their dilution, and their source

Antibody	Dilution	Source
Goat anti-mouse IgG, Alexa Fluor®549	IHC/ICC: 1:800	Life Technologies, Carlsbad, CA, USA
Goat anti-mouse IgG, Alexa Fluor®488	IHC/ICC: 1:800	Life Technologies, Carlsbad, CA, USA
Goat anti-mouse IgG, peroxidase-conjugate	WB: 1:10000	(Calbiochem) Merck Chemicals GmbH, Schwalbach, Germany
Goat anti-mouse IgG, peroxidase-conjugate	WB: 1:10000	(Calbiochem) Merck Chemicals GmbH, Schwalbach, Germany

Goat anti-rabbit IgG, Alexa Fluor®549	IHC/ICC: 1:800	Life Technologies, Carlsbad, CA, USA
Goat anti-rabbit IgG, Alexa Fluor®488	IHC/ICC: 1:800	Life Technologies, Carlsbad, CA, USA

IHC: Immunohistochemistry, ICC: Immunocytochemistry, WB: Western Blot

2.9 Enzymes

Table 9: Listed are enzymes used in this work, their purpose, and their source

Enzyme	Source
Antarctic phosphatase	New England Biolabs, Ipswich, MA, USA
BamHI-HF	New England Biolabs, Ipswich, MA, USA
KpnI-HF	New England Biolabs, Ipswich, MA, USA
NaeI	New England Biolabs, Ipswich, MA, USA
PNGase F	New England Biolabs, Ipswich, MA, USA
RevertAid™ Reverse Transcriptase	Thermo Fisher Scientific, Waltham, MA, USA
SpeI-HF	New England Biolabs, Ipswich, MA, USA
T4 DNA Ligase	New England Biolabs, Ipswich, MA, USA
T4 Polynucleotide Kinase	New England Biolabs, Ipswich, MA, USA
XhoI	New England Biolabs, Ipswich, MA, USA

2.10 Molecular weight standards

Table 10: Listed are molecular weight standards used in this work, their purpose, and their source

Molecular Weight Standard	Source
Color-coded Prestained Protein Marker, High Range (43-315 kDa)	Cell Signaling Technologies, Danvers, MA, USA
Gene Ruler DNA Ladder Mix	Thermo Fisher Scientific, Waltham, MA, USA
PageRuler™ Prestained Protein Ladder, 10 to 180 kDA	Thermo Fisher Scientific, Waltham, MA, USA

2.11 Kit systems

Table 11: Listed are kit systems used in this work and their source

Kit System	Source
Clarity Max™ Western Blotting Substrate	Bio-Rad Laboratories GmbH, Munich, Germany
Clarity ™ Western Blotting Substrate	Bio-Rad Laboratories GmbH, Munich, Germany
In Situ Cell Death Detection Kit, Fluorescein	Merck Chemicals GmbH, Schwalbach, Germany
NucleoBond® XtraMidi	MACHEREY-NAGEL GmbH & Co. KG, Düren, Germany
NucleoSpin® Gel and PCR Clean-up	MACHEREY-NAGEL GmbH & Co. KG, Düren, Germany
NucleoSpin® Plasmid	MACHEREY-NAGEL GmbH & Co. KG, Düren, Germany
Pierce™ Anti-c-Myc agarose beads	Thermo Fisher Scientific, Waltham, MA, USA
Protein A Sepharose 4B, Fast Flow von *Staphylococcus aureus*	Sigma-Aldrich, St. Louis, MO, USA
PureLink™ RNA Micro Kit	Invitrogen, Thermo Fisher Scientific, Waltham, MA, USA
Q5®Site-Directed Mutagenesis Kit	New England Biolabs, Ipswich, MA, USA
Mirus TransIT® -LTI Transfectionreagent	Mirus Bio LLC, Madison, WI, USA
BigDye Terminator v1.1, v3.1 Cycle Sequencing Kit	Life Technologies, Carlsbad, CA, USA

2.12 Chemicals and reagents

Table 12: Listed are chemicals and reagents used in this work and their source

Chemical/Reagent	Source
3-[(3-Cholamidopropyl)-dimethylammonio]-1-propansulfonat Hydrat (CHAPS), $C_{32}H_{58}N_2O_7S{\cdot}H_2O$	AppliChem GmbH, Darmstadt, Germany
4',6-Diamidin-2-phenylindol (DAPI)-Stain-solution	Life Technologies GmbH, Darmstadt, Germany
Acidic acid, CH_3COOH	Merck Chemicals GmbH, Schwalbach, Germany
Adenosine 5'-Triphosphate (ATP), $C_{10}H_{16}N_5O_{13}P_3$	Sigma-Aldrich, St. Louis, MO, USA
Agarose (Biozym LE)	Biozym Scientific GmbH, Hessisch Oldendorf, Germany
Ammonium heptamolybdate tetrahydrate, $(NH_4)_6Mo_7O_{24}$	Merck Chemicals GmbH, Schwalbach, Germany
Ammoniumperoxodisulfate (APS), $(NH_4)_2S_2O_8$	AppliChem GmbH, Darmstadt, Germany
Ampicillin Sodium salt, $C_{16}H_{18}N_3NaO_4S$	Carl Roth GmbH + Co. KG, Karlsruhe, Germany
Antarctic phosphatase buffer	New England Biolabs, Ipswich, MA, USA
Bacto Agar	BD Bioscience, Heidelberg, Germany
Bacto Yeast extract	BD Bioscience, Heidelberg, Germany
Bovine serum albumin (BSA)	New England Biolabs, Ipswich, MA, USA
Bromphenolblue sodium salt, $C_{19}H_9Br_4O_5SNa$	Sigma-Aldrich, St. Louis, MO, USA
Chloroquine, $C_{18}H_{26}ClN_3$	Merck Chemicals GmbH, Schwalbach, Germany
Citalopram-hydrochlorid, $C_{20}H_{21}FN_2O{\cdot}HCl$	Merck Chemicals GmbH, Schwalbach, Germany
Coomassie Brilliant Blue R-250, (sodium salt) $C_{45}H_{44}N_3NaO_7S_2$	VWR International Germany GmbH, Darmstadt, Germany
D (+) Galactose, $C_6H_{12}O_6$	Carl Roth GmbH + Co. KG, Karlsruhe, Germany
D (+) Glucose-Monohydrate, $C_6H_{12}O_6$	Merck Chemicals GmbH, Schwalbach, Germany
D (+) Mannose, $C_6H_{12}O_6$	Merck Chemicals GmbH, Schwalbach, Germany
Digoxin, $C_{41}H_{64}O_{14}$	Sigma-Aldrich, St. Louis, MO, USA
Dimethyl sulfoxide (DMSO), C_2H_6OS	AppliChem GmbH, Darmstadt, Germany
Disodium hydrogen phosphate dihydrate, Na_2HPO_4	Merck Chemicals GmbH, Schwalbach, Germany
Ethanol ≥99,8 p.a, C_2H_6O	Carl Roth GmbH + Co. KG, Karlsruhe, Germany
Ethidiumbromide-solution 0,07%, $C_{21}H_20BrN_3$ in H_2O	AppliChem GmbH, Darmstadt, Germany
Ethyleneglycol-bis N, N, N', N'- tetraacetic acid (EGTA), $C_{14}H_{24}N_2O_{10}$	Sigma-Aldrich, St. Louis, MO, USA
Fluorescent Mounting Medium	Agilent, Santa Clara, CA, USA
Fura-2/AM	Fluka, Buchs, Switzerland
Gluteralaldehyde 25%, $C_5H_8O_2$ in H_2O	Carl Roth GmbH + Co. KG, Karlsruhe, Germany
Glycerine 87%, $C_3H_8O_3$ in H_2O	University of Regensburg, Chemical Supplies
Glycin, $C_2H_5NO_2$	AppliChem GmbH, Darmstadt, Germany
Goat serum	Abcam, Cambridge, United Kingdom
HiDi™ Formamide, CH_3NO	Thermo Fisher Scientific, Waltham, MA, USA
Hydrochloric acid fuming 37%, HCl	Merck Chemicals GmbH, Schwalbach, Germany
Isopropanol, C_3H_8O	Merck Chemicals GmbH, Schwalbach, Germany
Liquid Barrier solution	Carl Roth GmbH + Co. KG, Karlsruhe, Germany

Magnesium chloride hexahydrate, $Cl_2H_{12}MgO_6$	Merck Chemicals GmbH, Schwalbach, Germany
Malachite green oxalate salt, $C_{23}H_{25}N_2$ C_2HO_4 $0.5C_2H_2O_4$	Sigma-Aldrich, St. Louis, MO, USA
Methanol, CH_4O	Merck Chemicals GmbH, Schwalbach, Germany
NEG 50™ Frozen Section Medium	Thermo Fisher Scientific, Waltham, MA, USA
Ouabain octahydrate, $C_{29}H_{44}O_{12} \cdot 8H_2O$	Sigma-Aldrich, St. Louis, MO, USA
Paraformyaldehyde (PFA), $(CH2O)_n$	AppliChem GmbH, Darmstadt, Germany
Pluronic 1-2-7	Thermo Fisher Scientific, Waltham, MA, USA
Potassium chloride, KCl	Merck Chemicals GmbH, Schwalbach, Germany
Rotiphorese Gel 40% Acrylamide/ Bisacrylamide	Carl Roth GmbH + Co. KG, Karlsruhe, Germany
Rotiszint eco plus	Carl Roth GmbH + Co. KG, Karlsruhe, Germany
Rotiszint eco plus	Carl Roth GmbH + Co. KG, Karlsruhe, Germany
Skimmed milk powder	Carl Roth GmbH + Co. KG, Karlsruhe, Germany
Sodiumchlorid, NaCl	VWR International Germany GmbH, Darmstadt, Germany
Sodiumdodecylsulfate (SDS) ≥99%, $C_{12}H_{25}NaO_4S$	Carl Roth GmbH + Co. KG, Karlsruhe, Germany
ß-Mercaptoethanol, $HSCH_2CH_2OH$	Sigma-Aldrich, St. Louis, MO, USA
T4 DNA Ligase buffer	New England Biolabs, Ipswich, MA, USA
Tetramethylethylendiamin (TEMED), $(CH_3)_2NCH_2CH_2N(CH_3)_2$	Merck Chemicals GmbH, Schwalbach, Germany
Tris(hydroxymethyl)-aminomethan (Tris), $NH_2C(CH_2OH)_3$	Affymetrix, Santa Clara, CA, USA
Tris-HCl	VWR International Germany GmbH, Darmstadt, Germany
Triton® X-100	AppliChem GmbH, Darmstadt, Germany
Trypsin Gold, mass spectrometry grade	Promega Corporation, Madison, WI, USA
Tryptone	Carl Roth GmbH + Co. KG, Karlsruhe, Germany

2.13 Buffer and solutions

Table 13: Listed are buffers and solutions used in this work, as well as their composition

Buffer/Solution	Ingredients	Amount
2x HBS	NaCl KCl Na_2HPO_4 HEPES $H_2O_{dest.}$	280 mM 10 mM 1,5 mM 50 mM
5x Laemmli-buffer	Bromphenolblue Tris-HCl pH 6,8 β-Mercaptoethanol SDS Glycerol $H_2O_{dest.}$	0,01% v/v 60 mM 5% w/v 2% w/v 10% v/v
Agarose gel solution	Agarose TBE pH 8.0	0.8 – 1.5% (w/v)
Ammoniummolybdate solution	Ammoniummolybdate Hydrochloric acid	4.2% 4 M
Antibody solution for FACS analysis	FCS PBS	1% v/v

Antibody solution for immunohistochemical/ immunocytochemical staining	Goat serum TritonX-100 PBS	2,5% v/v 0,1% v/v
Antibody solution for western blotting analysis	1x TBS-T Milk powder	 5% w/v
ATPase test buffer	Tris-HCl, pH 7,4 NaCl KCl MgCl2 $H_2O_{dest.}$	100 mM 130 mM 20 mM 3 mM
Blocking solution for immunofluorescence staining	Goat serum TritonX-100 PB	10% v/v 0,3% v/v
Bromphenolblue loading buffer	Bromphenolblue Glycerol 87% $H_2O_{dest.}$	0.01% (w/v) 40% (v/v)
Chloroquine-phosphate solution	Chloroquine-phosphate $H_2O_{dest.}$	0,025 M
Coomassie-de-staining solution	Methanol Acidic acid 100% Coomassie Brilliant Blue $H_2O_{dest.}$	30% v/v 10% v/v 0,1% w/v
Coomassie staining solution	Methanol Acidic acid 100% $H_2O_{dest.}$	30% v/v 10% v/v
Extracellular patch-clamp solution (pH 7.3)	NaCl KCl $CaCl_2$ $MgCl_2$ HEPES $H_2O_{dest.}$ KOH for pH 7.3	130 mM 5 mM 10 mM 2 mM 10 mM
Intracellular patch-clamp solution (pH 7.3)	KCl Na_2ATP $MgCl_2$, HEPES EGTA $H_2O_{dest.}$ KOH for pH 7.3	130 mM 4 mM 4 mM 10 mM 1 mM
LB-medium	Pepton yeast extract NaCl $H_2O_{dest.}$	1% w/v 0.5% w/v 1% w/v
Lysogeny Broth (LB) Agar	Tryptone Bacto-yeast extract NaCl Bacto-Agar $H_2O_{dest.}$	1% w/v 0,5% w/v 1% w/v 15% w/v
Malachit green solution	Malachite green oxalate salt H_2O dest.	0.05% (w/v)
PB, pH 7.2	Na_2HPO_4 NaH_2PO_4 $H_2O_{dest.}$	78 mM 26 mM

PBS, pH 7.4	NaCl KCl Na_2HPO_4 KH_2PO_4 $H_2O_{dest.}$	137 mM 0,27 mM 10 mM 1,8 mM
Phosphate reagent	Ammoniummolybdate solution Malachit green solution	25% v/v 75% v/v
Ringer solution, pH 7.4	NaCl KCl $MgCl_2$ Na_2HPO_4 NaH_2PO_4 $CaCl_2$ Glucose HEPES NaOH for pH 7.4	118 mM 5 mM 1.2 mM 2 mM 1.8 mM 5 mM 9.1 mM
SDS-buffer, pH 8.6	Tris-HCl Glycine SDS $H_2O_{dest.}$	0,25 mM 0,2 M 1% w/v
SOC medium	Tryptone Yeast extract NaCl KCl MgCl2 Glucose	2% (w/v) 0.5% (w/v) 10 mM 2.5 mM 10 mM 20 mM
TBE, pH 8.0	Tris Borsäure EDTA $H_2O_{dest.}$	100 mM 100 mM 1 mM
TBS, pH 7.5	Tris NaCl $H_2O_{dest.}$	50 mM 150 mM
TBS-T	Tween® 20 TBS	0,1% v/v
Towbin	Glycine Tris Methanol $H_2O_{dest.}$	190 mM 0,25 mM 20% v/v
TritonX-100-Lösung	TritonX-100 $H_2O_{dest.}$	1,5% v/v

2.14 Cell culture media and supplements

Table 14: Listed are cell culture media and supplements used in this work and their source

Medium/Supplement	Source
Concanavalin A Typ IV	Sigma-Aldrich, St. Louis, MO, USA
DMEM F-12 medium	Thermo Fisher Scientific, Waltham, MA, USA
Dulbecco's modified eagle medium (DMEM) high-glucose medium (4.5 g/L)	Thermo Fisher Scientific, Waltham, MA, USA
Dulbecco's PBS	Thermo Fisher Scientific, Waltham, MA, USA

Fetal Bovine Serum Gold (FBS)	Thermo Fisher Scientific, Waltham, MA, USA
FluoroBrite™ DMEM medium	Thermo Fisher Scientific, Waltham, MA, USA
Geneticin™ Selective Antibiotic (G418 Sulfate), $C_{20}H_4ON_4O_{10}*2H_2SO_4$	Thermo Fisher Scientific, Waltham, MA, USA
Gentamicin (5 mg/ml)/Amphotericin (125 µg/ml)	Thermo Fisher Scientific, Waltham, MA, USA
Hygromycin B (50 mg/ml)	Thermo Fisher Scientific, Waltham, MA, USA
Insulin (27 USP-units/mg)	Thermo Fisher Scientific, Waltham, MA, USA
L-Glutamin (200 mM)	Thermo Fisher Scientific, Waltham, MA, USA
OptiMEM™ medium	Thermo Fisher Scientific, Waltham, MA, USA
Penicillin (10.000 Units)/streptomycin (10 mg/ml), (Pen/Strep)	Thermo Fisher Scientific, Waltham, MA, USA
Poly-L-lysine Hydrobromide (0.1 mg/ml)	Sigma-Aldrich, St. Louis, MO, USA
Roswell Park Memorial Institute (RPMI) 1640 Medium	Thermo Fisher Scientific, Waltham, MA, USA

2.15 Consumables specifically required for experiments

Table 15: Listed are consumables specifically required for experiments conducted in this study and their sources

Material	Source
3 cm and 10 cm cell culture dishes	Sarstedt AG & Co., Nümbrecht, Germany
35 mm cell culture dish with ibidi polymer coverslip bottom	Ibidi GmbH, Gräfelfing, Germany
35 mm FluoroDish cell culture dish, 23 mm well poly-L-lysine coated	World Precision Instruments, Friedberg (Hessen), Germany
384-Well Reaction Plate with Barcode, MicroAmp™ Optical	Applied Biosystems, Inc., Waltham, MA, USA
4%–12% NUPAGE Bis-Tris gels	Invitrogen, Thermo Fisher Scientific, Waltham, MA, USA
5 mm and 18 mm glass coverslips	VWR International Germany GmbH, Darmstadt, Germany
58 x 27 mm Scintillation cups	Sarstedt AG & Co., Nümbrecht, Germany
6-, 12-, and 24- well cell culture plates	Greiner Bio-One GmbH, Frickenhausen, Germany
96-well flat bottom assay plate	Greiner Bio-One GmbH, Frickenhausen, Germany
Cell culture flasks 25 ml	Sarstedt AG & Co., Nümbrecht, Germany
Dako fluorescent mounting medium	Merck Chemicals GmbH, Schwalbach, Germany
Nuclepore Track Etch Filter	VWR International Germany GmbH, Darmstadt, Germany
Staining chamber StainTray™ Black lid	Carl Roth GmbH + Co. KG, Karlsruhe, Germany

2.16 Devices

Table 16: Listed are devices used in this work and their source

Devices	Source
Accu-jet Pipet Controller	Brand, Wertheim, Germany
Autoclave „Autoklav V-150“	Systec GmbH, Wettenberg, Germany
Axioskop2 mot plus microscope	Carl Zeiss Meditec, Oberkochen, Germany
BD FACSCanto™-II flow cytometer	BD Biosciences, San Jose, CA, USA
Bench Heraguard	Heraeus Holding GmbH, Hanau, Germany
Bunsen burner Gasprofi1	WLD Tec, Göttingen, Germany
CASY TT Cell Counter	Innovatis Roche AG, Bielefeld, Germany

Centrifuge 5415 R (refrigerated centrifuge, Eppendorf Cups)	Eppendorf AG, Hamburg, Germany
Centrifuge Biofuge fresco (Tablecentrifuge)	Heraeus Holding GmbH, Hanau, Germany
Centrifuge Megafuge 1.0R (refrigerated centrifuge Falcontube)	Heraeus Holding GmbH, Hanau, Germany
Centrifuge Sigma 2-5	Sigma-Aldrich, St. Louis, MO, USA
Cold microtom Leica CM1850	Leica Microsystems, Wetzlar, Germany
DMZ Zeitz-Puller	Zeitz-Instruments Vertriebs GmbH, Martiensried, Germany
Duomax 1030 Rocking Platform Shaker	Heidolph Instruments GmbH & Co.KG, Schwabach, Germany
FACSCanto-II flow cytometer	BD Biosciences, San Jose, CA, USA
Fine scales „Feinwaage Explorer“	OHAUS, Nänikon, Switzerland
Gelelectrophoresis chamber Blue Marine200	SERVA Electrophoresis GmbH, Heidelberg, Germany
Gelelectrophoresis chamber Mini PROTEAN®	Bio-Rad Laboratories GmbH, Munich, Germany
Icemachine AF 100	Scotsman, Vernon Hills, IL, USA
Incubator for bacteria 37°C	Memmert GmbH, Schwabach, Germany
Incubator Hera Cell 150	Thermo Fisher Scientific, Waltham, MA, USA
Leica TCS SP5 II confocal laser scanning microscope	Leica Microsystems, Wetzlar, Germany
LI-COR Odyssey Imaging System	LI-COR Biosciences, Lincoln, NE, USA
Microwave KOR-6D07	Daewoo, Seoul, Korea
Milli-Q-Synthesis Water Purification System	Merck Chemicals GmbH, Schwalbach, Germany
NanoDrop® ND1000 Spectrophotometer	NanoDrop, Wilmington, DE, USA
Odyssey FC Imager	LI-COR Biosciences, Lincoln, NE, USA
Olympus FV3000 confocal laser scanning microscope	Olympus Europa SE & Co. KG, Hamburg, Germany
Olympus IX73 microscope	Olympus Europa SE & Co. KG, Hamburg, Germany
pH Meter Lab 850	SI Analytics GmbH, Mainz, Germany
Power Pack Blue Power 500	SERVA Electrophoresis GmbH, Heidelberg, Germany
Power Pack Blue Power Plus	SERVA Electrophoresis GmbH, Heidelberg, Germany
Scintillation counter Tricarb 2910	PerkinElmer®, Rodgau, Germany
Trans-Blot® Turbo™ Transfer System	Bio-Rad Laboratories GmbH, München, Germany
UltiMate 3000 RSLCnano System	Thermo Fisher Scientific, Waltham, MA, USA
Zeiss Observer Z.1	Carl Zeiss Meditec, Oberkochen, Germany

2.17 Software

Table 17: Listed are software applications used in this work and their source

Software	Source
ApE - A Plasmid Editor	M.Wayne Davis, Department of Biology, University of Utah
CellSense Imaging Software	Olympus Europa SE & Co. KG, Hamburg, Germany
Compass 1.7 acquisition and processing software	Bruker Daltonics GmbH & Co. KG, Bremen, Germany
Corel PHOTO-PAINT	Corel Corporation, Ottawa, Ontario, Kanada
CorelDRAW Graphicsuite X8	Corel Corporation, Ottawa, Ontario, Kanada
Data Analysis 4.2	Bruker Daltonics GmbH & Co. KG, Bremen, Germany

Diva software	BD Biosciences, San Jose, CA, USA
FV3000 software	Olympus Europa SE & Co. KG, Hamburg, Germany
Image Studio	LI-COR Biosciences GmbH, Lincoln, NE, USA
ImageJ	Wayne Rasband, National Institutes of Health, USA
Ligation Calculator	University of Düsseldorf, Germany
Microsoft Office	Microsoft Cooperation, Redmond, WA, USA
NEBaseChanger®	New England Biolabs, Ipswich, MA, USA
Origin 2015G	OriginLab Corporation, Northampton, MA, USA
Patchmaster Software	HEKA, Lambrecht, Germany
Protein Scape 3.1.3	Bruker Daltonics GmbH & Co. KG, Bremen, Germany
SigmaPlot 12.5	Systat Software, San Jose, CA, USA
SnapGene	GSL Biotech LLC, Chicago, IL, USA

3 Methods

3.1 Cell culture

3.1.1 Cultivation of Hek293 cells

Hek293 cells were cultivated in 10 cm cell culture dishes in DMEM high-glucose medium (4.5 g/L) containing 10% fetal calf serum (FCS), 1% penicillin/streptomycin (10000 units/ml penicillin and 10000 µg/ml streptomycin), and 1% Geneticin™ Selective Antibiotic (G418 Sulfate). The cells were grown in a 37 °C incubator with a 5% CO_2 environment and were passaged with fresh medium at a ratio of 1:10 when they reached 90% confluency. Every two days, cells were checked microscopically.

For the cultivation of Hek293 cells stably expressing recombinant retinoschisin, hygromycin B (1500 µg/ml) was additionally applied to the medium. To obtain retinoschisin containing supernatant from this cell line, cells were kept in OptiMEM™ medium containing 1% penicillin/streptomycin and 1500 µg/ml hygromycin B for 72 h, and the supernatant was subsequently harvested.

3.1.2 Cultivation of Y-79 cells

Y-79 cells were cultivated in 25 cm^2 cell culture flasks in RPMI medium containing 10% FCS and 1% penicillin/streptomycin (10000 units/ml penicillin and 10000 µg/ml streptomycin). The cells were grown in a 37 °C incubator with a 5% CO_2 environment and were subcultured twice weekly in a ratio of 1:5. Every two days, cells were checked microscopically.

3.1.3 Transfection *via* TransIT®LTI transfection reagent

Transfection of Hek293 cells with Mirus TransIT®LTI transfection reagent (Mirus Bio LLC) was performed according to the manufacturer's instructions. After incubating the transfected Hek293 cells at 37 °C for 48 h, they were subjected to further experiments.

3.1.4 Transfection *via* calcium-phosphate method

The calcium-phosphate transfection method was applied only for heterologous expression of Myc-tagged retinoschisin or of retinoschisin mutant C59S (RS1_C59S). Hek293 cells were passaged in a 1:3 ratio to 10 cm cell culture dishes previously coated with poly-L-lysine. On the following day, cells were pretreated by replacing the cultivation medium with DMEM high-glucose medium (4.5 g/L) containing 10% FCS, 1% penicillin/streptomycin, and 1 µM chloroquine for 1 h at 37 °C. Meanwhile, the transfection mixture was prepared, consisting of 20 µg DNA (pCDNA3_RS1_Myc or pCDNA3_RS1_C59S_Myc, or pCDNA3 as control), 62 µl $CaCl_2$, filled up with 438 µl of sterile water. After brief vortexing, 500 µl of 2xHBS was added to the bottom of the reaction tube, the suspension was mixed by bubbling several times, and incubated for 15 min. The chloroquine-containing medium was substituted with normal DMEM high-glucose (4.5 g/L) cultivation medium containing 10% FCS, 1% penicillin/streptomycin, and

1% G418 Sulfate. The transfection mixture was added dropwise to the pretreated cells and after incubation for at least 7 h, the medium was changed to OptiMEM™ medium. The transfected cells were kept in the incubator for 72 h. Subsequently, the supernatant containing Myc-tagged retinoschisin variants or control supernatant (from pCDNA3 transfected cells) was collected and stored at - 20 °C until further use.

3.2 Purification of Myc-tagged retinoschisin variants

Purification of Myc-tagged proteins from the supernatant of Hek293 cells was performed by immunoaffinity chromatography using Pierce™ Anti-c-Myc agarose beads (Thermo Fisher Scientific). Before purification, 250 µl beads were spun down at 12.000 rpm for 30 s (Centrifuge Biofuge Fresco), resuspended in 100 µl TBS, and this washing step was repeated. After discarding the supernatant, the beads were incubated with 10 ml supernatant containing Myc-tagged retinoschisin, Myc-tagged retinoschisin mutant C59S, or control supernatant overnight at 4 °C in a rotator. The following day, purification of Myc-tagged proteins was performed according to the manufacturer's instructions. The concentration of the purified proteins was determined using the Bradford assay (Bio-Rad) according to manufacturer's instructions. Here, the protein concentration ranged from 20 to 50 ng/µl. Elution fractions were controlled by Coomassie staining (see 3.13 and **Figure 6A**) and western blot analysis (**Figure 6B**).

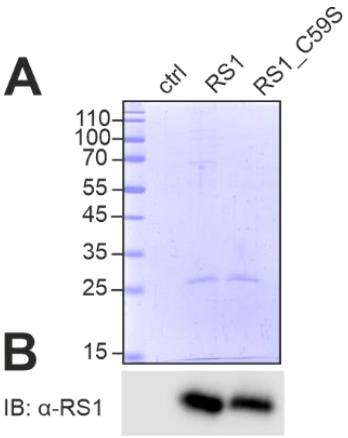

Figure 6: Analysis of purified Myc-tagged retinoschisin protein and retinoschisin variant C59S

Purification of Myc-tagged retinoschisin (RS1) protein and retinoschisin variant C59S (RS1_C59S) from the supernatant of transfected Hek293 cells was achieved by immunoaffinity chromatography. Supernatant from cells transfected with empty vector (ctrl) was used as a control. For purity analysis, Coomassie staining (**A**) and western blot analysis with antibodies against retinoschisin (**B**) was performed.

3.3 Animal models

Rs1^{tm1Web} mice were crossed onto a C57BL/6 background for more than 40 generations. Mice were housed under specific pathogen-free barrier conditions at the Central Animal Facility of the University of Regensburg, in strict compliance with European Union and German legal guidelines. Mice were sacrificed by cervical dislocation at different postnatal stages, in specific at P4, P7, P10, P14, P16, P18, P21, or P30 after inhalation of carbon dioxide or by decapitation when younger than P14.

The Atp1b2$^{-/-}$ mouse strain was kindly provided by Prof. Melitta Schachner (Keck Center for Collaborative Neuroscience and Department of Cell Biology and Neuroscience, Rutgers University, Piscataway, NJ, USA).

Porcine eyes for co-immunoprecipitations (see 3.14) were obtained fresh from a local slaughterhouse and handled on ice.

3.4 Cloning of expression constructs

In this work, the following expression constructs were generated: A bicistronic expression vector for a GFP-tagged retinal Na/K-ATPase (ATP1B2 and GFP-tagged ATP1A3 in pCDNA3 termed “pCDNA3_ATP1A3-GFP _ATP1B2”), and expression vectors for ATP1B2 mutants ATP1B2_T240S and ATP1B2_T240A, termed “pCEP_ATP1B2_T240S” and “pCEP_ATP1B2_T240A” (**Table 6**).

3.4.1 Generation of pCDNA_ATP1A3-GFP_ATP1B2

The cloning of plasmid pCDNA3_ATP1A3-GFP_ATP1B2 was performed as follows: The N-terminal part of the ATP1A3-GFP coding sequence was excised from pCEP_ATP1A3-OI-GFP (generated before as described in Plössl et al. (2017b) *via* the restriction enzymes KpnI-HF and NaeI. The C-terminal part of the ATP1A3 coding sequence was excised from pCEP_ATP1A3 (generated before as described in Friedrich et al. (2011) *via* NaeI and BamHI-HF. The two ATP1A3-fragments were phosphorylated and ligated with the KpnI-HF and BamHI-HF digested, dephosphorylated target vector pCEP4, resulting in vector pCEP_ATP1A3-GFP. The newly generated ATP1A3-GFP expression cassette was excised from pCEP_ATP1A3-GFP *via* SpeI-HF, dephosphorylated, and ligated into the SpeI-HF digested target vector pCDNA3_ATP1B2 (generated before as described in Friedrich et al. (2011). This resulted in a bicistronic expression vector termed “pCDNA3_ATP1A3-GFP_ATP1B2”.

3.4.2 Generation of pCEP_ATP1B2_T240S and pCEP_ATP1B2_T240A

Mutant clones ATP1B2_T240S and ATP1B2_T240A were generated with the Q5® Site-Directed Mutagenesis Kit according to the manufacturer's instructions (New England Biolabs). The vector pTLN1_ATP1B2, generated earlier as described in Plössl et al. (2017b), was used as a template and mutagenesis primers hATP1B2_T240A_F/R and hATP1B2_T240S_F/R (**Table 4**) were designed using the NEBaseChanger v1.2.6 tool. The newly generated ATP1B2_T240S and ATP1B2_T240A expression cassettes were excised from pTLN_ATP1B2_T240S and pTLN_ATP1B2_T240A *via* KpnI-HF and XhoI and ligated into the KpnI-HF and XhoI digested target vector pCEP. This resulted in the vectors termed “pCEP_ATP1B2_T240S” and “pCEP_ATP1B2_T240A”.

3.4.3 Restriction digestion

To generate expression constructs (for more detailed information see 3.4.1 and 3.4.2), the inserts of interest were cut out from existing constructs with selected restriction enzymes for the 5'-end (A) and 3'-end (B), which were selected *via* ApE - A Plasmid Editor. For inserts to be excised from pCEP or pTLN, 2 – 3 µg of DNA and for the target vectors pCEP or pCDNA3, 0.5 µg of DNA was digested with the same restriction enzymes. The reaction mixture was prepared as described in **Table 18** and incubated overnight at 37 °C.

Table 18: Reaction mixture of restriction digestion

Component	Amount
Expression construct	2 -3 µg insert containing vector or 0.5 µg target vector
Restriction enzyme (A)	1 µl
Restriction enzyme (B)	1 µl
CutSmart® buffer	1 µl
$H_2O_{dest.}$	Ad 10 µl

3.4.4 Purification of PCR products from agarose gels

Agarose gel electrophoresis was used for separating DNA fragments after restriction digestion. Depending on the sizes of DNA fragments to be separated, the agarose concentration in the gel ranged from 0.8% (800 bp – 12 kb) to 1.5% (200 bp – 3kb). Agarose gels were generated by heating 0.8 – 1.5% agarose in TBE buffer until the agarose was solved completely. To later visualize DNA under UV light, two drops of a 0.07% ethidiumbromide-solution were added to the cooled solution. Bromphenolblue loading buffer (5x solution) was added to the samples before loading them onto the gel together with 5 µl GeneRuler™ DNA Ladder Mix, which served as a size standard. Electrophoretic separation was performed at 190 V for 30 min. Subsequently, the bands were visualized by a UV transilluminator. By using a scalpel, the bands with the required fragment lengths were cut out. The DNA fragments were extracted using NucleoSpin® Gel and PCR Clean-up Kit according to the manufacturer's instructions (MACHEREY-NAGEL GmbH). Insert DNA was eluted from the columns in 25 µl $H_2O_{dest.}$ and target vector DNA in 50 µl H_2O_{dest}. Extracted DNA was stored at -20 °C until further use.

3.4.5 Ligation into target vector

Insert and corresponding target vector were ligated overnight at 4 °C applying the reaction mixture described in **Table 19**. The amounts of insert and target vector were calculated in a vector to insert ratio of 1 to 3 by using the Ligation Calculator from the University of Düsseldorf.

Table 19: Reaction mixture for ligation

Component	Amount
Target vector	10 - 20 ng
Insert	Calculated by Ligation Calculator
T4 DNA Ligase	1 µl
10x T4 DNA Ligase buffer	1 µl
$H_2O_{dest.}$	Ad 10 µl

For ligation of the N-terminal part of ATP1A3-GFP and the C-terminal part of ATP1A3 into pCEP, and of ATP1A3-GFP into pCDNA3_ATP1B2, the inserts were phosphorylated, and the target vector was dephosphorylated. The reaction mixture for the 5'- insert phosphorylation *via* T4 Polynucleotide kinase, prepared as depicted in **Table 20**, was incubated for 1 h at 37 °C and followed by incubation at 65 °C for 20 min. To avoid vector re-ligation, vector 5'-end and 3'-end dephosphorylation was performed by adding antarctic phosphatase. The following reaction mixture was prepared (**Table 21**) and incubated for 1 h at 37 °C and afterward for 20 min at 75 °C.

Table 20: Reaction mixture for insert phosphorylation *via* T4 Polynucleotide Kinase

Component	Amount
Insert	5 µl
T4 Polynucleotide Kinase	1 µl
10x T4 Polynucleotide Kinase buffer	1 µl
ATP (100 µM)	1 µl
$H_2O_{dest.}$	Ad 10 µl

Table 21: Reaction mixture for vector dephosphorylation *via* antarctic phosphatase

Component	Amount
Target vector	500 ng
Antarctic phosphatase	1 µl
Antarctic phosphatase buffer	2 µl
$H_2O_{dest.}$	Ad 20 µl

3.4.6 Heat shock transformation

100 µl of DH5α cells were thawed on ice, 5 µl of the ligation product was added, incubated on ice for 30 min and heat shocked for 45 s at 42 °C. Subsequently, cells were incubated for 10 min and 400 µl of SOC medium was added. The DNA-bacteria mixture was placed on a shaker for at least 45 min at 37 °C and 300-500 rpm. In the final step, 200 µl of the transformation product was plated on a pre-warmed LB-ampicillin (100 µg/ml) agar plate. The plate was incubated overnight at 37 °C.

3.4.7 Colony PCR

Single bacteria clones were picked from the agar plate with a pipette tip, resuspended in 20 µl LB-medium containing ampicillin (100 µg/ml), and incubated for 2 h at 37 °C. After incubation, the reaction mixture for colony PCR was prepared (**Table 22**). Colony PCR was performed in the thermocycler with the program given in **Table 23.**

Table 22: Reaction mixture for colony PCR

Component	Amount
5x GoTaq® Reaction Buffer	5 µl
dNTPs (2 mM)	0.5 µl
T7 forward Primer (10 µM)	1 µl
BGH reverse Primer (10 µM)	1 µl
Template (*E. Coli* suspension)	3 µl
GoTaq® DNA-Polymerase	0.4 µl
$H_2O_{dest.}$	14.1 µl

Table 23: Thermocycler program for colony PCR

Step of reaction	Temperature	Time	Cycle
Initial denaturation	94 °C	3 min	
Denaturation	94 °C	30 s	29 cycles
Annealing	58 °C	30 s	
Elongation	72 °C	1 min	
Final elongation	72 °C	5 min	
Break	15 °C	∞ min	

To identify positive clones, the probes were analyzed *via* agarose gel electrophoresis (see 3.4.4). Constructs containing the expected insert were visualized by exhibiting a PCR product of the expected length. The respective clones were inoculated for subsequent plasmid DNA preparation in a ng range (“Mini” Preparation).

3.4.8 Plasmid DNA “Mini” preparation

10 -20 µl of the *E. Coli* suspension was inoculated in 5 ml LB-medium containing ampicillin (100 µg/ml), and incubated overnight at 37 °C. The DNA preparation was carried out on the following day by using NucleoSpin® Plasmid Kit according to the manufacturer's instructions. To elute DNA, 25 µl $H_2O_{dest.}$ was used. The DNA concentration and quality were measured *via* NanoDrop® spectrophotometer.

3.4.9 Sanger sequencing

The generated expression constructs were sequenced using the BigDye Terminator v1.1, v3.1 Cycle Sequencing Kit (Life Technologies). The reaction mixture for cycle sequencing was prepared as shown in **Table 24**. Inserts and adjacent vector sequences were fully sequenced

using primers given in **Table 4**. Amplification was performed by using a thermocycler with the program given in **Table 25.**

Table 24: Reaction mixture for cycle sequencing

Component	Amount
Expression construct (20 ng/µl)	2 µl
BigDye® Terminator reaction mix	0,3 µl
5x BigDye® Terminator sequencing buffer	2 µ
Primer (10 µM)	1 µl
$H_2O_{dest.}$	Ad 10 µl

Table 25: Thermocycler program for sanger sequencing

Step of reaction	Temperature	Time	Cycle
Initial denaturation	94 °C	3 min	
Denaturation	94 °C	30 s	27 cycles
Annealing	58 °C	30 s	
Elongation	60 °C	3 min	
Final elongation	60 °C	5 min	
Break	15 °C	∞ min	

Precipitation of amplified DNA was performed as follows: After the addition of 2 µl sodium acetate (3 M) and 25 µl ethanol (100%), the mixture was centrifugated for 30 min at 4 °C and 4000 rpm (Centrifuge Megafuge 1.0R). The supernatant was removed by briefly centrifuging the reaction tubes overhead on an absorbent paper towel (< 400 rpm). The pellet was washed by adding 100 µl of ethanol (70%), followed by centrifugation (20 min, 4000 rpm, 4 °C). The supernatant was discarded as described above. Finally, the DNA was solved in 15 µl of HiDi™ formamide, transferred to a sequencing plate, and analyzed *via* Abi3130x1 Genetic Analyzer. The evaluation of the obtained sequences was performed using the ApE - Ape Plasmid Editor software.

3.5 Plasmid DNA “Midi” preparation

Plasmid DNA preparation in a µg range (“Midi” preparation) was used to isolate expression constructs on a larger scale for transfection of Hek293 cells. For this purpose, 100 ml LB-medium containing ampicillin (100 µg/ml) was inoculated with corresponding *E. coli* clones and shaken overnight at 37 °C. *Via* the NucleoBond® XtraMidi Kit, plasmid DNA was isolated according to the manufacturer's instructions, except for plasmid DNA elution 100 µl $H_2O_{dest.}$ was used. The DNA concentration and quality were determined using NanoDrop® Spectrophotometer and the plasmids were stored at -20 °C until use.

3.5.1 Glycerol stock preparation for long-term storage

For long-term storage of bacterial cultures, glycerol stocks were prepared. 825 µl of fresh overnight culture and 175 µl of sterile 87% glycerol were mixed, transferred in CryoPure tubes,

and stored at -80 °C. Datasheets of plasmid constructs and their storage location were entered into the database of the Institute of Human Genetics at the University of Regensburg.

3.6 Retina preparation

Mice were sacrificed as described in 3.3, eyes were dissected using curved forceps and transferred into PBS. For retina preparation, performed as described by Léger et al. (2019), the eyes were dissected through circumcision along the ora serrata. Cornea, lens, and vitreous body were separated from choroid and sclera. Subsequently, the retina was carefully detached from the retinal pigment epithelium and either frozen at -80 °C for further analysis or transferred into prewarmed OptiMEM™ medium for subsequent cultivation.
Retina preparation of porcine eyes was performed likewise.

3.7 Cultivation of retinal explants

To test the effect of retinoschisin and cardiac glycosides on retinal integrity, 3 ml of medium for culturing retinal explants (**Table 26**) was mixed with purified retinoschisin (333 ng/ml) or the same volume of control eluate, as well as with 0 M or 10^{-4} M ouabain, or 0 M or 10^{-6} M digoxin, respectively. After retina preparation, retinae of retinoschisin-deficient mice (P18) were set on Nucleopore Track-Etch Membrane Filters in 3 cm cell culture dishes and covered with a drop of the cultivation medium. The retinal explants were cultivated for four days at 37 °C applying a medium change to 3 ml of fresh medium after two days. After four days, they were processed for immunohistochemical analyses.

Table 26: Composition of retinal explants cultivation medium

Component	Amount
DMEM Hams F12	18 ml
FCS	2 ml
Gentamicin (5 mg/ml) / Amphotericin (125 µg/ml)	40 µl
Penicillin-streptomycin-L-Glutamin (200 mM)	200 µl
Insulin (27 USP-units/mg)	10 µl

3.8 Preparation of retinal cryosections from murine retinae or eyes

Murine retinae from retinal cultivation experiments or whole eye preparations were transferred into a 3 cm cell culture dish and washed with PBS. For fixation, PBS was replaced with 4% PFA followed by a 10 min incubation step for retinal explants or a 1 h incubation step for whole eyes. Afterwards, the tissues were washed twice with PBS, transferred into 30% sucrose, and incubated overnight on a shaker. For embedding, pouring molds on dry ice were filled with NEG-50™ frozen section medium and the retinal tissue was carefully placed in the center. Using a cryostat, 10 µm cryosections of frozen tissue samples were prepared, transferred onto microscope slides, and stored at -80 °C until further use or subjected to immunolabeling or TUNEL staining.

3.9 Immunocytochemical analysis

To perform immunocytochemical analysis, Hek293 and Y-79 cells were seeded on glass coverslips (5 mm). After retinoschisin binding assays (see 3.16) were performed, the glass coverslips were transferred into a 24-well cell culture plate for immunocytochemical analysis. First, cells were washed twice with PBS and incubated with 300 µl of 2% PFA for 10 min. After three washing steps with PBS for 5 min, the blocking solution for immunofluorescence staining (**Table 13**) was added for 30 min. Next, the cells were incubated with primary antibodies (given in **Table 7**) in antibody solution for immunocytochemical staining overnight at 4 °C. The following day, three washing steps with PBS were performed and the staining solution with secondary antibodies and DAPI (given in **Table 8**) was applied for 1 h in the dark. Later, the coverslips were placed upside down on a drop of Dako fluorescent mounting medium on a slide. Fluorescence microscopy was performed with an Axioskop2 mot plus microscope at 40x magnification.

3.10 Quantitative real-time PCR

RNA was isolated from murine retinae using the PureLink™ RNA Micro Kit (Invitrogen), according to the manufacturer's instructions. One microgram of total RNA was transcribed into cDNA using Random Hexamer Primers and the RevertAid M-MuLV Reverse Transcriptase according to the manufacturer's instructions. Quantitative real-time PCR (qRT-PCR) was performed in three technical replicates using KiCqStart® probe assays from Sigma Aldrich (primers and probes or catalog numbers given in **Table 5**) and the QuantStudio5 System. The reaction mixture and the PCR conditions are given in **Table 27** and **Table 28**, respectively. The results were analyzed by applying the ΔΔCt method for relative quantification (Livak and Schmittgen 2001).

Table 27: Reaction mixture for qRT-PCR

Component	Amount
cDNA (20 ng/µl)	2.5 µl
2x TaqMan Gene expression master mix	5 µl
Forward Primer (10 µM)	1 µ
Reserve Primer (10 µM)	1 µl
KiCqStart®Probe	0.125
$H_2O_{dest.}$	Ad 10 µl

Table 28: QuantStudio5 PCR program for qRT-PCR

Stage of reaction	Step of reaction	Temperature	Time	Cycle
Holding Stage	Polymerase Activation	95 °C	10 min	
Cycling Stage	Denaturation	95 °C	15 s	40 cycles
	Annealing	60 °C	1 min	

3.11 Sodiumdodecylsulfate polyacrylamide gel electrophoresis

For the electrophoretic separation of proteins according to their size, SDS-gels composed of a 12.5% separation gel and a 3% collection gel were prepared as described in **Table 29**. Subsequent western blot analyses were performed with 1.5 mm thick gels and Coomassie staining with 0.75 mm thick gels. For mass spectrometric analysis of co-immunoprecipitations, 4%–12% NUPAGE Bis-Tris gels (Invitrogen) were used instead of self-prepared gels.

Table 29: Composition of 12.5% separation and 3% collection gel

Component	12.5% separation gel	3% collection gel
1 M Tris/HCl pH 8.8	3.83 ml	-
1M Tris/HCl pH 6.8	-	2.76 ml
$H_2O_{dest.}$	3.045 ml	1.69 ml
Acrylamide (40%)	3.125 ml	0.55 ml
SDS (20%)	100 µl	50 µl
APS (10%)	100 µl	50 µl
TEMED	10 µl	5 µl

Samples subjected to SDS-PAGE were mixed with 5xLaemmli buffer (Laemmli 1970) and heated to 95 °C for 3 min. Subsequently, samples and size standards (3.5 µl of PageRuler™ Prestained Protein Ladder (10-180 kDa) or 5 µl of color-coded Prestained Protein Marker (43 – 315 kDa)) were loaded onto the gel. The gel run was performed at 50 V until protein samples had passed through the collection gel, afterward the voltage was increased to 150 V.

3.12 Western blot analysis

After SDS-PAGE separation, proteins were blotted onto a PVDF membrane using the semi-dry western blot method. For this purpose, the PVDF membrane was activated in methanol for 30 s and subsequently soaked in Towbin buffer together with the SDS-gel and two 3 mm Whatman papers. These components were assembled into a blotting sandwich and protein transfer was performed by the Trans-Blot®Turbo™Transfer system for 40 min at 24 V. The membrane was then blocked in antibody solution for western blot analysis (**Table 13**) for at least 1 h and incubated overnight at 4 °C with primary antibodies (given in **Table 7**) in antibody solution for western blot analysis. The next day, three 5 min washing steps with TBS-T were performed before incubating the membrane for 1 h with secondary antibodies (given in **Table 8**). The three washing steps with TBS-T were repeated before the membrane was briefly incubated in Clarity™ Western ECL Blotting Substrate (Bio-Rad Laboratories GmbH). Chemiluminescence detection was performed on a LI-COR Odyssey Imaging System. If the signal was too weak, the membrane was incubated again in Clarity Max™ Western Blotting Substrate (Bio-Rad Laboratories GmbH) which provides increased chemiluminescence signal intensity.

3.13 Coomassie staining

The SDS-gels were stained in Coomassie staining solution overnight. The next day, the gels were incubated in Coomassie de-staining solution until the protein-free parts of the gel were free of Coomassie stain. After washing three times with distilled water, the Coomassie gel was scanned in a transparent glass film for subsequent scanning. The staining and washing procedure were carried out under gentle agitation on a shaker.

3.14 Co-Immunoprecipitation analysis of retinal lysates

Co-immunoprecipitation analyses were performed in retinal lysates of porcine retinae or wildtype mice (P18).

50 µl of Protein A Sepharose 4B beads (Sigma-Aldrich) were washed three times with 1 ml of PBS and spun down for 2 min at 2000 rpm at 4°C (Centrifuge Megafuge 1.0R). After discarding the supernatant, the beads were conjugated with the antibodies given in **Table 7**. For antibody coupling, beads were mixed with 100 µl PBS and 2 µg antibodies, rotated at 4 °C for 1 h and centrifugated for 2 min at 2000 rpm at 4 °C. The supernatant was discarded, and the antibody-coupled beads were mixed with the retinal lysates as input.

Retinal lysates were prepared as follows: For each co-immunoprecipitation experiment, 10 mg of porcine retinae was dissolved in 3 ml of 10 mM CHAPS in TBS followed by sonification for 45 s at 40%. Alternatively, four retinae of wildtype mice (P18) were homogenized in 1 ml of 10 mM CHAPS in TBS and sonicated for 10 s at 40%. The suspensions were rotated at 4 °C for 1 h and cell debris was removed *via* centrifugation for 20 min at 13.000 rpm and 4 °C. The supernatant containing the retinal lysate was collected and used as “input”.

Input (3 ml of porcine lysate or 800 µl of murine lysate) was added to the antibody-coupled beads. After overnight rotation at 4 °C, the beads were spun down for 2 min at 2000 rpm and 4°C. 50 µl of the supernatant was collected as “flow through” fraction, the rest was discarded. To remove unbound protein, beads were washed five times with 1 ml of 10 mM CHAPS (centrifugation as described at each step) and 100 µl of the last wash fraction (“wash”) was collected. Precipitated proteins were eluted with 1xLaemmli-buffer and input, flow through, and wash fractions were mixed with 5xLaemmli-buffer. Samples were denatured at 93°C for 10 min and subjected to Coomassie staining for subsequent mass spectrometric or western blot analysis.

3.15 Fluorescence-activated cell sorting analysis

Fluorescence-activated cell sorting (FACS) was performed with Hek293 cells transfected with expression constructs for ATP1B2 mutants. The transfected cells were harvested, washed twice in 300 µl PBS containing 1% FCS *via* centrifugation (5 min, 300 × *g*, 4 °C; Centrifuge Biofuge Fresco), and incubated with primary antibodies (given in **Table 7**) in antibody solution for FACS analysis for 25 min at 4 °C. The cells were washed again in 300 µl of PBS containing

1% FCS (5 min, 300 × *g*) and incubated with secondary antibodies (given in **Table 8**) for 25 min at 4 °C. After two washing steps, the cell pellets were resuspended in 100 µl PBS containing 1% FCS and subjected to FACS analysis using a BD FACSCanto™-II flow cytometer run by Diva software. During the whole procedure, cells were kept on ice and pre-cooled solutions were applied.

3.16 Retinoschisin binding assays

3.16.1 Retinoschisin binding analyzed *via* western blot analysis

Retinoschisin binding assays with Hek293 cells were performed as follows: Cells of a confluent-grown plate were passaged at a ratio of 1:24 into a 6-well cell culture plate. On the next day, Hek293 cells were transfected with expression vectors for the retinal Na/K-ATPase *via* the Mirus TransIT®LTI transfection method. After 24 h, the binding assay was performed: First, the medium of transfected Hek293 cells was replaced by 2 ml of input (supernatant of Hek293 stably secreting retinoschisin diluted 1:8 with OptiMEM™ medium) followed by an incubation of 1 h at 37 °C. The Hek293 cells were then resuspended in 2 ml PBS, transferred into a 2 ml reaction tube, and centrifuged at 1000 rpm for 3 min (Centrifuge Biofuge Fresco). The supernatant was discarded, and the cell pellet was resuspended in 1 ml PBS, followed by a 3 min centrifugation step at 4600 rpm. This washing step was repeated three times. Finally, the cell pellet was resuspended in 200 µl PBS, sonicated at 38% for 10 s, mixed with 5xLaemmli buffer, and heated up for 3 min at 95 °C for western blot analysis as described in sections 3.12.

For retinoschisin binding assays with Y-79 cells: Retinoschisin binding to Y-79 cells was performed likewise, but with $4x10^6$ cells resuspended in 2 ml retinoschisin containing supernatant and without transfection as Y-79 express the retinal Na/K-ATPase endogenously (Friedrich et al. 2011).

3.16.2 Retinoschisin binding analyzed *via* immunocytochemical analysis

Retinoschisin binding assays analyzed *via* immunocytochemical instead of western blot analysis were performed similarly, but the cells (Hek293 or Y- 79) were seeded on poly-L-lysine coated coverslips in a 24-well cell culture plate. After 24 h, the binding assay was performed. First, the medium was replaced by 500 µl of input (supernatant of Hek293 stably secreting retinoschisin diluted 1:8 with OptiMEM™ medium) followed by an incubation of 2 h at 37 °C. After three washing steps with 300 µl PBS, which was added carefully by pipetting against the wall of the cell culture dish, the cells were subjected to immunolabeling as described in section 3.9.

3.16.3 Retinoschisin binding after enzymatic deglycosylation of Hek293 cells

The assay was performed as described in 3.16.2, but before adding recombinant retinoschisin containing supernatant, a deglycosylation of transfected Hek293 cells was performed by PNGase F treatment. Two days after transfection with expression vectors for the retinal Na/K-ATPase, the medium was removed and Hek293 cells were incubated for 18 h at 37 °C in a total volume of 100 µl containing 83 µl TBS, 10 µl 10X Glycobuffer 2, and 7 µl (3500 U) of PNGase F or control buffer. After two washing steps with PBS, the retinoschisin containing supernatant was added and the binding assay was performed as described in 3.16.2.

3.16.4 Retinoschisin binding in presence of different sugars

In the binding assay in presence of different sugars the same protocol was used as described before (3.16.1; 3.16.2), but galactose, glucose, or mannose (0, 0.5, and 0.75 M) were added to the input.

3.16.5 Retinoschisin binding in presence of cardiac glycosides

The binding assay in presence of cardiac glycosides was performed with transfected Hek293 and Y-79 cells as described in 3.16.1 and 3.16.2, but ouabain (at 0 M, 10^{-7} M, 10^{-5} M, 10^{-3} M, and 10^{-2} M for western blot or 0 M and 10^{-3} M for immunocytochemical analysis) or digoxin (at 0 M, 10^{-8} M, 10^{-7} M, 10^{-6} M, and 10^{-5} M for western blot or 0 M and 10^{-6} M immunocytochemical analysis) were added to the input.

3.16.6 Binding of purified retinoschisin or retinoschisin variants to transfected Hek293 cells

This binding assay used the same protocol as described before (3.16.1 and 3.16.2), but instead of applying recombinant retinoschisin containing supernatant, purified retinoschisin (1 µg/ml), RS1_C59S (1 µg/ml), RS1_R141H (1 µg/ml), or the equal amount of control eluate were directly added to the medium.

3.17 Tritium (^{3}H)-labeled ouabain binding analysis to the Na/K-ATPase

Hek293 cells of a confluent-grown plate were transferred onto a 12-well cell culture plate in a ratio of 1:40. On the following day, Hek293 cells were transfected with pCEP_ATP1A3_ATP1B2 (1 µg/µl) or an empty pCEP4 vector using Mirus TransIT®LTI transfection reagent and cultured for 48 h. Subsequently, two different experimental approaches were applied.

In approach #1, 300 µl DMEM cultivation medium containing purified recombinant retinoschisin (1.5 µg/ml) or an equal amount of control eluate was added. The cells were incubated for 30 min at 37 °C, followed by the addition of ^{3}H-labeled ouabain, (at 0, 0.5×10^{-9}, 1.0×10^{-8}, 2.5×10^{-8}, 5.0×10^{-8}, or 1.0×10^{-7} M) and incubation for 30 min at 37 °C.

In approach #2, cells were subjected to different concentrations of purified retinoschisin (0, 0.5, 1.0, 1.5, or 2.0 µg/ml) or the same volume of control eluate for 30 min, followed by the addition of 10^{-7} M ^{3}H-labeled ouabain and an incubation for 30 min.

Hek293 cells were resuspended in 1 ml PBS, centrifuged, and washed twice with PBS. The pellet was dissolved in 100 µl 5% SDS and transferred to scintillation cups with 5 ml of scintillation cocktail. Radioactivity of cell pellet bound ^{3}H-labeled ouabain was determined in a scintillation counter for 1 min.

Similar to the Hek293 cell treatment, the same two approaches were applied to Y-79 cells, with the following modifications: 8.5×10^{5} cells were seeded in 24-well plates coated with poly-L-lysine. After 24 h, the medium was replaced by 1 ml of RPMI 1640 medium (Thermo Fisher Scientific) and purified retinoschisin (0, 75, 150, 225, or 350 ng/ml).

3.18 Immunohistochemical analysis of retinal cryosections

For immunolabeling of retinal cryosections, a staining chamber (StainTray™; Carl Roth GmbH) was used to ensure adequate humidity. First, sections of murine eyes or retinal explants were thawed, bordered twice with Liquid Barrier solution, and moistened with 30-50 µl of PB. The PB was replaced by a blocking solution for immunofluorescence staining (**Table 13**) and sections were incubated for 30 min. Subsequently, the primary antibodies (given in **Table 7**) were diluted in antibody solution for immunofluorescence staining and sections were incubated overnight at 4 °C. The next day, three washing steps with PB for 5 min were performed. For staining with light-sensitive secondary antibodies, the 30 min incubation was done in the dark. In addition, secondary antibodies and DAPI (given in **Table 8**) were also added to the secondary antibody solution. After three washes with PB for 5 min, a drop of Dako medium was added, the slides were covered with a coverslip and dried until microscopic analysis.

Photographs of labeled cryosections from murine eyes (see 3.8 and results section 4.3.1.2, 4.3.4.2,and 4.3.3.2) were taken with an Olympus Fv3000 confocal laser scanning microscope at 20x magnification. Co-localization analysis from these samples were performed using 60x magnification and confocal z stacks (3 slides, 0.25 µM z-distance). Confocal image stacks were processed *via* the 3D-deconvolution tool Wiener with a subvolume overlap of five pixels using Olympus CellSens image processing software (CellSens Dimension). The overlap of two signals was analyzed using the co-localization tool from the CellSens Dimension software.

Pictures of labeled cryosections from retinal explants after long-term incubation (see 3.7 and results section 4.2.3) were analyzed in confocal microscopic images taken with TCS SP5 confocal microscope at 40× magnification.

3.19 TUNEL-assay in retinae of retinoschisin-deficient mice

TUNEL staining of cultivated retinal explants (see 3.7 or 3.8) was performed using the *In Situ* Cell Death Detection Kit (Merck Chemicals GmbH) according to the manufacturer's

instructions. Subsequently, confocal images were taken with a TCS SP5 confocal microscope, at 40x magnification and TUNEL-positive nuclei were counted with the Cell Counter plugin for ImageJ (https://imagej.nih.gov/ij/plugins/cell-counter.html).

3.20 Mass spectrometric analysis after co-immunoprecipitation

The Liquid Chromatography-Tandem Mass Spectrometry (LC-MS/MS) analyses were performed by Dr. Astrid Bruckmann (Institute of Biochemistry Center Regensburg, Laboratory for RNA Biology, University of Regensburg).

After co-immunoprecipitation in porcine retinal lysates with antibodies targeting ATP1A3 (and anti-6*His-tag antibodies as control), the precipitates were loaded on a 4%–12% NUPAGE Bis-Tris gel (Invitrogen), proteins were stained with Coomassie and analyzed *via* LC-MS/MS.

LC-MS/MS analyses were described earlier in Hasler et al. (2020). Subsequent database searches (https://www.uniprot.org) were done in the Swiss-Prot *Sus scrofa* and *mammalian* database applying the following parameters: Enzyme specificity trypsin with one missed cleavage allowed precursor tolerance 0.02 Da, MS/MS tolerance 0.04 Da, Mascot-score cut-off 30. Deamidation of asparagine and glutamine, oxidation of methionine, carbamidomethylation, or propionamide modification of cysteine were set as variable modifications.

3.21 Comparison of protein levels in murine retinal lysates

Protein levels of the retinal Na/K-ATPase and putative interaction partners (see 4.3.3.4) in wildtype and retinoschisin-deficient mice (P10, P14, P18, P21, and P30) were compared by sonicating the two retinae of a single mouse in 100 µl of PBS followed by the addition of 25 µl of 5xLaemmli-buffer. Samples were heated to 93°C for 5 min and subjected to SDS-PAGE (3.11) followed by western blot analysis (3.12).

3.22 Na/K-ATPase specific ATP hydrolysis assay

First, plasma membrane-enriched fractions were collected from retinoschisin-deficient, and wildtype murine retinae as follows: A single retina was sonicated in 200 µl TBS. After a centrifugation step (5 min, 2500 rpm, Centrifuge Biofuge Fresco) the supernatant was collected, and cellular debris was discarded. Additional centrifugation of the collected supernatant for 30 min at 13.000 rpm was performed and the pellet, containing retinal membranes, was resuspended and sonicated in ATPase test buffer. Protein concentrations of retinal membrane fractions were determined using the Bradford assay (Bio-Rad) according to manufacturer's instructions. For testing the effect of retinoschisin on cardiac glycoside-induced inhibition, two different approaches were performed.

In approach #1, membrane fractions of retinoschisin-deficient and wildtype retinae (3 µg protein/µl) were mixed with ATPase test buffer containing different concentrations of ouabain

(final concentration: 0, 5.0×10^{-8}, 1.0×10^{-7}, 2.5×10^{-7}, 5.0×10^{-7}, 7.5×10^{-7}, 1.0×10^{-6}, 1.25×10^{-6}, 1.5×10^{-6}, 1.75×10^{-6}, 2×10^{-6}, 2.25×10^{-6}, 2.5×10^{-6}, 5.0×10^{-6}, and 1.0×10^{-5} M) or digoxin (final concentration 0, 1.0×10^{-7}, 5.0×10^{-7}, 7.5×10^{-7}, 1.0×10^{-6}, $5 \times 1.0 \times 10^{-6}$, and 1.0×10^{-5} M) in a total volume of 40 µl and incubated for 30 min.

In approach #2, membrane lysates of retinoschisin-deficient retinae (3 µg protein/µl) were mixed with ATPase test buffer and purified retinoschisin (1 µg/ml) or an equal amount of control eluate in a total volume of 40 µl for 30 min, followed by another 30 min incubation after the addition of ouabain/digoxin (concentration as described in approach #1).

After incubation with cardiac glycosides, 10 µl of ATP solution (3 mM) was added to each sample. 10 µl of the mixture was directly transferred to a 96-well flat-bottom assay plate and stored on ice (timepoint 0 min). The rest was incubated at 37 °C for 60 min. Subsequently, 10 µl were pipetted into the 96-well flat-bottom assay plate and stored on ice.

To determine the ATP hydrolysis activity, the cardiac-sensitive Pi release (Jones et al. 2005) was measured colorimetrically (Howard and Ridley 1990) by adding 300 µl phosphate reagent containing Malachite green solution and ammoniummolybdate solution (freshly prepared during the 1 h incubation step, Triton-X added right before use), as also described in Plössl et al. (2017b). After incubation for 3 min, the colorimetric reaction was stopped by adding 60 µl of 34% citric acid. The photometric measurement was then measured on a FLUOstar™ OPTIMA Microplate Reader at 630 nm. For determination of enzymatic activity, a phosphate calibration curve containing defined amounts of phosphate (1, 2, 3, 4, 5, 6, and 7 nM) was added and the values obtained at 10^{-3} M ouabain, representing unspecific (not Na/K-ATPase-catalyzed) ATP cleavage (Jones et al. 2005) were subtracted from the other values readings. During the entire procedure, cells were kept on ice and pre-cooled solutions were applied. Data processing was performed by nonlinear regression using Sigma Plot Graph System 12.5.

3.23 Patch-clamp analysis of Kv channels in Y-79 cells

Glass coverslips (18 mm) were placed in 3 cm cell culture dishes, coated with concanavalin-A (0.5% in 1 M NaCl) for 2 h at 37°C, and then rinsed with distilled water. Next, 2.5×10^5 Y-79 cells were seeded onto coated coverslips in 3 ml RPMI medium containing 10% FCS and 1% penicillin/streptomycin and cultured for 24 h in medium containing purified retinoschisin (333 ng/ml) or the same volume of control eluate. Electrophysiological measurements of potassium channel currents were performed as described in Gomez et al. (1993), with slight modifications: Patch pipettes had a tip resistance of 3-4 MΩ and were filled with intracellular patch-clamp solution and cells were bathed in extracellular patch-clamp solution. Single cells (without contact to other cells) were voltage-clamped at a holding potential of -60 mV with voltage steps between -60 mV to 80 mV in 10 mV increments. The whole-cell voltage-clamp recordings were obtained by using an EPC-10 USB amplifier on an Olympus IX73 microscope (Olympus Europa SE & Co. KG, Hamburg, Germany) and the Patchmaster Software (HEKA, Lambrecht,

Germany). To test whether the measured outward current was generated by potassium channels, KCl in intracellular and extracellular solutions was replaced by CsCl or the specific voltage-gated potassium channel inhibitor citalopram (Gayet-Primo et al. 2018) (50 µM and 200 µM, respectively) was added to the extracellular solution.

3.24 Imaging of intracellular calcium in Y-79 cells

35 mm cell culture dishes with an ibidi polymer coverslip bottom were incubated for 1 h at 37 °C with poly-L-lysine. Subsequently, 3×10^5 Y-79 cells were seeded onto the coated coverslips in RPMI medium containing 10% FCS and 1% penicillin/streptomycin. After incubation for 1 h at 37 °C, purified recombinant retinoschisin (1 µg/µl) or an equal volume of control eluate was added. The next day, 2 µM Fura-2/AM and 2 µM Pluronic F1-2-7 were added to OptiMEM™ and after an incubation of 30 min at 37 °C, the medium was replaced by Ringer solution (**Table 13**). Intracellular calcium levels were measured using an Olympus IX73 inverted microscope that detected fluorescence intensity at 510 nm after illuminating Y-79 cells with light at 340 nm and 380 nm, respectively. Single cells were selected with FIJI/ImageJ and intracellular calcium level was measured as fluorescence ratio at 510 nm after excitation at 340 and 380 nm.

3.25 Fluorescence correlation spectroscopy analysis

The conception of the project was made in collaboration with Prof. Friedrich (Technical University of Berlin, Department of Physical and Theoretical Chemistry). Data analysis was performed together with Albert Prause (Technical University of Berlin, Department of Physical Chemistry).

Hek293 cells of a confluent-grown plate were passaged at a ratio of 1:18 into a 35 mm FluoroDish cell culture dish with a poly-L-lysine coated glass bottom for cell imaging and cultured in normal Hek293 cultivation medium. After 24 h, the medium was replaced by FluoroBrite™ DMEM medium containing 10% FCS and 1% penicillin/streptomycin followed by transfection with pCDNA3_ATP1A3-GFP_ATP1B2 using Mirus TransIT®LTI transfection reagent. Two days after transfection, retinoschisin, retinoschisin mutant C59S (333 ng/µl), or the same volume of control eluate was added, and cells were incubated for 1 h. The fluorescence correlation spectrometry analysis measurements were performed with a Leica TCS SP5 II confocal laser scanning microscope with a fluorescence correlation spectrometry set-up from PicoQuant. The Hek293 cells were excited with a 488 nm Argon laser line and the measurements were performed in the horizontal cell walls, where the GFP-tagged Na/K-ATPase was localized at the plasma membrane. The obtained fluorescence correlation data were analyzed by Albert Prause as follows:

The signal detected was split into 20 s intervals to minimize the effects of sample movement and photobleaching. Each interval was correlated *via* pseudo-cross correlation to eliminate the influence of detector after-pulsing. The obtained data were preselected according to the

presence of a correlation (all data without a correlation were discarded without further evaluation). The selected correlated data were fitted with two components 2D diffusion model.

$$G(\tau) = \sum_i G_{i,\mathrm{F}}(\tau) \text{ with } G_{i,\mathrm{F}}(\tau) = \rho_i \cdot \left(1 + \frac{\tau}{\tau_{\mathrm{xy}}}\right)^{-1}$$

where ρ_i is a weighting factor for the contribution of each species (the average number of fluorescent species $\langle N \rangle = \frac{1}{\sum_i \rho_i}$) and τ_{xy} is the correlation time in the horizontal xy-plane (i.e., parallel to the cell wall).

4 Results

4.1 Analyses on retinoschisin binding to the retinal Na/K-ATPase

4.1.1 ATP1B2 / Retinoschisin interface – analysis of the influence of ATP1B2 glycosylation

An earlier study demonstrated that retinoschisin localization to the plasma membrane implicitly requires the ATP1B2 subunit of the retinal Na/K-ATPase as a binding partner (Plössl et al. 2017b). As this subunit is highly glycosylated (Tokhtaeva et al. 2010) and retinoschisin was shown to exhibit a high affinity for galactose (Dyka et al. 2008), it was now tested whether retinoschisin binds to the ATP1B2 subunit *via* an interaction with the oligosaccharide side chains of this protein.

To this end, three independent experimental approaches were chosen: First, retinoschisin binding to the recombinantly expressed retinal Na/K-ATPase was tested in the presence of different (putatively competitive) sugars. Second, retinoschisin binding to the recombinantly expressed retinal Na/K-ATPase was tested after enzymatic deglycosylation of the enzyme and third, ATP1B2 binding capacities of retinoschisin and retinoschisin mutant RS1_R141H proteins, both exhibiting similar galactose affinities (Dyka et al. 2008), were compared.

For the first experimental approach, Hek293 cells recombinantly expressing the retinal Na/K-ATPase subunits ATP1A3 and ATP1B2 were incubated with retinoschisin in the presence of galactose, glucose, or mannose (0, 0.5, and 0.75 M). As shown in western blot analysis of the cells after several washing steps (**Figure 7**), the presence of galactose or glucose decreased retinoschisin binding to the cells with a statistically significant difference ($p < 0.05$) for 0.75 M galactose (reduction to 29.0 + 41.8%) and 0.75 M glucose (reduction to 33.2 + 22.8%).

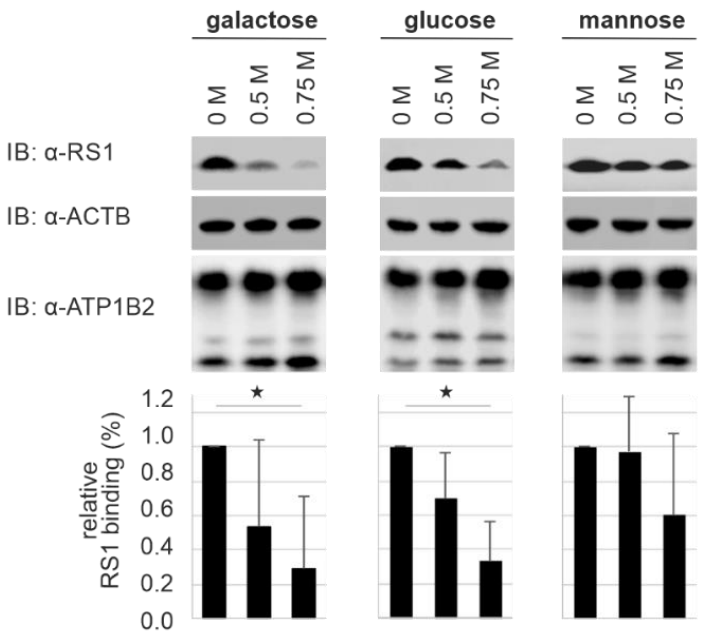

Figure 7: Retinoschisin binding to transfected Hek293 cells in the presence of galactose, glucose, or mannose analyzed *via* western blot analysis

Hek293 cells were transfected with pCEP_ATP1A3_ATP1B2. After two days, cells were incubated for 1 h with purified retinoschisin and 0, 0.5 or 0.75 M galactose, glucose, or mannose. After serval washing steps, retinoschisin binding was analyzed by western blot analysis with antibodies against retinoschisin. ACTB staining served as a loading and ATP1B2 as a transfection control. Densitometric quantification was performed on immunoblots of four individual experiments. Retinoschisin signals were normalized against ATP1B2 and calibrated against signals for 0 M sugar. Data show the mean + SD. Asterisks represent statistically significant differences (*P < 0.05; Kruskal-Wallis test followed by Dunn's multiple comparison test and Bonferroni correction). (Figure modified from Plössl et al. 2019)

Mannose (0.5 M or 0.75 M) exerted a weaker effect on retinoschisin binding to the heterologously expressed Na/K-ATPase (**Figure 7**), with no effect at 0.5 M mannose and a reduction of retinoschisin binding to only 60.0 + 48.1% at 0.75 M mannose ($p > 0.05$). Immunocytochemical staining was also applied to investigate the effect of galactose, glucose, or mannose on retinoschisin binding to Hek293 cells heterologously expressing the retinal Na/K-ATPase. In these experiments, cells were incubated with retinoschisin and the different sugars (0.75 M) for 1 h and 7 h. After both incubation times, retinoschisin binding (red signals in **Figure 8A** and **B**) was only detected to transfected Hek293 cells (identified *via* green ATP1B2 signals), but not to non-transfected cells (visualized *via* DAPI staining, not exhibiting green ATP1B2 labeling) (**Figure 8A** and **B**). In line with western blot analyses, immunocytochemical analyses revealed strongly reduced retinoschisin binding after incubation with 0.75 M galactose or glucose, and no (1 h, **Figure 8A**) or a weaker (7 h, **Figure 8B**) inhibitory effect on retinoschisin binding by 0.75 M mannose.

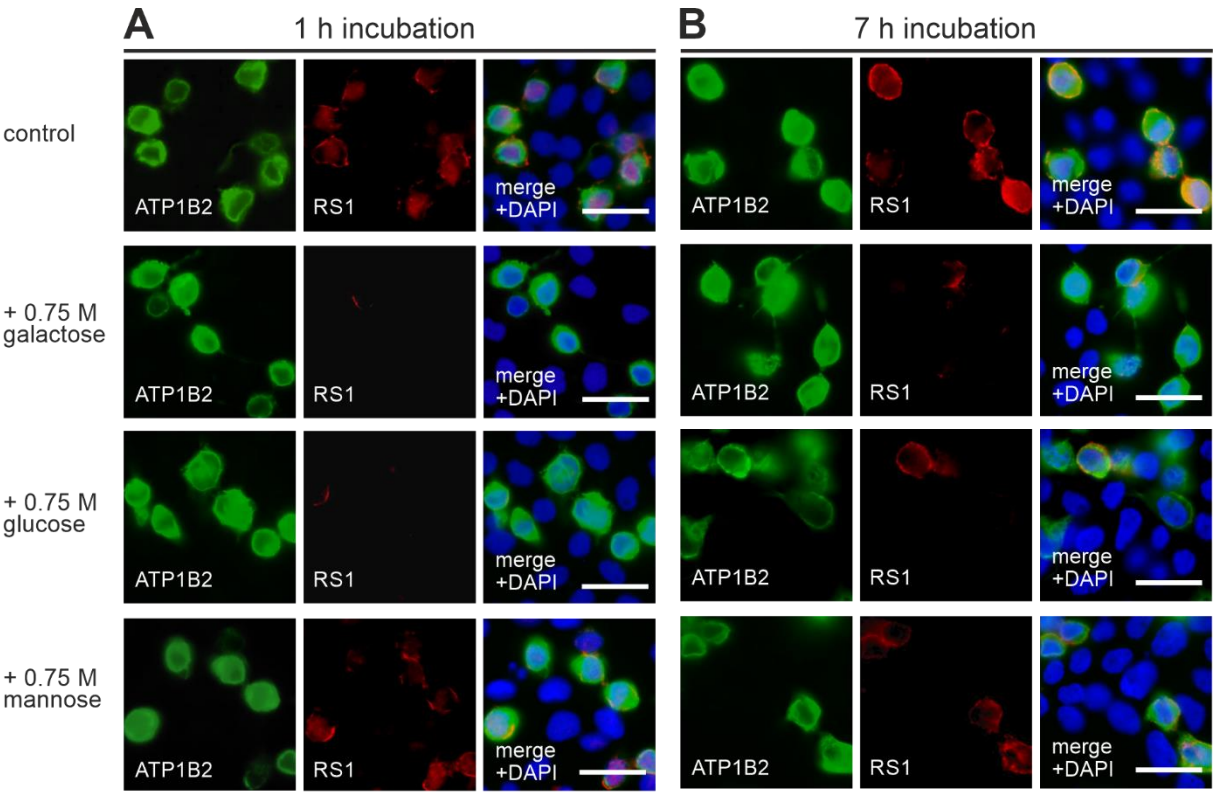

Figure 8: Retinoschisin binding to transfected Hek293 cells in the presence of galactose, glucose, or mannose analyzed *via* immunocytochemical analysis

Hek293 cells were transfected with pCEP_ATP1A3_ATP1B2. After two days, cells were incubated for 1 h (**A**) or 7 h (**B**) with purified retinoschisin (1 µg/ml) and 0, 0.5, or 0.75 M galactose, glucose, or mannose. After several washing steps, retinoschisin binding was analyzed *via* immunocytochemical analysis with antibodies against retinoschisin (red), ATP1B2 (green, used as a transfection marker), as well as DAPI staining (blue, depicting nuclei). Scale bars: 40 µm, (Figure modified from Plössl et al. 2019).

For the second experimental approach (testing retinoschisin binding to deglycosylated ATP1B2), Hek293 cells heterologously expressing ATP1A3 and ATP1B2 were subjected to

PNGase F treatment for 18 h. As a control, the same treatment but without enzyme was performed on transfected Hek293 cells. Western blot analysis, performed by Dr. Karolina Plössl (Institute of Human Genetics, Regensburg), confirmed full deglycosylation of the ATP1B2 after this treatment (Plössl et al. 2019). After incubation with recombinant retinoschisin, immunocytochemical analyses (**Figure 9**) revealed similarly strong retinoschisin binding (red signals in **Figure 9**) to deglycosylated (+ PNGase F) and non-deglycosylated (- PNGase F) cells.

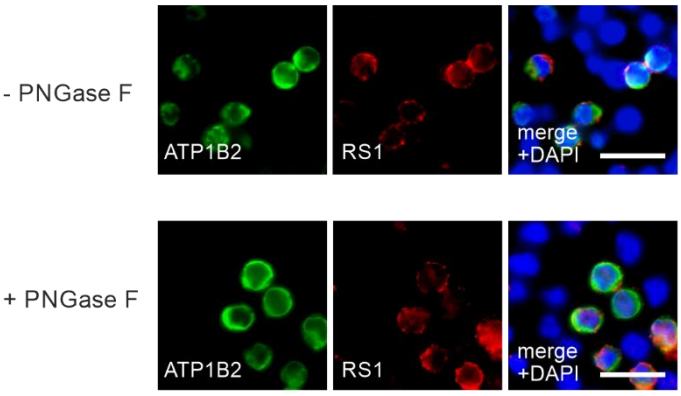

Figure 9: Retinoschisin binding to Hek293 cells heterologously expressing the retinal Na/K-ATPase after PNGase F treatment

Hek293 cells were transfected with pCEP_ATP1A3_ATP1B2. After two days, cells were subjected to enzymatic deglycosylation *via* PNGase F (+ PNGase F) or to the same treatment without the enzyme (- PNGase F). After 1 h incubation with recombinant retinoschisin, retinoschisin binding was analyzed *via* immunocyto-chemical analysis with antibodies against retinoschisin (red), ATP1B2 (green, used as a transfection marker), as well as DAPI staining (blue, depicting nuclei) Scale bars: 40 µm, (Figure modified from Plössl et al. 2019).

The third experimental approach compared ATP1B2 binding of retinoschisin and retinoschisin mutant RS1_R141H. Hek293 cells heterologously expressing the retinal Na/K-ATPase were incubated for 1 h with purified recombinant retinoschisin or recombinant RS1_R141H and their binding to the cells was investigated *via* immunocytochemistry (**Figure 10**). In line with previous studies (Plössl et al. 2018), only retinoschisin, but not RS1_R141H showed binding to Hek293 cells expressing the retinal Na/K-ATPase (**Figure 10**).

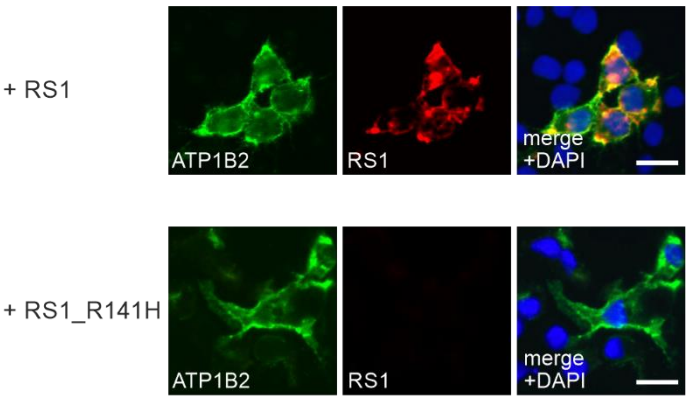

Figure 10: Binding of retinoschisin and retinoschisin mutant R141H to transfected Hek293 cells

Hek293 cells were transfected with pCEP_ATP1A3_ATP1B2. After two days, cells were incubated for 1 h with recombinant retinoschisin (+RS1) or retinoschisin mutant R141H (+RS1_R141H). Retinoschisin binding was analyzed *via* immuno-cytochemical analysis with antibodies against retinoschisin (red), ATP1B2 (green, used as a transfection marker), as well as DAPI staining (blue, depicting nuclei) Scale bars: 40 µm, (Figure modified from Plössl et al. 2019).

4.1.2 Role of threonine 240 in ATP1B2 as a possible retinoschisin binding site of the retinal Na/K-ATPase

A combination of bioinformatic analyses and binding assays with ATP1B2 mutants revealed threonine 240 and the surrounding hydrophobic patch in ATP1B2 as crucial for retinoschisin binding to ATP1B2 (Plössl et al. 2019). In these studies, the substitution of the polar and small threonine 240 by the bulky and neutral leucine interfered with retinoschisin binding but did not affect the overall surface structure of ATP1B2, as shown by FACS analysis.

To further investigate the role of ATP1B2 aa 240 in retinoschisin binding, two more ATP1B2 mutants at aa 240 were generated: In mutant 1 (ATP1B2_T240A), threonine 240 was replaced by the non-bulky, chemically inert alanine and in mutant 2 (ATP1B2_T240S), by the chemically similar serine. Retinoschisin binding assays were performed with Hek293 cells heterologously expressing ATP1A3 and ATP1B2 or the ATP1B2_T240 mutants. After 1 h of incubation with recombinant retinoschisin, retinoschisin binding was investigated by western blot analysis. Retinoschisin binding was detected to normal ATP1B2 and to ATP1B2_T240S but not to ATP1B2_T240A (**Figure 11A**). Densitometric quantification of ATP1B2 expression revealed no effect of the introduced aa exchanges on ATP1B2_T240A and ATP1B2_T240S expression levels, suggesting that the lack of retinoschisin binding to cells transfected with ATP1B2_T240A expression vectors is not a consequence of absent ATP1B2_T240A protein (**Figure 11B**).

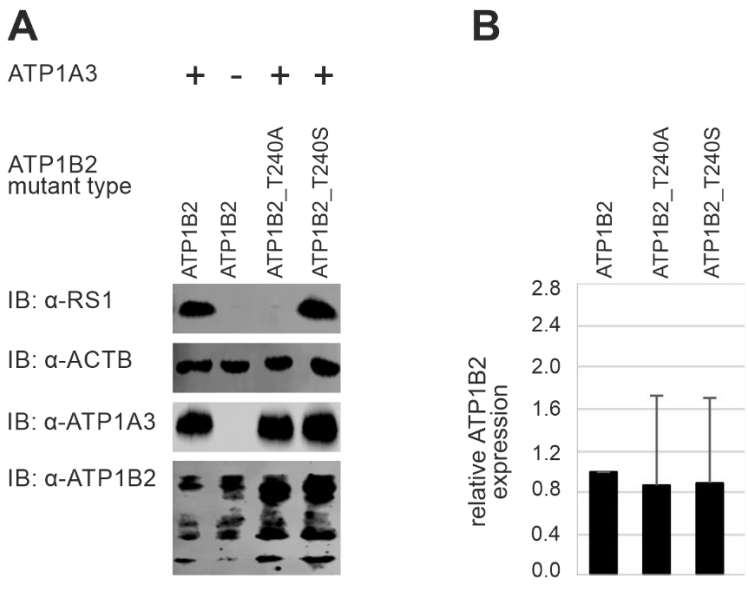

Figure 11: Retinoschisin binding to Hek293 cells heterologously expressing ATP1A3 and ATP1B2 mutants of amino acid site 240

A: Hek293 cells were co-transfected with expression constructs for ATP1A3 and ATP1B2, ATP1B2_T240A or ATP1B2_T240S. After two days, cells were incubated with recombinant retinoschisin for 1 h. Cells transfected with expression constructs for only ATP1B2 served as a negative control (see also Friedrich et al. 2011), cells transfected with expression constructs for ATP1A3 and normal ATP1B2 served as a positive control in the retinoschisin binding assay. After several washing steps, heterologous protein expression as well as retinoschisin binding was investigated by western blot analysis with antibodies against retinoschisin, ATP1A3, and ATP1B2. ACTB staining served as loading control. **B**: Densitometric quantification of ATP1B2 expression was performed on immunoblots

from three individual experiments. Signals were normalized against ACTB and calibrated against ATP1B2. Data represent the mean + SD. (Figure modified from Plössl et al. 2019)

In FACS analyses with antibodies against ATP1B2, both mutants were detected, revealing membrane localization and accessible surface structure of ATP1B2. Nevertheless, ATP1B2_T240A showed a reduced mean fluorescence intensity compared to ATP1B2 and ATP1B2_T240S (**Figure 12**, **Table 30**).

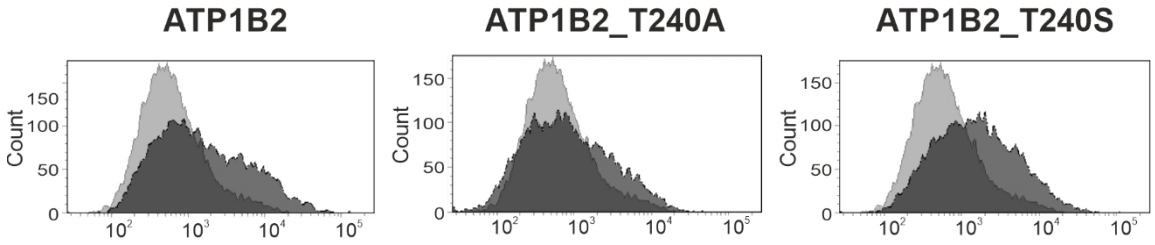

Figure 12: FACS analysis of ATP1B2 and ATP1B2 mutants T240A and T240S

Hek293 cells were co-transfected with expression constructs for ATP1A3 and ATP1B2_T240A or ATP1B2_T240S. After two days, cells were subjected to FACS analysis applying anti-ATP1B2 antibodies, representative histograms are given in this figure. Light grey: Histogram of untransfected Hek293 cells (negative control) depicting unspecific background signals. Dark grey: Histogram of transfected Hek293 cells. (Figure modified from Plössl et al. 2019).

Table 30: Quantitative FACS analysis of ATP1B2 mutants of amino acid site 240 (modified from Plössl et al. 2019)

ATP1B2 mutant	MFI (% of non-mutant ATP1B2)
Negative control	31.1 +/- 6.4
Normal ATP1B2	100 +/- 0.0
ATP1B2_T240L	119.9 +/- 40.4
ATP1B2_T240A	62.4 +/- 29.5
ATP1B2_T240S	106.9 +/- 34.0

Mean fluorescence intensity (MFI) from total cell population, calibrated against normal ATP1B2. Given is the mean +/- SD of three (ATP1B2_T240A and ATP1B2_T240S) or four (negative control, ATP1B2, and ATP1B2_T240L) independent experiments. Negative. control: Untransfected cells.

4.1.3 Influence of retinoschisin on the lateral diffusion of the Na/K-ATPase

A possible effect of retinoschisin on the lateral diffusion of the retinal Na/K-ATPase was assessed *via* fluorescence correlation spectroscopy analyses in cooperation with Prof. Dr. Thomas Friedrich (Technical University of Berlin, Department of Physical and Theoretical Chemistry) and with Albert Prause (Technical University of Berlin, Department of Physical Chemistry).

First, a bicistronic expression vector for a GFP-tagged retinal Na/K-ATPase, required for fluorescence monitoring of the Na/K-ATPase at the plasma membrane, was generated (see 3.4.1). This vector, termed pCDNA3_ATP1A3-GFP_ATP1B2, contained the coding sequences for ATP1B2 and GFP-tagged ATP1A3. Transfection efficacy was tested, the capacity to enable expression of the GFP-tagged retinal Na/K-ATPase in transfected Hek293 cells was determined as well as the capacity of the heterologously expressed retinal Na/K-ATPase to

bind retinoschisin. As shown in **Figure 13A**, around 40% of Hek293 cells transfected with pCDNA3_ATP1A3-GFP_ATP1B2, revealed a green fluorescence due to GFP-expression. Transfection in Hek293 cells yielded a successful expression of ATP1A3 and ATP1B2 (**Figure 13B**). After incubation with purified retinoschisin or the retinoschisin mutant RS1_C59S, the transfected Hek293 cells revealed binding of retinoschisin, but not of retinoschisin mutant RS1_C59S (**Figure 13B**), which is in line with results for the non-tagged retinal Na/K-ATPase (see **Figure 7** and **Figure 11**, (Friedrich et al. 2011; Plössl et al. 2017b)

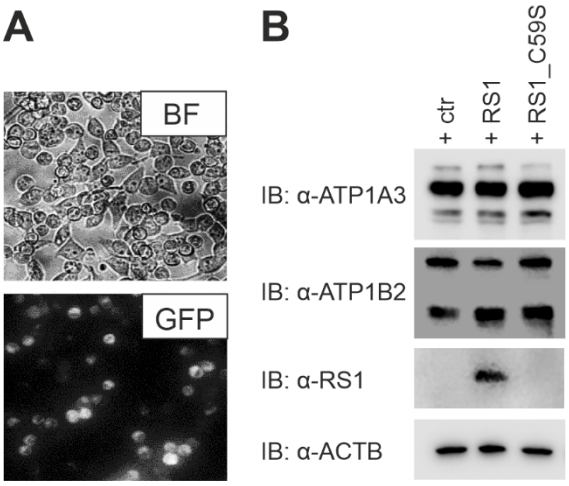

Figure 13: Characterization of the generated expression vector pCDNA3_ATP1A3-GFP_ATP1B2

Hek293 cells were transfected with pCDNA3_ATP1A3-GFP_ATP1B2. **A:** After two days, transfection efficacy and the expression of the GFP-tagged Na/K-ATPase was analyzed *via* brightfield (BF) and subsequent GFP-fluorescence microscopy (GFP) or **B:** Hek293 cells were subjected to recombinant retinoschisin (+ RS1; 333 ng/µl), RS1_C59S (+RS1_C59S¸333 ng/µl), or the equal amount of control eluate (+ctrl) for 1 h. Heterologous protein expression as well as retinoschisin binding was investigated by western blot analysis with antibodies against retinoschisin, ATP1A3, and ATP1B2. ACTB staining served as loading control.

For fluorescence correlation spectroscopy analyses, Hek293 cells were transfected with pCDNA3_ATP1A3-GFP_ATP1B2 and incubated with recombinant retinoschisin, RS1_C59S, or an equal volume of control eluate. Only transfected Hek293 cells, which showed plasma membrane-bound expression of the GFP-tagged Na/K-ATPase at the horizontal cell walls (**Figure 14A,** indicated by white arrows) were used for measurements. As shown in **Figure 14B**, the heterologously expressed retinal Na/K-ATPase showed two distinct diffusion times ($\overline{\tau_1}$: fast, lower curve, and $\overline{\tau_2}$: slow, upper curve), as observed before for Na/K-ATPases (Junghans et al. 2017). Both, the diffusion times ($\overline{\tau_1}$: fast and $\overline{\tau_2}$: slow) and the diffusion coefficients (D1: fast and D2: slow) exhibited no significant differences between retinoschisin, RS1_C59S, or control treatment (**Figure 14B, Table 31**).

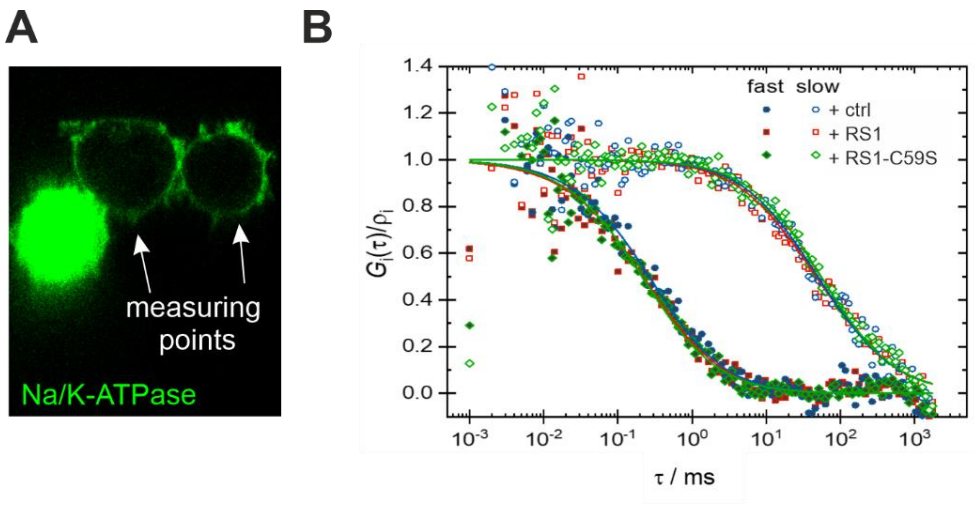

Figure 14: Fluorescence correlation spectroscopy analysis of transfected Hek293 cells

Hek293 cells were transfected with pCDNA3_ATP1A3-GFP_ATP1B2. After two days, the medium was changed to DMEM FluoroBrite medium and cells were subjected to recombinant retinoschisin (+RS1; 333 ng/µl), RS1_C59S (+RS1_C59S¸333 ng/µl), or the equal amount of control eluate (+ctrl) for 1 h. **A:** Fluorescence correlation spectroscopy measurements were performed at the horizontal cell walls, where the GFP-tagged Na/K-ATPase (green) was localized at the plasma membrane (marked by white arrows). **B**: The correlation data of Hek293 cells treated with control eluate (ctrl, blue circle, n = 73), recombinant retinoschisin (RS1, red square, n = 55) and recombinant RS1_C59S (RS1_C59S, green rhomb, n = 80) were fitted against a 2D diffusion model. Empty symbols show slow, filled symbols show fast diffusion times. (Figure B was generated by Albert Prause).

Table 31: Fluorescence correlation spectroscopy analysis of Hek293 cells heterologously expressing GFP-tagged Na/K-ATPase

	$\overline{\tau_1}$ (ms) (fast)	D_1 (m^2s^{-1}) (fast)	$\overline{\tau_2}$ (ms) (slow)	D_2 (m^2s^{-1}) (slow)
ctrl	$0.25 \pm {}^{0.42}_{0.16}$	$(3.6 \pm {}^{6.2}_{2.3}) \cdot 10^{-11}$	$50 \pm {}^{73}_{30}$	$(1.8 \pm {}^{2.7}_{1.1}) \cdot 10^{-13}$
RS1	$0.20 \pm {}^{0.42}_{0.14}$	$(4.4 \pm {}^{9.1}_{3.0}) \cdot 10^{-11}$	$45 \pm {}^{82}_{29}$	$(2.0 \pm {}^{3.7}_{1.3}) \cdot 10^{-13}$
RS1_C59S	$0.20 \pm {}^{0.34}_{0.13}$	$(4.4 \pm {}^{7.3}_{2.8}) \cdot 10^{-11}$	$55 \pm {}^{68}_{30}$	$(1.6 \pm {}^{2.1}_{1.0}) \cdot 10^{-13}$

Mean diffusion times (†) and mean correlation diffusion coefficients (D) and their standard deviations of the GFP-tagged Na/K-ATPase of the fast (1) and slow (2) species analyzed *via* fluorescence correlation spectroscopy in transfected Hek293 cells after the incubation with control eluate (ctrl), recombinant retinoschisin (RS1), and recombinant RS1_C59S (RS1_C59S).

4.2 Analysis of retinoschisin and cardiac glycosides crosstalk at the retinal Na/K-ATPase

Cardiac glycosides like ouabain and digoxin are well known binding partners and important regulators of Na/K-ATPase (Schoner and Scheiner-Bobis 2007). In the following project, a potential interplay of retinoschisin and cardiac glycosides at the Na/K-ATPase interface and possible consequences of this interplay for retinal integrity were investigated.

4.2.1 Retinoschisin binding to the retinal Na/K-ATPase in presence of cardiac glycosides

First, an effect of cardiac glycosides on the binding of retinoschisin to the retinal Na/K-ATPase was investigated. Hek293 cells heterologously expressing the retinal Na/K-ATPase were incubated with recombinant retinoschisin and different concentrations of ouabain (0 M, 10^{-7} M,

10^{-5} M, 10^{-3} M, and 10^{-2} M for subsequent western blot analyses or 0 M and 10^{-3} M for subsequent immunocytochemical analyses) or digoxin (0 M, 10^{-8} M, 10^{-7} M, 10^{-6} M, and 10^{-5} M for subsequent western blot analyses or 0 M and 10^{-6} M subsequent immunocytochemical analyses). Western blot analyses revealed a concentration dependent inhibitory effect of both ouabain and digoxin on the binding of retinoschisin to Hek293 cells heterologously expressing the retinal Na/K-ATPase (**Figure 15**). Digoxin showed a stronger effect than ouabain. Specifically, no effect of ouabain on retinoschisin binding was observed at 10^{-5} M ouabain (however 10^{-2} M ouabain reduced retinoschisin binding to 33.0 + 16.3%, $P < 0.05$ compared to control) (**Figure 15A**), while 10^{-5} M digoxin reduced retinoschisin binding to 46.9 + 21.0% ($P < 0.05$ compared to control) (**Figure 15B**).

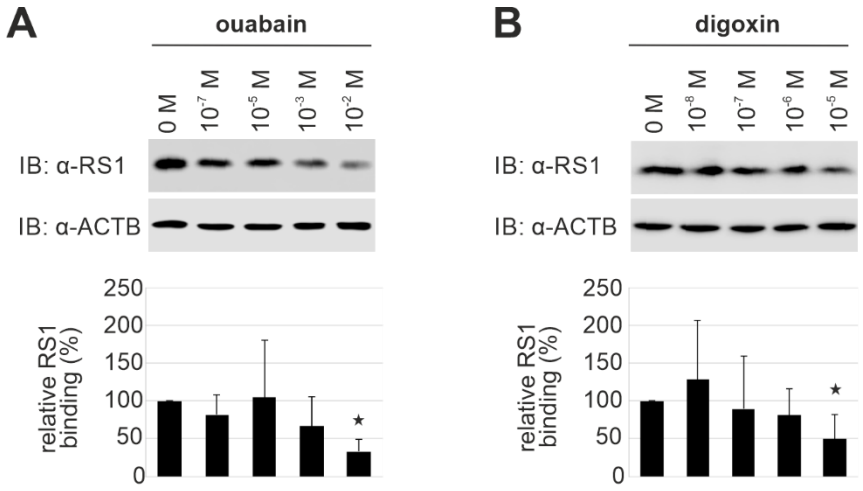

Figure 15: Retinoschisin binding to transfected Hek293 cells in the presence of cardiac glycosides analyzed *via* western blot analysis

A, B: Hek293 cells were co-transfected with pCEP_ATP1A3 and pCEP_ATP1B2. After two days, the cells were incubated with retinoschisin in the presence of 0 (control), 10^{-7}, 10^{-5}, 10^{-3}, or 10^{-2} M ouabain (**A**) or 0 (control), 10^{-8}, 10^{-7}, 10^{-6}, or 10^{-5} M digoxin (**B**) for 1 h. After several washing steps, retinoschisin binding was investigated by western blot analysis with antibodies against retinoschisin. ACTB staining served as loading control. Densitometric quantification was performed on immunoblots from five (**A**, ouabain treatment) or seven (**B**, digoxin treatment) individual experiments. Retinoschisin signals were normalized against ACTB and calibrated against the control. Data represent the mean + SD. Asterisks represent statistically significant differences compared to control (*P < 0.05; Kruskal–Wallis test followed by Dunn's multiple comparison test and Bonferroni correction). (Figure modified from Schmid et al. 2020).

In line with the results from western blot analyses, a significant decrease of retinoschisin binding by cardiac glycoside treatment was also observed after immunocytochemical staining (reduction to 53.9 + 5.1% at 10^{-3} M ouabain and to 24.8 + 19.1% at 10^{-6} M digoxin; $P < 0.05$ compared to control) (**Figure 16**). The inhibitory effect of cardiac glycosides on retinoschisin binding was even more pronounced than in western blot analyses, probably due to different sensitivity of the two experimental approaches (western blot and immunocytochemistry).

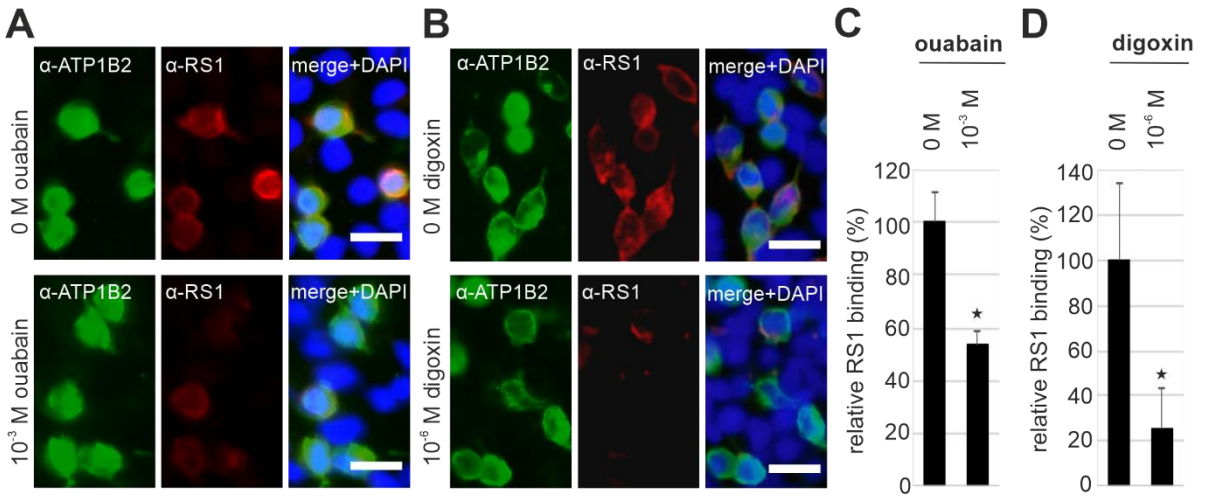

Figure 16: Retinoschisin binding to transfected Hek293 cells in the presence of cardiac glycosides analyzed *via* immunocytochemical analysis

A- D: Hek293 cells were co-transfected with pCEP_ATP1A3 and pCEP_ATP1B2. After two days, they were subjected to recombinant retinoschisin for 2 h in the presence of 0 M (control) or 10^{-3} M ouabain (**A**) or in the presence of 0 M (control) or 10^{-6} M digoxin (**B**). After several washing steps, retinoschisin binding was analyzed *via* immunocytochemistry with antibodies against retinoschisin (red), ATP1B2 (green), as well as DAPI staining (blue, depicting nuclei). Scale bars: 25 µm. Retinoschisin signals of 20 ATP1B2-expressing cells per biological replicate were measured using ImageJ. Data represent the mean + SD of four (**C**, ouabain treatment) or five (**D**, digoxin treatment) biological replicates, calibrated against the control. Asterisks show statistically significant differences compared to control (*P < 0.05; Mann–Whitney U test). (Figure modified from Schmid et al. 2020).

The effect of cardiac glycosides on retinoschisin binding was also investigated in Y-79 cells, a human retinoblastoma cell line that endogenously expresses the retinal Na/K-ATPase, but not retinoschisin, and which can bind externally added retinoschisin (Plössl et al. 2017a). Consistent with the results for Hek293 cells expressing the retinal Na/K-ATPase, Y-79 cells exhibited reduced retinoschisin binding with increasing cardiac glycoside concentrations (ouabain: 0 M, 10^{-6} M, 10^{-5} M, 10^{-4} M, 10^{-3} M, and 10^{-2} M or digoxin: 0 M, 10^{-7} M, and 10^{-6} M). Again, digoxin exerted a stronger effect than ouabain (reduction to 41.3 + 43.6% at 10^{-2} M ouabain and 42.4 + 7.2% at 10^{-6} M digoxin; $P < 0.05$ compared to control) (**Figure 17**).

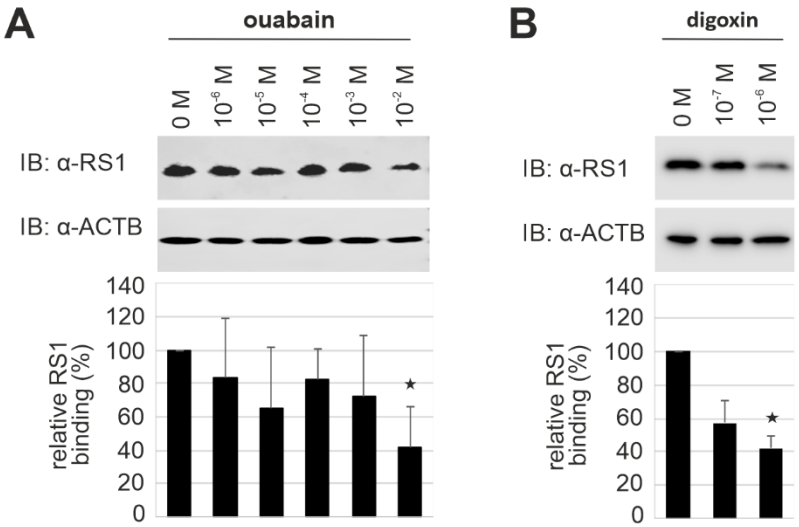

Figure 17: Retinoschisin binding to Y-79 cells in the presence of cardiac glycosides

A, B: Y-79 cells were subjected to recombinant retinoschisin for 1 h in the presence of 0 (control), 10^{-6}, 10^{-5}, 10^{-4}, 10^{-3}, or 10^{-2} M ouabain (**A**) or 0 (control), 10^{-7}, or 10^{-6} M digoxin (**B**). After several washing steps, retinoschisin binding was investigated by western blot analysis with antibodies against retinoschisin. ACTB staining served as loading control. Densitometric quantification was performed on immunoblots from six (**A**, ouabain treatment) or four (**B**, digoxin treatment) individual experiments. Retinoschisin signals were normalized against ACTB and calibrated against the control. Data represent the mean + SD. Asterisks show statistically significant differences compared to control (*P < 0.05; Kruskall–Wallis test followed by Dunn's multiple comparison test and Bonferroni correction). (Figure modified from Schmid et al. 2020).

To exclude that the observed retinoschisin binding behavior is not a consequence of cellular processes other than a competitive effect of both molecules at the retinal Na/K-ATPase additional analyses were conducted.

First, a putative influence of cardiac glycosides on the expression of the retinoschisin binding partner ATP1B2 was investigated. Thus, ATP1B2 levels of the transfected Hek293 cells from the retinoschisin binding assays (**Figure 15**) were quantified *via* western blot analysis. As shown in **Figure 18** no difference in ATP1B2 protein expression was observed after the incubation with ouabain (**Figure 18A**) or digoxin (**Figure 18B**).

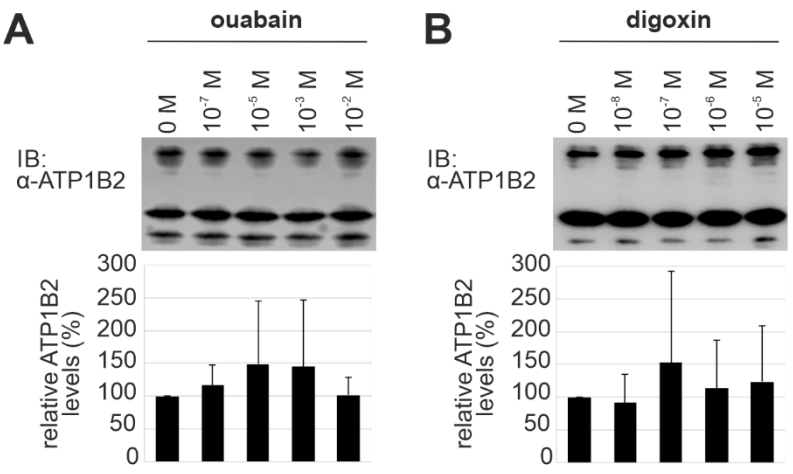

Figure 18: Effect of cardiac glycosides on ATP1B2 levels

A, B: ATP1B2 levels in the Hek293 cells used in retinoschisin binding experiments before (Figure 15) were analyzed by western blot analysis with antibodies against ATP1B2. Densitometric quantification of retinoschisin binding was performed on immunoblots from five (**A**, ouabain treatment) or seven (**B**, digoxin treatment) individual experiments. ATP1B2 signals were normalized against ACTB and calibrated against the control (0 M). Data represent the mean + SD (Figure modified from Schmid et al. 2020).

Second, a putative effect of cardiac glycosides on retinoschisin levels in the supernatant was addressed. Hek293 cells heterologously expressing the retinal Na/K-ATPase were incubated with cardiac glycosides (ouabain: 0 M, 10^{-3} M, and 10^{-2} M, or digoxin: 0 M,10^{-6} M, and 10^{-5} M) and retinoschisin for 1 h (comparable to western blot analysis) or for 2 h (comparable to immunocytochemical analysis). Afterwards retinoschisin protein expression in the supernatant were investigated in western blot analyses. No effect of cardiac glycosides on retinoschisin levels was observed (**Figure 19A** and **B**).

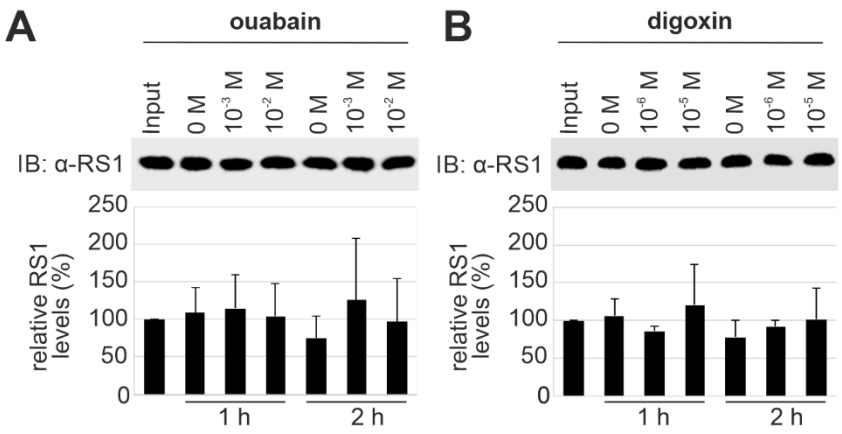

Figure 19: Effect of cardiac glycosides on retinoschisin levels in the supernatant

A, B: Hek293 cells were co-transfected with pCEP_ATP1A3 and pCEP_ATP1B2. After two days, retinoschisin (RS1) containing supernatant (input) was added as well as 0 (control), 10^{-3}, or 10^{-2} M ouabain (**A**) or 0 (control), 10^{-6}, or 10^{-5} M digoxin (**B**). After 1 h and 2 h, samples were taken from the supernatant and subjected to western blot analysis with antibodies against retinoschisin. Densitometric quantification of retinoschisin was performed on immunoblots from six individual experiments. Signals were calibrated against the control. Data represent the mean + SD (Figure modified from Schmid et al. 2020).

Finally, cardiac glycoside dependent retinoschisin binding to an ouabain-insensitive ATP1A3 mutant ("ATP1A3-OI") was investigated. Due to two point mutations at the ouabain binding site (Q108R and N119D), ATP1A3-OI remains fully functional but can no longer bind ouabain (Price and Lingrel 2002; Plössl et al. 2017b). As crystal structures revealed similar interaction sites for ouabain or digoxin at the α-subunit of the Na/K-ATPase, ATP1A3-OI should also fail to bind digoxin (Laursen et al. 2013). Binding assays with Hek293 cells heterologously expressing ATP1A3-OI and ATP1B2 in the presence of ouabain (0, 10^{-7}, 10^{-5}, 10^{-3}, or 10^{-2} M) or digoxin (0, 10^{-8}, 10^{-7}, 10^{-6}, or 10^{-5} M) were conducted as before (**Figure 15**) and retinoschisin binding was analyzed *via* western blot analysis. In contrast to the inhibitory effect of cardiac glycosides on the binding of retinoschisin to the normal retinal Na/K-ATPase (**Figure 15**), ouabain (**Figure 20A**) or digoxin (**Figure 20B**) did not affect binding of retinoschisin to the ouabain-insensitive Na/K-ATPase.

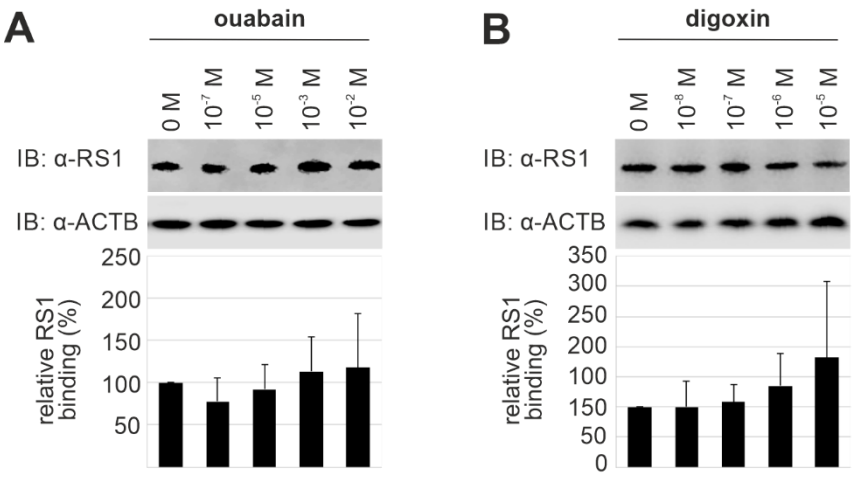

Figure 20: Retinoschisin binding to Hek293 cells heterologously expressing ATP1A3 mutant ATP1A3-OI and ATP1B2 in the presence of cardiac glycosides analyzed *via* western blot analysis

A, B: Hek293 cells were co-transfected with pCEP_ATP1A3-OI (ouabain-insensitive) and pCEP_ATP1B2. After two days, cells were incubated with retinoschisin in the presence of 0 (control), 10^{-7}, 10^{-5}, 10^{-3}, or 10^{-2} M ouabain (**A**) or 0 (control), 10^{-8}, 10^{-7}, 10^{-6}, or 10^{-5} M digoxin (**B**) for 1 h. After several washing steps, retinoschisin binding was investigated by western blot analysis with antibodies against retinoschisin. ACTB staining served as loading control. Densitometric quantification was performed on immunoblots from each of five individual experiments. Retinoschisin signals were normalized against ACTB and calibrated against the control. Data represent the mean + SD. (Figure modified from Schmid et al. 2020).

Immunocytochemical analyses confirmed this observation. Neither ouabain (10^{-3} M) (**Figure 21A** and **C**) nor digoxin (10^{-6} M) (**Figure 21B** and **D**) affected the binding of retinoschisin to Hek293 cells expressing the ouabain-insensitive retinal Na/K-ATPase (**Figure 15**).

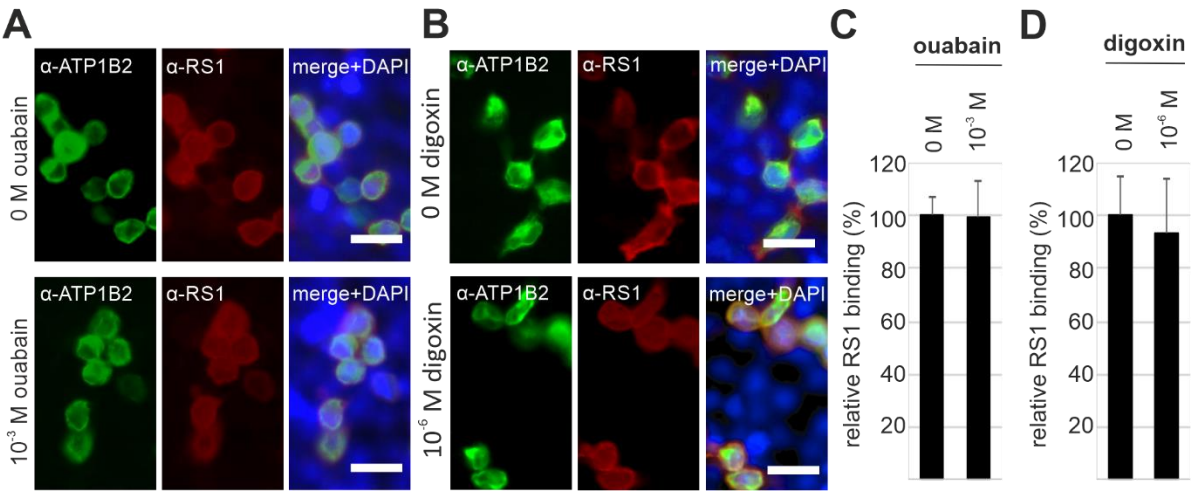

Figure 21: Retinoschisin binding to Hek293 cells heterologously expressing ATP1A3 mutant ATP1A3-OI and ATP1B2 in the presence of cardiac glycosides analyzed *via* immunocytochemical analysis

A- D: Hek293 cells were co-transfected with pCEP_ATP1A3-OI (ouabain-insensitive) and pCEP_ATP1B2. After two days, cells were subjected to recombinant retinoschisin for 2 h in the presence of 0 M (control) or 10^{-3} M ouabain (**A**) or in the presence of 0 M (control) or 10^{-6} M digoxin (**B**). Subsequently, retinoschisin binding was analyzed *via* immunocytochemistry with antibodies against retinoschisin (red), ATP1B2 (green), as well as DAPI staining (blue, depicting nuclei). Scale bars*:* 25 µm. Retinoschisin signals of 20 ATP1B2 expressing cells per biological replicate were measured using ImageJ. Data represent the mean + SD of four (**C,** ouabain treatment) or five (**D**, digoxin treatment) biological replicates, calibrated against the control. (Figure modified from Schmid et al. 2020).

4.2.2 Cardiac glycosides binding to the retinal Na/K-ATPase in dependence of retinoschisin

Next, an effect of retinoschisin on cardiac glycoside binding was investigated, applying two experimental approaches: First, the retinoschisin dependent binding of radioactive ^{3}H-labeled ouabain to the retinal Na/K-ATPase was analyzed. Second, the influence of retinoschisin on the cardiac glycoside-induced inhibition of the active ion transport of the Na/K-ATPase was explored.

^{3}H-labeled ouabain binding to the retinal Na/K-ATPase heterologously expressed in Hek293 or Y-79 cells was explored. Before conducting the experiments, binding assays with different retinoschisin concentrations (without cardiac glycosides) were performed to determine the retinoschisin input concentration to allow maximal cellular retinoschisin binding (meaning the strongest signals of bound retinoschisin after western blot analysis). For Hek293 cells (**Figure 22A**) maximal retinoschisin binding was observed from a retinoschisin concentration of 1 µg/ml, and for Y-79 cells (**Figure 22B**) from a retinoschisin concentration of 75 ng/ml. The following experiments testing binding of ^{3}H-labeled ouabain were conducted in the presence of an excess amount of retinoschisin, 1,5 µg/ml for transfected Hek293 cells and 125 ng/µl for Y-79 cells.

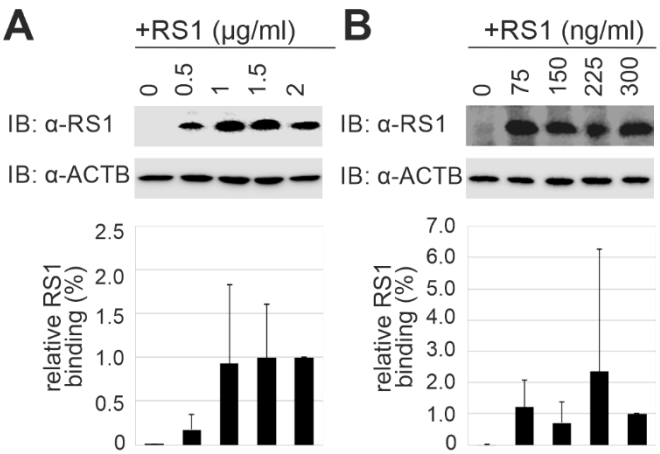

Figure 22: Effect of protein concentration on retinoschisin binding efficiency

A: Hek293 cells were transfected with pCEP_ATP1A3_ATP1B2. After two days, Hek293 cells were subjected to 0, 0.5, 1.0, 1.5, or 2.0, µg/ml of recombinant retinoschisin (+RS1) **B**: Y-79 cells were subjected to 0, 75, 150, 225, or 300 ng/ml recombinant retinoschisin (+RS1). After 30 min of incubation and several washing steps, retinoschisin binding was investigated by western blot analysis with antibodies against retinoschisin. ACTB staining served as loading control. Densitometric quantification of retinoschisin binding was performed on immunoblots from four (**A**) or six (**B**) individual experiments. Signals were normalized against ACTB and calibrated against signals for 2 µg/ml (**A**), or 300 ng/ml (**B**) retinoschisin. Data represent the mean + SD (Figure modified from Schmid et al. 2020).

In the first experimental approach, Hek293 cells heterologously expressing the retinal Na/K-ATPase or Y-79 cells were subjected to 1.5 µg/ml recombinant retinoschisin or the same volume of control eluate and increasing concentrations of ^{3}H-labeled ouabain (0, 0.5×10^{-9}, 1.0×10^{-8}, 2.5×10^{-8}, 5.0×10^{-8}, or 1.0×10^{-7} M). Alternatively, the cells were incubated with 10^{-7} M ^{3}H-labeled ouabain and with increasing concentrations of retinoschisin (Hek293 cells: to 0, 0.5, 1.0, 1.5, or 2.0 µg/ml, Y-79 cells: 0, 75, 150, 225, or 350 ng/ml) or the same volume of control eluate. The bound radioactivity and thus the binding of ^{3}H-labeled ouabain to

transfected Hek293 cells or Y-79 cells was measured subsequently as counts per minute *via* a scintillation detector.

For the applied ouabain concentrations (**Figure 23A**), Hek293 cells transfected with pCEP_ATP1A3_ATP1B2 showed an approximately twofold increase in bound radioactivity compared to control cells (transfected with pCEP4), apparently reflecting additional ouabain binding by the heterologously expressed retinal Na/K-ATPase. No differences in bound radioactivity and thus on ouabain binding were observed between cells treated with or without retinoschisin (**Figure 23A**). When binding of 10^{-7} M ^{3}H-labeled ouabain in the presence of increasing amounts of retinoschisin was investigated, retinoschisin did not affect ouabain binding to the retinal Na/K-ATPase heterologously expressed in Hek293 cells, even under the highest applied retinoschisin concentration of 2 µg/ml (**Figure 23B**).

Y-79 cells (**Figure 23C,D**) showed no effect of retinoschisin on the binding of ^{3}H-labeled ouabain, neither for different ouabain concentrations (**Figure 23C**) nor under increasing concentrations of retinoschisin (**Figure 23D**).

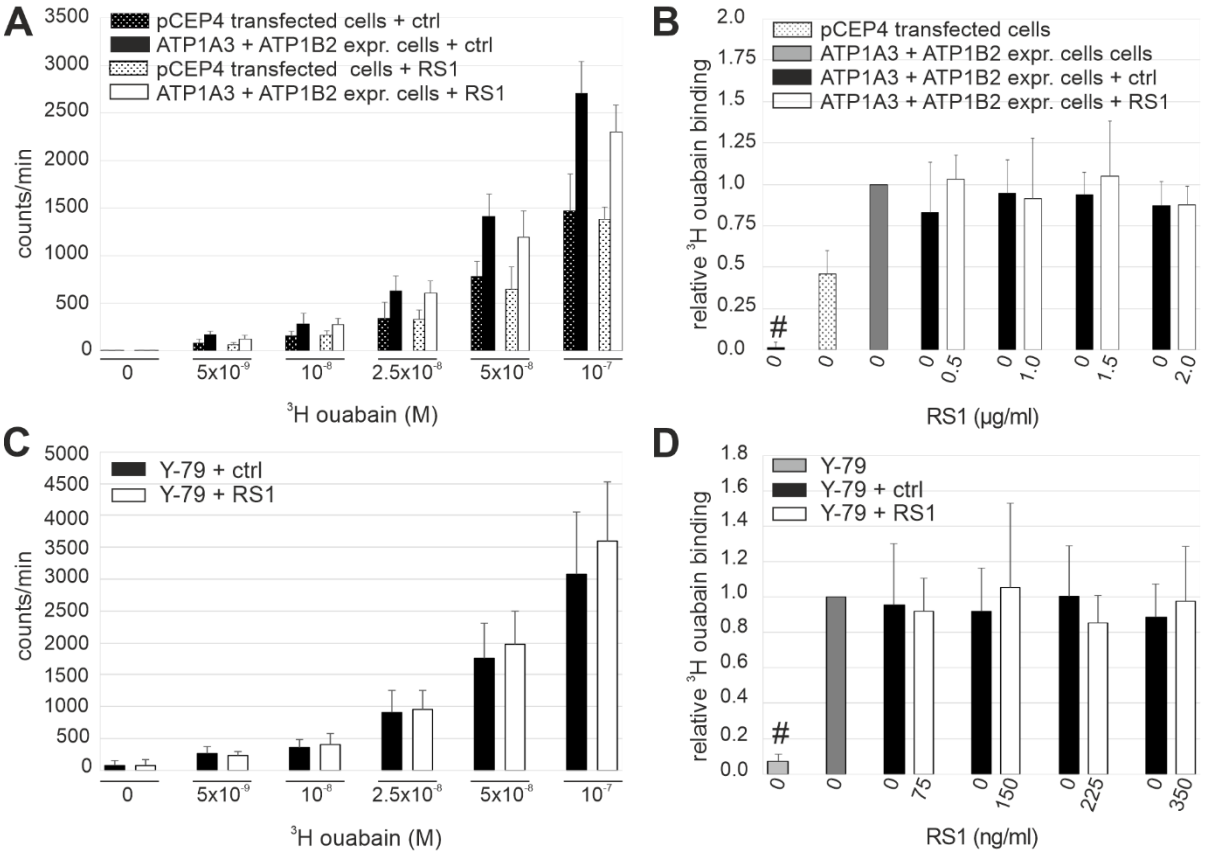

Figure 23: ^{3}H-labeled ouabain binding to transfected Hek293 cells in the presence of retinoschisin

A, B: Hek293 cells were transfected with pCEP4 or with pCEP_ATP1A3_ATP1B2. **A**: After two days, cells were subjected to 1.5 µg/ml recombinant retinoschisin (RS1) or the same volume of control eluate (ctrl) for 30 min, followed by the addition of 0, 0.5×10^{-9}, 1.0×10^{-8}, 2.5×10^{-8}, 5.0×10^{-8}, or 1.0×10^{-7} M ^{3}H-labeled ouabain for 30 min. **B**: Alternatively, cells were subjected to 0, 0.5, 1, 1.5, or 2 µg/ml retinoschisin (RS1) or the same volume of control eluate (ctrl) for 30 min, followed by the addition of 10^{-7} M ^{3}H-labeled ouabain for 30 min (#, without ^{3}H-

labeled ouabain). **C**: Y-79 cells were subjected to 120 ng/mL recombinant retinoschisin (RS1) or the same volume of control eluate (ctrl) for 30 min, followed by the addition of 0, 0.5 × 10^{-9}, 1.0 × 10^{-8}, 2.5 × 10^{-8}, 5.0 × 10^{-8}, or 1.0 × 10^{-7} M ^{3}H-labeled ouabain. **D**: Alternatively, Y-79 cells were subjected to 0, 75, 150, 225, or 350 ng/ml recombinant retinoschisin (RS1) or the same volume of control eluate (ctrl) for 30 min, followed by the addition of 10^{-7} M ^{3}H-labeled ouabain and 30 min of incubation (#, without ^{3}H-labeled ouabain). **A–D**: After incubation with retinoschisin and ouabain, cells were washed and lysed, and bound radioactivity was determined in a scintillation counter. (**A, C**) Data represent the mean + SD of measured counts/minute of five (**A**) or nine (**C**) biological replicates. (**B, D**) Data represent the mean + SD of five (**B**) or seven (**D**) biological replicates, calibrated against signals of cells incubated with ^{3}H-labeled ouabain but without retinoschisin or control eluate (gray bar). (Figure modified from Schmid et al. 2020).

In the second experimental approach, the influence of retinoschisin on the cardiac glycoside-induced inhibition of the active ion transport of the Na/K-ATPase was explored. A cardiac glycoside-sensitive ATP hydrolysis assay was performed to compare Na/K-ATPase activity in murine retinal membranes of wildtype and retinoschisin-deficient mice (**Figure 24A**), or to compare Na/K-ATPase activity in murine retinoschisin-deficient retinal membranes in the presence of recombinant retinoschisin or control eluate (**Figure 24B**). With increasing concentrations of digoxin (0 – 10 µM; **Figure 24**), the Na/K-ATPase activity decreased in both assays. Notably, the presence of endogenous (**Figure 24A**) or recombinant (**Figure 24B**) retinoschisin did not alter the inhibitory capacity of digoxin ($P > 0.05$ compared with retinoschisin-deficient retinae at all concentrations of digoxin). In addition, the ATP hydrolysis tests were also performed in the presence of ouabain by Carina Schmied (M.Sc. student at the Institute of Human Genetics, Regensburg), and comparable results were obtained (published in Schmid et al. 2020).

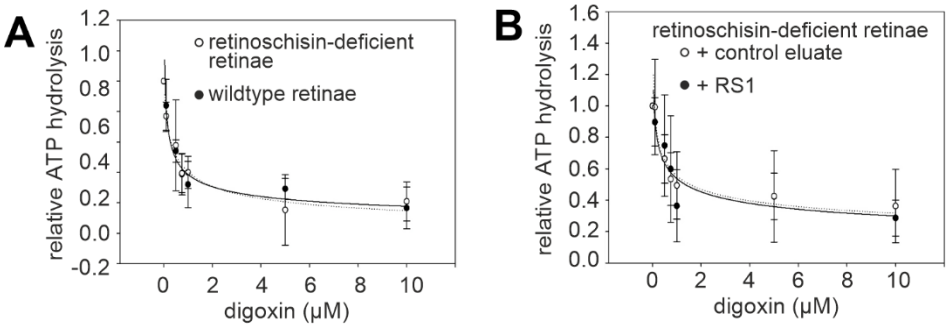

Figure 24: Effect of retinoschisin on inhibition of retinal Na/K-ATPase pump activity by cardiac glycosides

A, B: Na/K-ATPase catalyzed ATP hydrolysis in murine retinal membrane fractions from (**A**) retinoschisin-deficient (open circles) and wildtype mice (closed circles) or from (**B**) retinoschisin-deficient mice pre-incubated for 30 min with recombinant retinoschisin (RS1, 1 µg/ml, closed circles) or control eluate (open circles). Assays were performed in the presence of 0, 1.0 × 10^{-7}, 5.0 × 10^{-7}, 7.5 × 10^{-7}, 1.0 x 10^{-6}, 5.0 × 10^{-6}, and 1.0 × 10^{-5} M digoxin. Data represent the mean ± SD of five biological replicates, calibrated against values obtained for 0 M digoxin. (Figure modified from Schmid et al. 2020).

4.2.3 The reciprocal effect of cardiac glycosides and retinoschisin on photoreceptor degeneration

In retinoschisin-deficient mice, apoptotic photoreceptor degeneration is observed, with a peak of apoptotic nuclei around P18 (Gehrig et al. 2006; 2007). Photoreceptor degeneration in retinal explants of retinoschisin-deficient mice was shown to be reduced by externally added

retinoschisin (Plössl et al. 2018). The following experiment now addressed the effect of cardiac glycosides on the protective capacity of retinoschisin against apoptotic photoreceptor degeneration.

Retinae of retinoschisin-deficient mice were explanted at P18 and incubated with recombinant retinoschisin or control eluate and with or without ouabain or digoxin. After four days, apoptotic cell death was followed by TUNEL-staining. Explants incubated with retinoschisin showed less apoptotic nuclei in outer nuclear layer (9.1 + 5.3%) than explants incubated with control eluate (23.3 + 19.9%) (**Figure 25**). After the incubation with 10^{-5} M ouabain, the number of apoptotic nuclei increased to 54.3 + 31.1%, after the incubation with 10^{-5} M ouabain and retinoschisin to 40.3 + 17.9% (**Figure 25**). The difference in the percentages of apoptotic nuclei between only retinoschisin- or only ouabain-treated explants reached statistical significance ($P < 0.05$) (**Figure 25**).

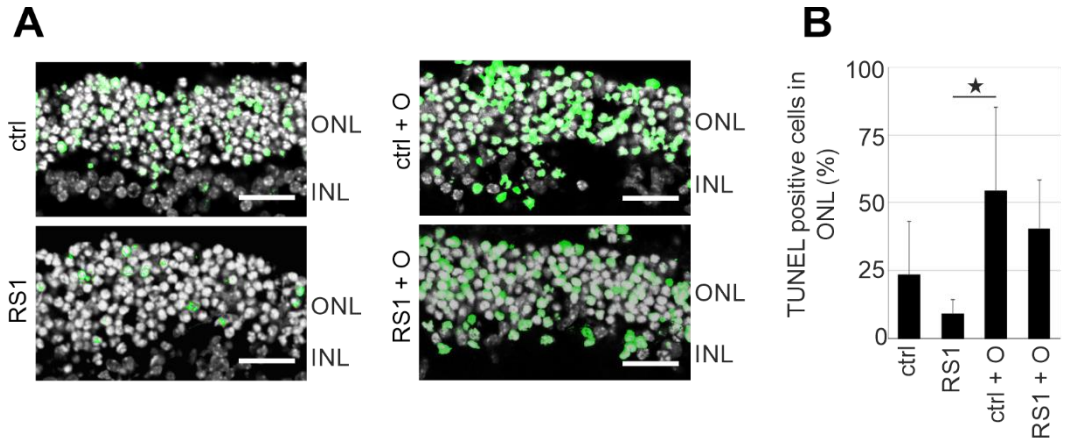

Figure 25: Effect of ouabain and retinoschisin on photoreceptor degeneration in retinal explants

A: Retinoschisin-deficient retinae explanted at postnatal day18 were cultivated for four days in medium containing retinoschisin (RS1) or control eluate (ctrl) in the presence of 0 or 10^{-5} M ouabain (O). Cryosections of the explants were subjected to TUNEL staining to visualize apoptotic nuclei (green), as well as to DAPI staining to visualize all nuclei (gray). Scale bars: 25 µm. ONL, outer nuclear layer; INL, inner nuclear layer. **B:** TUNEL-positive nuclei and all nuclei were counted in each cryosection with the Cell Counter plugin for ImageJ, and the percentage of TUNEL-positive nuclei was calculated. Data represent the mean + SD of five biological replicates calibrated against the control. Asterisks represent statistically significant differences compared with the control (*$P < 0.05$; ANOVA test followed by Tukey's multiple comparison test). (Figure modified from Schmid et al. 2020).

For the retinal explants incubated with digoxin, similar effects were observed. Again, retinoschisin exerted a protective effect against apoptosis (13.9 + 16.7% apoptotic nuclei in retinoschisin treated explants compared to 24.0 + 19.9% in control explants), while treatment with 10^{-6} M digoxin strongly increased apoptosis in the outer nuclear layer (55.4 + 27.6% apoptotic nuclei; $P < 0.05$ compared to retinoschisin-treated explants) (**Figure 26**). In explants incubated with retinoschisin and digoxin 36.4 + 22.0% apoptotic nuclei were detected (**Figure 26**).

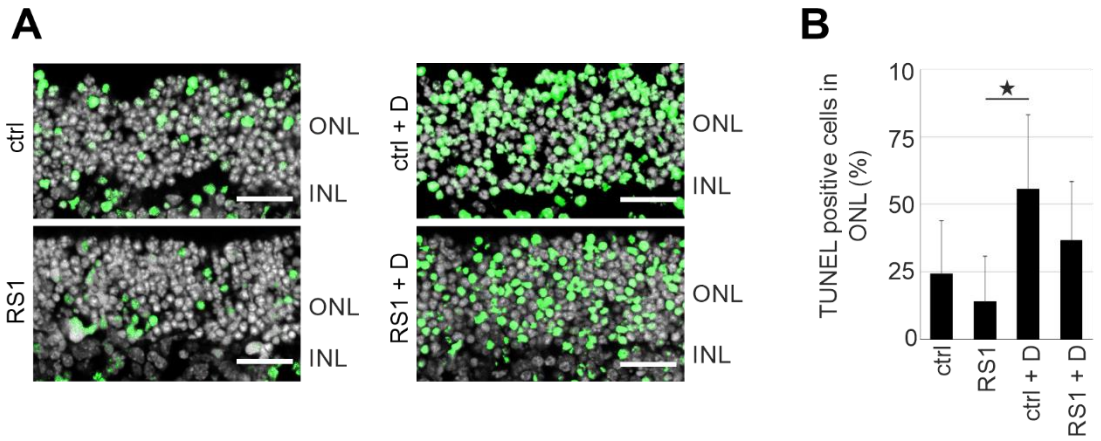

Figure 26: Effect of digoxin and retinoschisin on photoreceptor degeneration in retinal explants

A: Retinoschisin-deficient retinae explanted at postnatal day 18 were cultivated for four days in medium containing retinoschisin (RS1) or control eluate (ctrl) in the presence of 0 or 10^{-6} M digoxin (D). Cryosections of the explants were subjected to TUNEL staining to visualize apoptotic nuclei (green), as well as to DAPI staining to visualize all nuclei (gray). Scale bars: 25 µm. ONL, outer nuclear layer; INL, inner nuclear layer. **B:** TUNEL-positive nuclei and all nuclei were counted in each cryosection with the Cell Counter plugin for ImageJ, and the percentage of TUNEL-positive nuclei was calculated. Data represent the mean + SD of six biological replicates calibrated against the control. Asterisks represent statistically significant differences compared with the control (*P < 0.05; Kruskal-Wallis test followed by Dunn's multiple comparison test and Bonferroni correction). (Figure modified from Schmid et al. 2020).

4.3 Detailed analysis of the retinal Na/K-ATPase

The ATP1A1-containing Na/K-ATPase complex interacts with several signal transducers such as SRC, PLC, RAS or PI3K leading to the formation of a so-called “signalosome complex” (Reinhard et al. 2013; Cui and Xie 2017). In addition, the transmembrane ion exchanger NCX and the adaptor protein ANKB were suggested as close interaction partners of the Na/K-ATPase in cardiomyocytes, together playing an important role in maintaining ion homeostasis and stabilizing the protein complex (Mohler et al. 2005; Reinhard et al. 2013).

In the retina, the retinal Na/K-ATPase was also reported to be complexed with ANKB and tethered to β2-spectrin (Kizhatil et al. 2009). Apart from the latter work, little is known about further interaction partners of the retinal Na/K-ATPase and thus about a putative function of the retinal Na/K-ATPase at the photoreceptor inner segments. The aim of this subproject was to identify further interaction partners of the retinal Na/K-ATPase and the consequences of retinoschisin-deficiency on such a macromolecular complex.

4.3.1 Targeted approach: Analysis of known ATP1A1-containing Na/K-ATPase complex associated proteins

4.3.1.1 Co-Immunoprecipitation analysis targeting known ATP1A1-containing Na/K-ATPase complex associated proteins

The identification of interacting proteins of the retinal Na/K-ATPase was initially addressed following a targeted approach. After co-immunoprecipitation of porcine retinal lysates with antibodies against ATP1A3, western blot analyses were performed of the precipitate applying

antibodies against known ATP1A1-containing Na/K-ATPase complex associated proteins, such as SRC, PI3K, RAS, NCX, and PLC (summarized in Reinhard et al. 2013)

As shown in **Figure 27A** (top), ATP1A3 as well as ATP1B2 were identified in the precipitate of the ATP1A3 co-immunoprecipitation experiment but not in the precipitate of the negative control experiment, a 6*His-tag co-immunoprecipitation. In the staining of ATP1B2 a weak molecular weight species staining slightly higher than the band obtained for ATP1B2 was observed in the precipitate of the 6*His-tag co-immunoprecipitation, which is likely due to unspecific labeling of the heavy chains of the antibodies (molecular weight of both ATP1B2 and heavy antibody chain around 55 kDa).

In contrast to the two retinal Na/K-ATPase subunits, the known ATP1A1 interaction partner SRC (**Figure 27A**, top) showed a very weak staining of similar intensity in the precipitates of both anti-ATP1A3 and 6*His-tag co-immunoprecipitation. The precipitation of SRC might thus rather be a consequence of its unspecific interaction with the column material or antibody backbones. The analysis of PI3K (molecular weight = 85 kDa), showed no immunolabeling in the precipitate of ATP1A3, whereas a faint staining of the same size was detectable in the control co-immunoprecipitation targeting 6*His-tag (**Figure 27A** middle), likely indicating unspecific binding of the PI3K to the 6*His-Tag. The western blot analysis of RAS in the co-immunoprecipitations of ATP1A3 and 6*His-tag showed signals in input and flow through fractions equivalent to the molecular weight of RAS (21 kDa), whereas in the precipitates of both experiments only an antibody binding at a higher molecular weight was detected, which most likely represents unspecific detection of the light chains of the antibodies (molecular weight = 25 kDa) (**Figure 27A** middle). As shown in **Figure 27A** (bottom), the known ATP1A1 complex partners NCX (molecular weight = 120 kDa) and PLC (molecular weight = 150 kDa) only showed a weak staining in both precipitates (ATP1A3 and 6*His-tag). Similar to the SRC staining, the observed labeling might be a consequence of unspecific interaction with the column material or antibody backbones.

To confirm specificity, additional co-immunoprecipitations targeting ATP1A1 were conducted (**Figure 27B**). Again, ATP1B2, as a possible Na/K-ATPase β-subunit, was detected in the precipitate of ATP1A1 co-immunoprecipitation, whereas only unspecific labeling of likely heavy chains of the antibodies was observed in the precipitate of the 6*His-tag co-immunoprecipitation (**Figure 27B**, top). In contrast to the weak SRC staining in the co-immunoprecipitation targeting ATP1A3 (**Figure 27A,** top), a strong SRC staining was obtained in the co-immunoprecipitation targeting ATP1A1 while again, only a weak band was detected in the control co-immunoprecipitation (6*His-tag) (**Figure 27B**, top). In contrast to the co-immunoprecipitation targeting ATP1A3, the staining of PI3K revealed a positive reaction in the co-immunoprecipitation targeting ATP1A1, while a weaker staining was detected in the control experiments using 6*His-tag antibodies (**Figure 27B**, middle). RAS could not be detected in

the co-immunoprecipitation with ATP1A1 antibodies (**Figure 27B,** middle). Like in the co-immunoprecipitation with ATP1A3 antibodies, probably the heavier light chains of the antibodies were stained in the precipitates. In the co-immunoprecipitation targeting ATP1A1, both NCX and PLC were precipitated (strong labeling), and only NCX showed a weak unspecific molecular weight staining in the co-immunoprecipitation with 6*His-tag antibodies (**Figure 27B**, bottom).

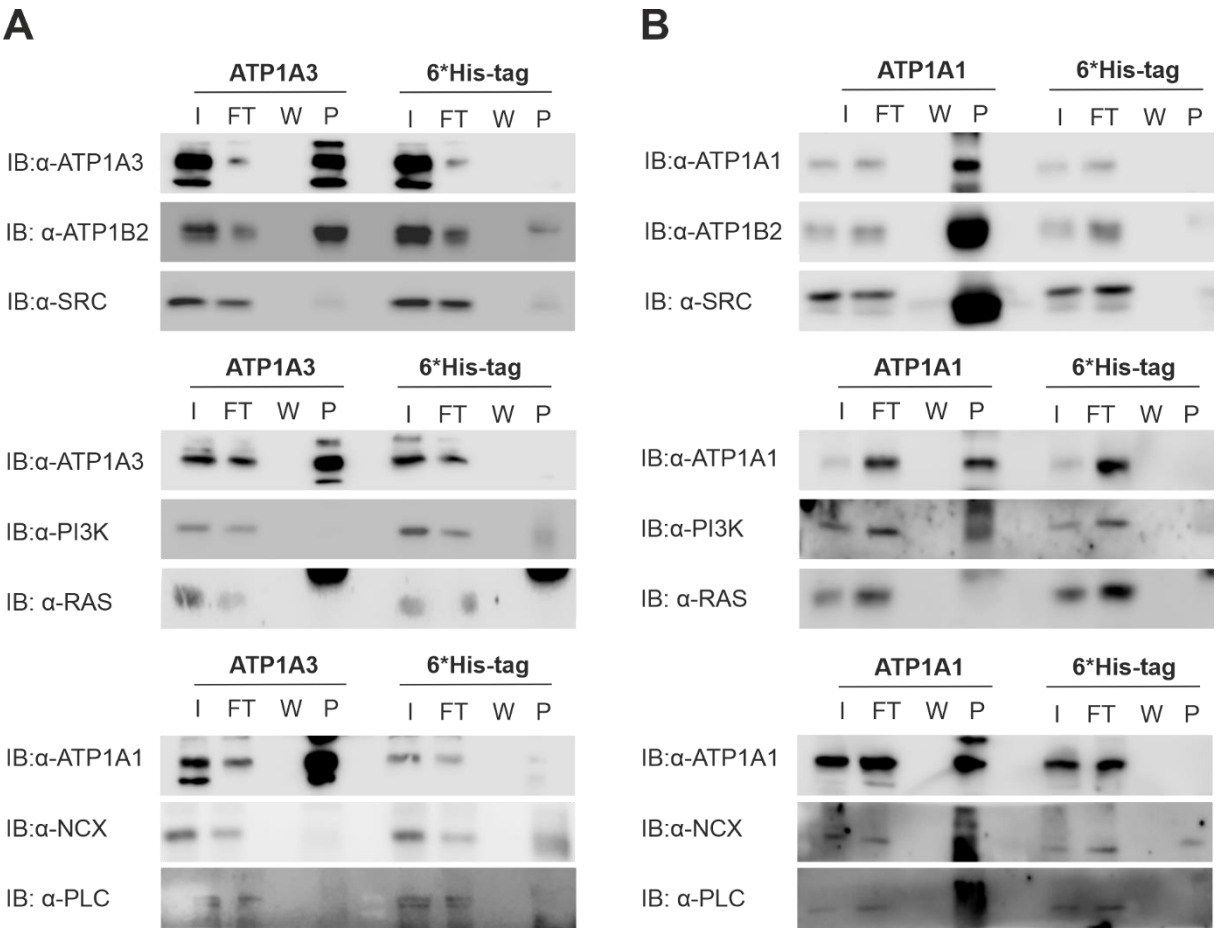

Figure 27: Co-Immunoprecipitation from porcine retinal lysates to test the interaction between ATP1A1-containing Na/K-ATPase complex associated proteins and the retinal Na/K-ATPase

Co-immunoprecipitations from porcine retinal lysates were performed with antibodies against ATP1A3 (**A**), ATP1A1 (**B**), and 6*His-tag as a control. Samples of input (I), flow through (FT), the last washing step (W), and precipitate (P, contains co-immunoprecipitated proteins) were stained with antibodies against ATP1A3, ATP1A1, ATP1B2, SRC, PI3K, RAS, NCX, and PLC.

4.3.1.2 Effect of retinoschisin-deficiency on the localization of retinal Na/K-ATPase interaction partner AnkyrinB

Kizhatil and colleagues (2009) presented evidence for a complex formation of the retinal Na/K-ATPase and AnkB in murine photoreceptor inner segments, with important consequences on the localization of this complex.

In the present work, co-immunoprecipitation analysis to confirm this direct interaction was not performed because the large molecular weight of AnkB (220 kDa) prevented the detection in SDS-PAGE separation.

Previous studies demonstrated that retinoschisin-deficiency affects the correct localization of the retinal Na/K-ATPase during murine retinal development with first visible differences occurring around P14 (Friedrich et al. 2011). Thus, an effect of retinoschisin-deficiency on AnkB localization was investigated in wildtype and retinoschisin-deficient mice from P4 to P30 as well, by measuring the AnkB signal intensity in inner segments and outer nuclear layer and calculating the ratio from inner segments to outer nuclear layer, r(IS/ONL). From P7 to P14, the distribution of AnkB in inner segments and outer nuclear layer was comparable in wildtype and retinoschisin-deficient mice with an r(IS/ONL) around 1.5 (**Figure 28A** and **B**). In contrast, from P18 onward, a significant difference in the distribution of AnkB was detected between wildtype and retinoschisin-deficient mice with an r(IS/ONL) of 2.74 + 0.22 in wildtype retinae compared to 1.62 + 0.29 in retinoschisin-deficient retinae at P18 ($P < 0.01$) (**Figure 28A** and **B**).

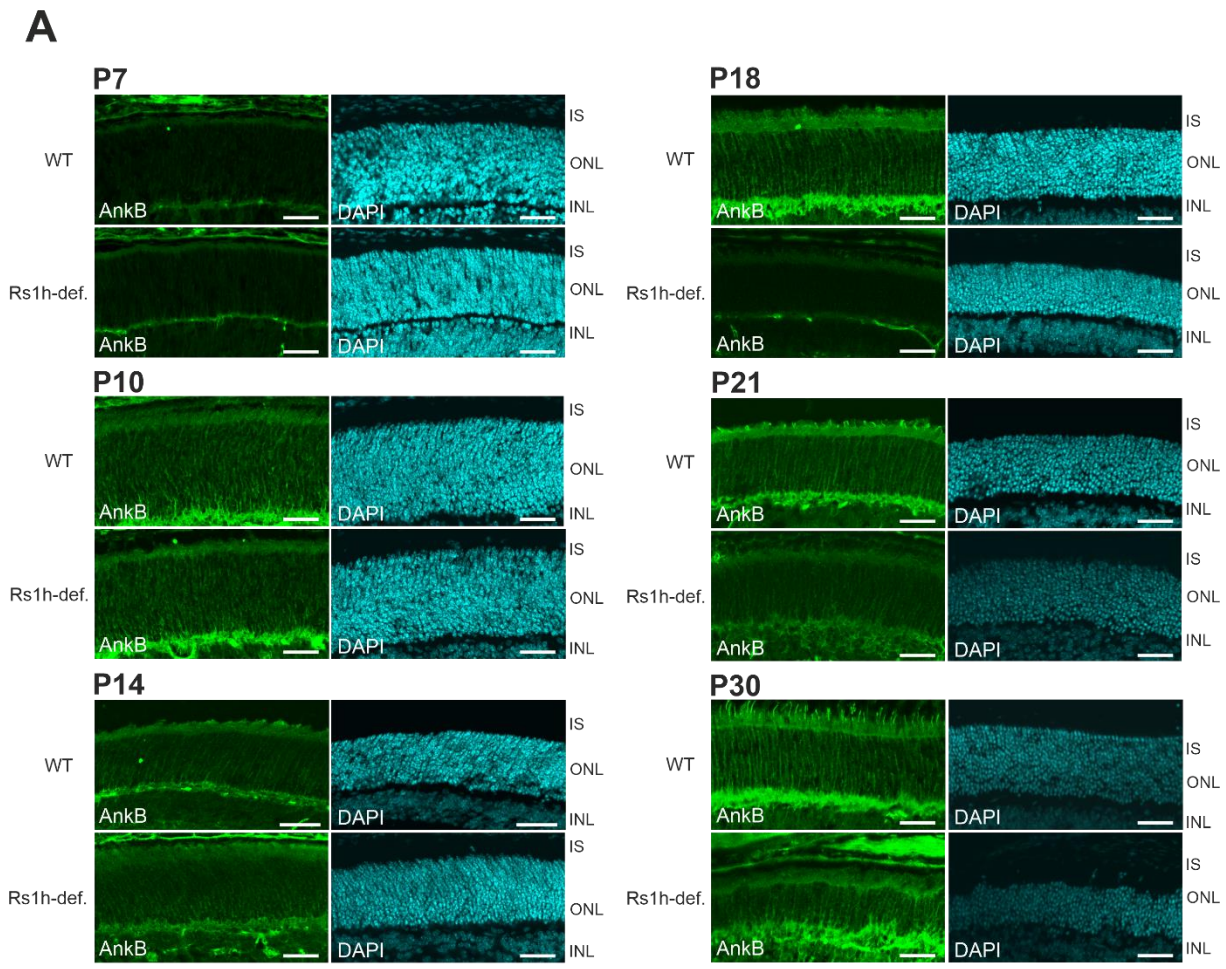

Figure 28: Localization of AnkB in the retina of wildtype and retinoschisin-deficient mice of different postnatal stages

A: Cryosections of eyes of wildtype (WT) and retinoschisin-deficient (Rs1h-def.) mice of different postnatal stages (P7, P10, P14, P18, P21, and P30) were subjected to staining with antibodies against AnkB (green), as well as DAPI staining (blue, depicting nuclei). Confocal microscopy was performed at 20x magnification. Scale bars: 40 µm; IS, inner segments; ONL, outer nuclear layer; INL, inner nuclear layer **B:** AnkB signals in the inner segments and outer nuclear layer were measured using ImageJ. Data show the ratio of signal intensity from inner to outer segments r(IS/ONL), given as mean + SD of five biological replicates. Asterisks represent statistically significant differences (*P < 0.05; two-tailed Student's t-test)

4.3.2 Nondirected approach: Mass spectrometric analysis of ATP1A3-targeted co-immunoprecipitation

As the targeted co-immunoprecipitation approach failed to reveal additional interaction partners of ATP1A3-containing Na/K-ATPases, a nondirected co-immunoprecipitation approach was chosen. After co-immunoprecipitations from porcine retinal lysates targeting ATP1A3 or 6*His-tag (control), the precipitates were subsequently analyzed using LC-MS/MS analysis. The workflow is illustrated in **Figure 29**.

First, the precipitates were loaded onto a NuPAGE gel and proteins were stained with Coomassie. All protein species detected (**Figure 29**, indicated with red arrows) were excised,

and subjected to LC-MS/MS analysis. The data were then mapped against the Swiss-Prot *Mammalian* database. From the unique proteins identified *via* the Mammalian database keratins, representing well-known impurities, were subtracted, leaving a total number of 436 identified proteins. Of these, 66 were detected only in the precipitate of the 6*His-tag control, 82 in both precipitates, and 288 only in the precipitate of ATP1A3 co-immunoprecipitation. Next, candidate prioritization of the 288 proteins was conducted to select suitable candidates for further laboratory testing. For candidate prioritization the following parameters were chosen a) for the Mascot-score a threshold of 100 was set, b) the number of peptides, which were identified in the precipitate, should be higher than 1. It should be mentioned that proteins with a Mascot-score below 100 can also be possible interaction partners, since the Mascot-score is defined as the sum of the individual peptides and can therefore be lower for very small proteins. Consequently, these proteins should also be considered in further data analysis. In addition to the specific mass spectrometric parameters, localization of the proteins in the retina (favoring an inner segment localization, close to the retinal Na/K-ATPase) and their function was included in the prioritization (**Figure 29**).

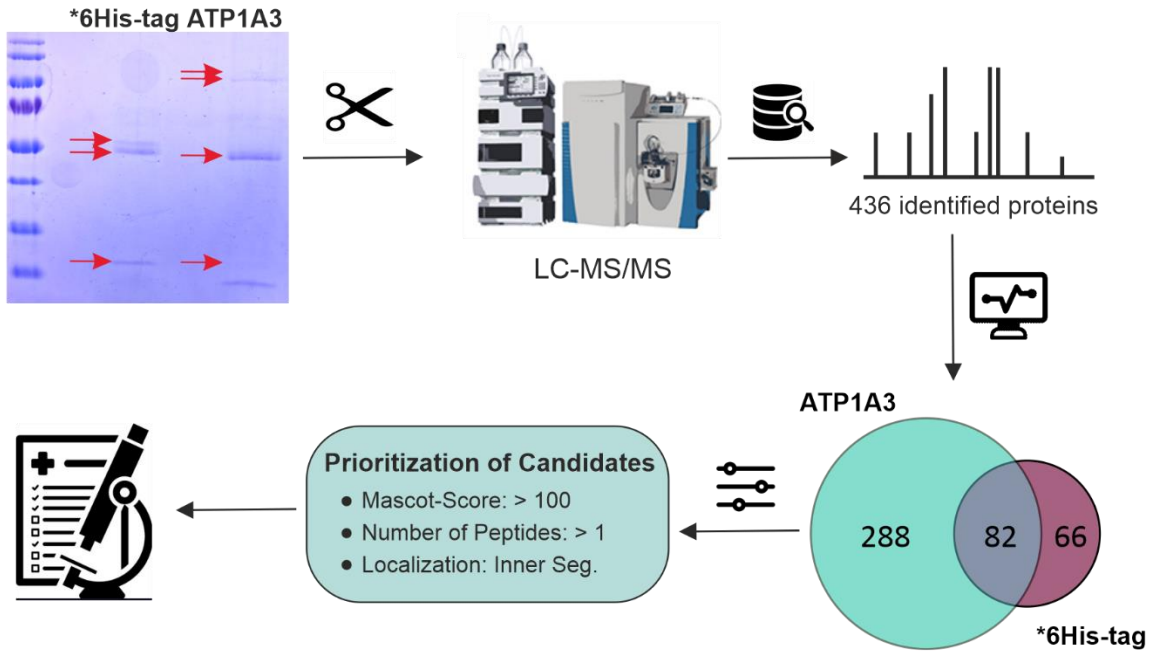

Figure 29: Workflow of the nondirected approach to identify new interaction partners of the retinal Na/K-ATPase *via* mass spectrometric analysis of the precipitate of the co-Immunoprecipitation from porcine retinal lysates targeting ATP1A3.

After applying prioritization parameters, the most promising interaction candidates were again mapped against the Swiss-Prot *Sus scrofa* database.

Table 32 shows the results for ATP1A3, ATP1B2, and retinoschisin (highlighted in grey), which were exclusively detected in the co-immunoprecipitation targeting ATP1A3, but not in the co-

immunoprecipitation targeting the 6*His-tag. It summarizes the ten most promising candidates for interaction partners of the retinoschisin-Na/K-ATPase complex (**Table 32**).

The ATP1A3 protein showed both the highest score and the highest number of identified peptides. ATP1B2 and retinoschisin were also detected, with a score above 100 and more than one identified peptide (**Table 32**), demonstrating the capacity of the co-immunoprecipitation approach to precipitate ATP1A3-interacting proteins (like ATP1B2) and proteins attached to ATP1A3 binding proteins (like the ATP1B2 binding partner retinoschisin).

In this study, three of the ten most promising candidates were selected for first laboratory analysis, due to their functional relevance and localization in the retina (**Table 32**, highlighted in light green): The voltage-gated potassium channel subfamily B member 1 (Kv2.1 or KCNB1), the voltage-gated potassium channel subfamily V member 2 (Kv8.2 or KCNV2), and AnnexinA2 (ANXA2).

Table 32: Overview of the ten most promising interaction partners of the retinal Na/K-ATPase, examined *via* co-immunoprecipitation targeting ATP1A3 and *6His-tag as a control and subsequent mass spectrometric analysis of the precipitates from porcine retinal lysates, and additional prioritization.

Listed are the identified proteins (LC-MS/MS data mapped against Swiss-Prot *Sus scrofa* database), their gene name, mass spectrometric parameters such as Mascot-score, the number of identified peptides (Pept.) and the sequence coverage (SC %) score as well as the protein function. Proteins of the retinoschisin-Na/K-ATPase complex are highlighted in light grey, and proteins, which were further analyzed in this work, are highlighted in light green

Protein	Gene	Mascot-score	Pept.	SC [%]	Protein Function
ATP1A3	*ATP1A3*	5503.6	67	43.2	See 1.2
ATP1B2	*ATP1B2*	785.6	11	32.1	See 1.2
Retinoschisin	*RS1*	212.9	4	18.9	See 1.1.2 and 1.1.5
Voltage-gated potassium channel subfamily B member 1 (Kv2.1)	*KCNB1*	362.9	7	12.8	Kv2.1 and Kv8.2, are high-voltage activated and they generate delayed rectifier Kv currents that regulate the rate and repolarization of action potentials (Liu and Bean 2014). Kv2.1 and Kv8.2 form heterotetrametric complexes in photoreceptor inner segments (Gayet-Primo et al. 2018).
Voltage-gated potassium channel subfamily V member 2 (Kv8.2)	*KCNV2*	217.3	4	6.4	
AnnexinA2 (ANXA2)	*ANXA2*	361.9	5	18	Annexins are cytosolic proteins, with a soluble and a stable form, which reversibly interacts with components of the cell membrane (Mirsaeidi et al. 2016). AnxA2 is involved in many processes, including organization of specialized membrane microdomains, signal transduction, and regulation of additional membrane dynamic events (Moss and Morgan 2004; Jiang and Xu 2019; Dallacasagrande and Hajjar 2020).
Enolase-1	*ENO1*	1259.4	17	56.6	Enolase 1 is a glycolytic enzyme and thus plays an important role in the cellular energy metabolism (Wold and Ballou 1957). It is also involved in the regulation of dynamics of cytoskeletal filaments (Keller et al. 2007), signaling cascades (Dai et al. 2018), or stress responses (Graven et al. 1993).
S-Arrestin	*SAG*	695.0	11	53.1	S-Arrestin 1 is involved in multiple signaling pathways and desensitizes rod photoreceptors by the small G-protein in rods from binding to phosphorylated rhodopsin (Hanson et al. 2007).
Aminopeptidase B	*RNPEP*	245.5	6	9,1	Aminopeptidase B is a ubiquitous enzyme, and it catalyzes the amino-terminal cleavage of basic residues of peptide or protein substrates, indicating a role in precursor processing.

					The physiological role is still not clear, but preliminary analysis of rat retina analysis indicates that Aminopeptidase B, the glucose transporter GLUT3 and choline acetyltransferase share a similar expression pattern in retina (Piesse et al. 2004).
Lamin B1	*LMNB1*	271,2	6	14.5	Lamins are components of the nuclear lamina, a fibrous layer on the nucleoplasmic side of the inner nuclear membrane. Lamin B1 and lamin B2 have crucial but distinct functions in the development of the retina. In specific, lamin B1 is extremely important for the survival of retinal neurons (Razafsky et al. 2016).
Vinculin	*VCL*	108.0	2	3.1	The focal adhesion protein vinculin is an actin filament-binding protein involved in cell-matrix adhesion and cell-cell adhesion and it may also play important roles in cell morphology and locomotion (Le Clainche et al. 2010).
Arginase-1	*ARG1*	157.5	4	11.5	Arginase is mainly expressed in the liver, where it plays an essential role in the urea cycle. In the retina, arginase activity mediates retinal inflammation in endotoxin-induced uveitis (Zhang et al. 2009).
Rab GDP dissociation inhibitor beta	*GDI2*	162.2	3	11.2	Rab GDP dissociation inhibitors (GDIs)1 are relatively abundant cytosolic proteins that bind prenylated Rab-GTPases. GDIs have the capacity to deliver Rab proteins to their specific membrane-bound compartments (Pfeffer et al. 1995).

4.3.3 Studies on voltage-gated potassium channel subunits Kv2.1 and Kv8.2 as possible interaction partners of the retinoschisin-Na/K-ATPase complex

4.3.3.1 Analysis of Na/K-ATPase and Kv channel subunits Kv2.1 and Kv8.2 interaction in murine retinae

To verify the interaction between the retinal Na/K-ATPase and Kv channel subunits Kv2.1 and Kv8.2 observed in the undirected porcine co-immunoprecipitation experiment (**Table 32**), murine retinal lysates were subjected to co-immunoprecipitation analysis with antibodies against Atp1a3 (**Figure 30A**). The precipitate was analyzed for Kv2.1 and Kv8.2 (as well as Atp1a3, Atp1b2, and retinoschisin as positive controls) *via* western blot analysis.

Kv2.1 (molecular weight = 120 kDa) and Kv8.2 (molecular weight = 65 kDa) were detected in the precipitate of the co-immunoprecipitation targeting Atp1a3, together with Atp1b2 and retinoschisin. In control experiments targeting 6*His-tag, Kv2.1, Atp1b2, and retinoschisin were absent from the precipitate (**Figure 30A**). In contrast, immunostaining against Kv8.2 revealed a signal with a slightly reduced molecular weight compared to Kv8.2 in the precipitate of the 6*His-tag co-immunoprecipitation, which is most likely explained by unspecific detection of the heavy chains of the antibodies (Kv8.2 = 65 kDa, heavy antibody chain = 55 kDa).

Additional co-immunoprecipitation experiments were performed targeting Kv2.1 (**Figure 30B**) or Kv8.2 (**Figure 30C**). In both experiments, the two subunits of the retinal Na/K-ATPase (Atp1a3 and Atp1b2), retinoschisin, and the corresponding Kv channel subunit were precipitated with Kv2.1 and Kv8.2, respectively. Again, control experiments using 6*His-tag antibodies did not reveal any of these proteins in the precipitate (**Figure 30B** and **C**).

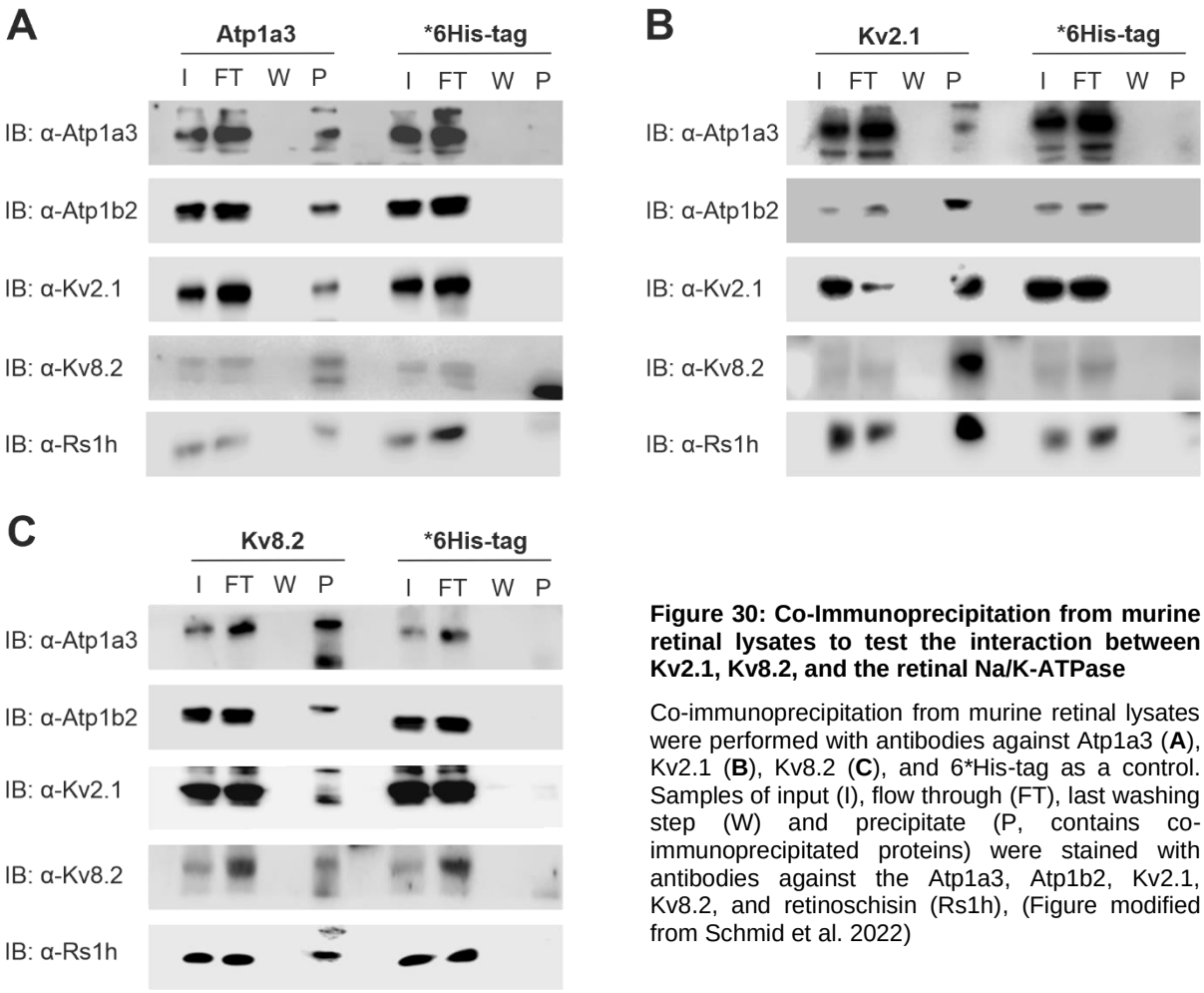

Figure 30: Co-Immunoprecipitation from murine retinal lysates to test the interaction between Kv2.1, Kv8.2, and the retinal Na/K-ATPase

Co-immunoprecipitation from murine retinal lysates were performed with antibodies against Atp1a3 (**A**), Kv2.1 (**B**), Kv8.2 (**C**), and 6*His-tag as a control. Samples of input (I), flow through (FT), last washing step (W) and precipitate (P, contains co-immunoprecipitated proteins) were stained with antibodies against the Atp1a3, Atp1b2, Kv2.1, Kv8.2, and retinoschisin (Rs1h), (Figure modified from Schmid et al. 2022)

4.3.3.2 Localization of the retinoschisin-Na/K-ATPase-Kv channel complex in murine retina

In a next step, (co-)localization of Kv2.1, Kv8.2 and the retinal Na/K-ATPase was investigated. As both Kv channel subunits were primarily detected in photoreceptor inner segments in previous analyses (Gayet-Primo et al. 2018), a close-up confocal microscopic analysis was performed focusing on the inner segments after immunohistochemical staining of retinal cryosections. As shown in **Figure 31A** and **B**, Kv2.1 as well as the constituents of retinoschisin-Na/K-ATPase complex, Atp1a3, Atp1b2, and retinoschisin, are clearly localized in the plasma membrane of the photoreceptor inner segments. Kv8.2 signals were rather weak and punctate, and, while labeling in the inner segments was obvious, membrane localization could not be confirmed with this experiment (**Figure 31B**). The co-labeling of the Kv channel subunits and the Atp1b2 subunit of the retinal Na/K-ATPase revealed an extensive overlap of Kv2.1 with Atp1b2 signals in the plasma membrane of the inner segments (white overlay signals in **Figure 31C**, right panel). Kv8.2 was also found to co-localize with Atp1b2 (white overlay signals in **Figure 31D**, right panel), but to a lesser extent due to weaker and punctuate Kv8.2 staining.

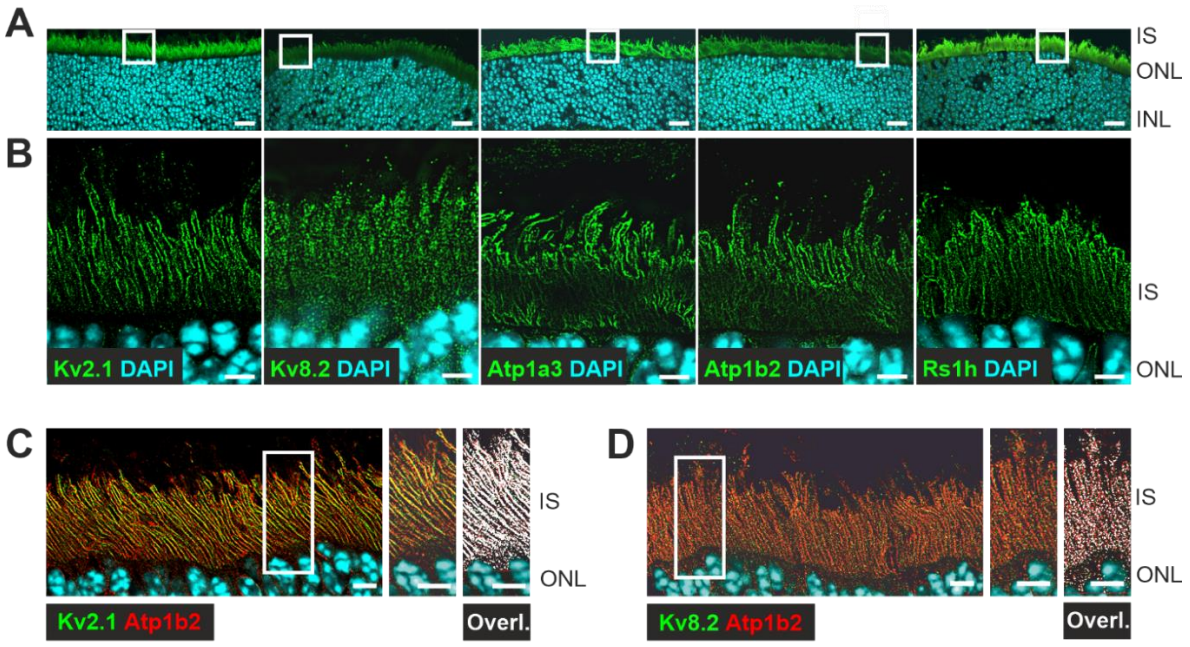

Figure 31: Localization and co-localization analysis of the retinoschisin-Na/K-ATPase-Kv channel complex in the photoreceptor inner segments

Cryosections of eyes from wildtype mice (postnatal day 18) were analyzed *via* confocal microscopy (60x magnification) after immunohistochemical staining. Nuclei were visualized with DAPI staining (blue). IS, inner segments; ONL, outer nuclear layer. **A**, **B**: Immunohistochemical staining with antibodies against Kv2.1, Kv8.2, Atp1a3, Atp1b2 and retinoschisin (Rs1h, green). **A**: Overview images show the distribution of the complex partners in the murine outer retina. Scale bars: 20 µm. Regions of subsequent close-up images shown in (**B**) are marked by white boxes. **B**: Close-up images focusing on photoreceptor inner segments. Scale bars: 5 µm. **C, D:** Immunohistochemical staining with antibodies against Kv2.1 (**C**) or Kv8.2 (**D**) (green) and Atp1b2 (red). Overview images (left panels) show the localization of the Kv channels Kv2.1 (**C**) and Kv8.2 (**D**) and Atp1b2 in the inner segments. Scale bars: 5 µm. Regions of subsequent close-up images shown in the right panels are marked by white boxes. Close-up images (right panels) show the overlap (white coloration) of signals for the Kv channels Kv2.1 or Kv8.2 and Atp1b2. Scale bars: 5 µm. (Figure modified from Schmid et al. 2022)

To further confirm the interaction between the retinal Na/K-ATPase, Kv2.1, and Kv8.2, immunohistochemical stainings were performed with murine retinal cryosections from wildtype and Atp1b2-deficient retinae (AMOG mouse) at different postnatal stages (P10, P14, and P18). As described before (Friedrich et al. 2011) wildtype murine retinae showed strong Atp1a3 and Atp1b2 signals in photoreceptor inner segments with increasing intensity during retinal maturation (**Figure 32A** and **B**). Atp1a3 and Atp1b2 immunolabeling of synaptic contacts in outer nuclear layer, outer, and inner plexiform layers was observed as well, but to a lesser extent. In contrast, Atp1b2-deficient mice exhibited very weak or no signals for both retinal Na/K-ATPase subunits Atp1a3 and Atp1b2 in the photoreceptor inner segments, and only residual signals of Atp1a3 at the outer nuclear layer (**Figure 32A** and **B**). Wildtype mice exhibited strong immunolabeling of Kv2.1 and Kv8.2 in the inner segments (increasingly with age) and much weaker staining in the outer nuclear and outer plexiform layer (**Figure 32C** and **D**). As illustrated in **Figure 32C** and **D**, Atp1b2-deficient mice showed a strong reduction in the signals for both Kv channels (Kv2.1 and Kv8.2) in photoreceptor inner segments and an increase in the outer nuclear layer compared to wildtype mice. This effect was observed in all analyzed postnatal stages but was most pronounced at P18.

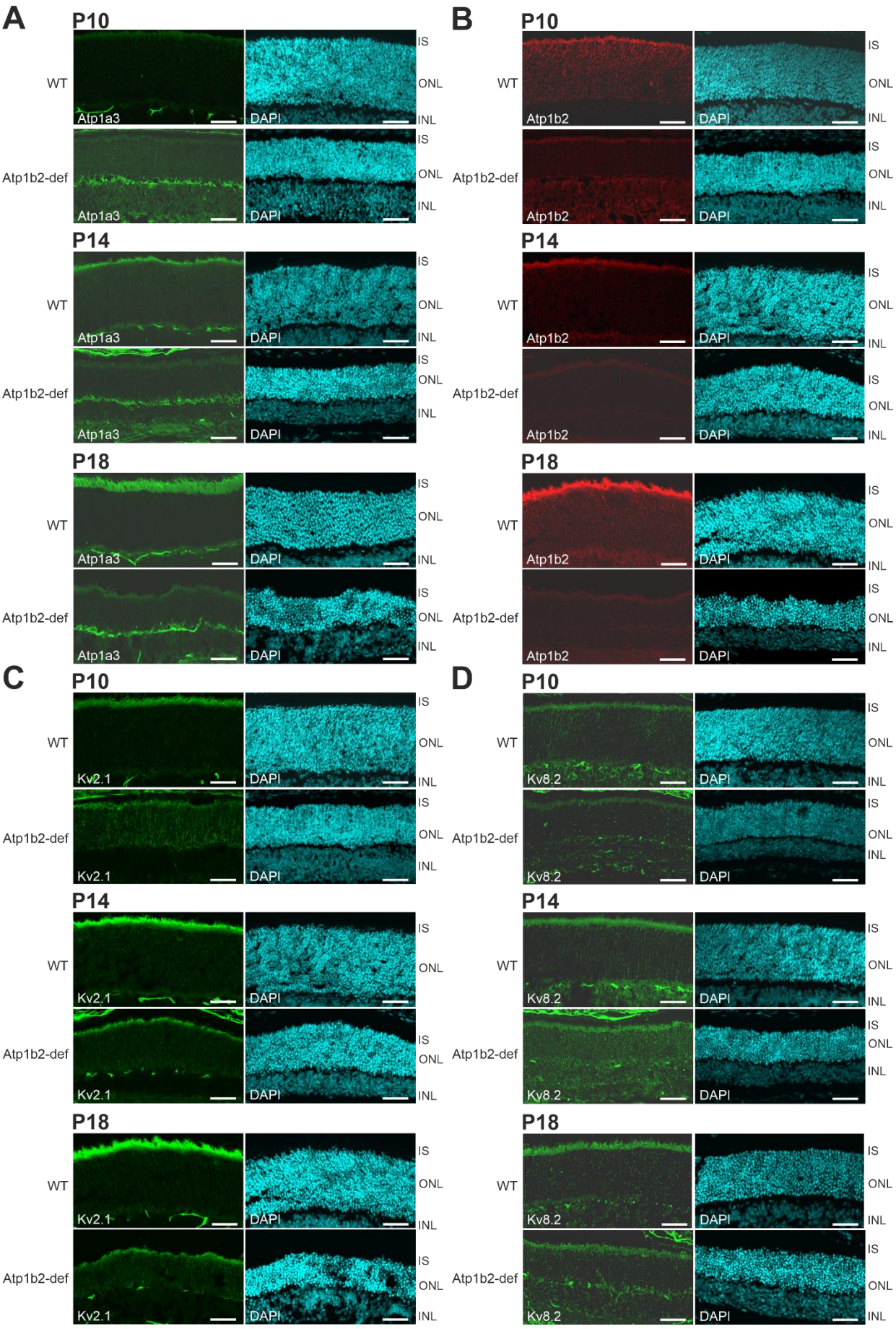
A
P10
WT
Atp1b2-def
Atp1a3
DAPI
IS
ONL
INL
P14
P18
B
Atp1b2
C
Kv2.1
D
Kv8.2

Figure 32: Localization of the retinoschisin-Na/K-ATPase-Kv channel complex in the retina of wildtype and Atp1b2-deficient mice of different postnatal stages

Cryosections of eyes from wildtype (WT) and Atp1b2-deficient (Atp1b2-def.) mice of different postnatal stages (P10, P14, and P18) were subjected to staining with antibodies against Atp1a3 (green) (**A**), Atp1b2 (red) (**B**), Kv2.1 (green) (**C**), Kv8.2 (green) (**D**), as well as DAPI staining (blue, depicting nuclei). Confocal microscopy was performed at 20x magnification. Scale bars: 40 µm; IS, inner segments; ONL, outer nuclear layer; INL, inner nuclear layer. (Figure modified from Schmid et al. 2022)

4.3.3.3 Effect of retinoschisin-deficiency on the localization of Kv2.1 and Kv8.2 in the murine retina

Comparable to the localization analysis of AnkB (4.3.1.2), the consequences of retinoschisin-deficiency were also investigated for Kv2.1 and Kv8.2 in retinal cryosections of wildtype and retinoschisin-deficient mice at different postnatal stages from P4 to P30. After immunolabeling with antibodies against Kv2.1 and Kv8.2, the signal intensities of Kv2.1 and Kv8.2 in inner segments and outer nuclear layer were measured as the ratio from inner segments to outer nuclear layer, “r(IS/ONL)”.

Similar to the retinal Na/K-ATPase, the Kv2.1 and Kv8.2 immunolabeling increased in the photoreceptor inner segments with increasing age (r (IS/ONL) from around 1 at P4 to around 4 at P14 and this process was negatively affected by retinoschisin-deficiency (**Figure 33A** and **Figure 34A**). Notably, the effect of retinoschisin-deficiency on Kv channel localization occurred earlier than on retinal Na/K-ATPase localization: A statistically significant difference in the r(IS/ONL) of Kv2.1 between wildtype and retinoschisin-deficient mice was already obvious at P7 (**Figure 33B**, r (IS/ONL) = 2.55 + 0.37 in wildtype retinae compared to 1.40 + 0.25 in retinoschisin-deficient retinae, $p < 0.01$) and at P14 for Kv8.2 (**Figure 34B,** r (IS/ONL) = 4.63 + 0.42 in wildtype retinae compared to 2.08 ± 0.33 in retinoschisin-deficient retinae, $p < 0.01$).

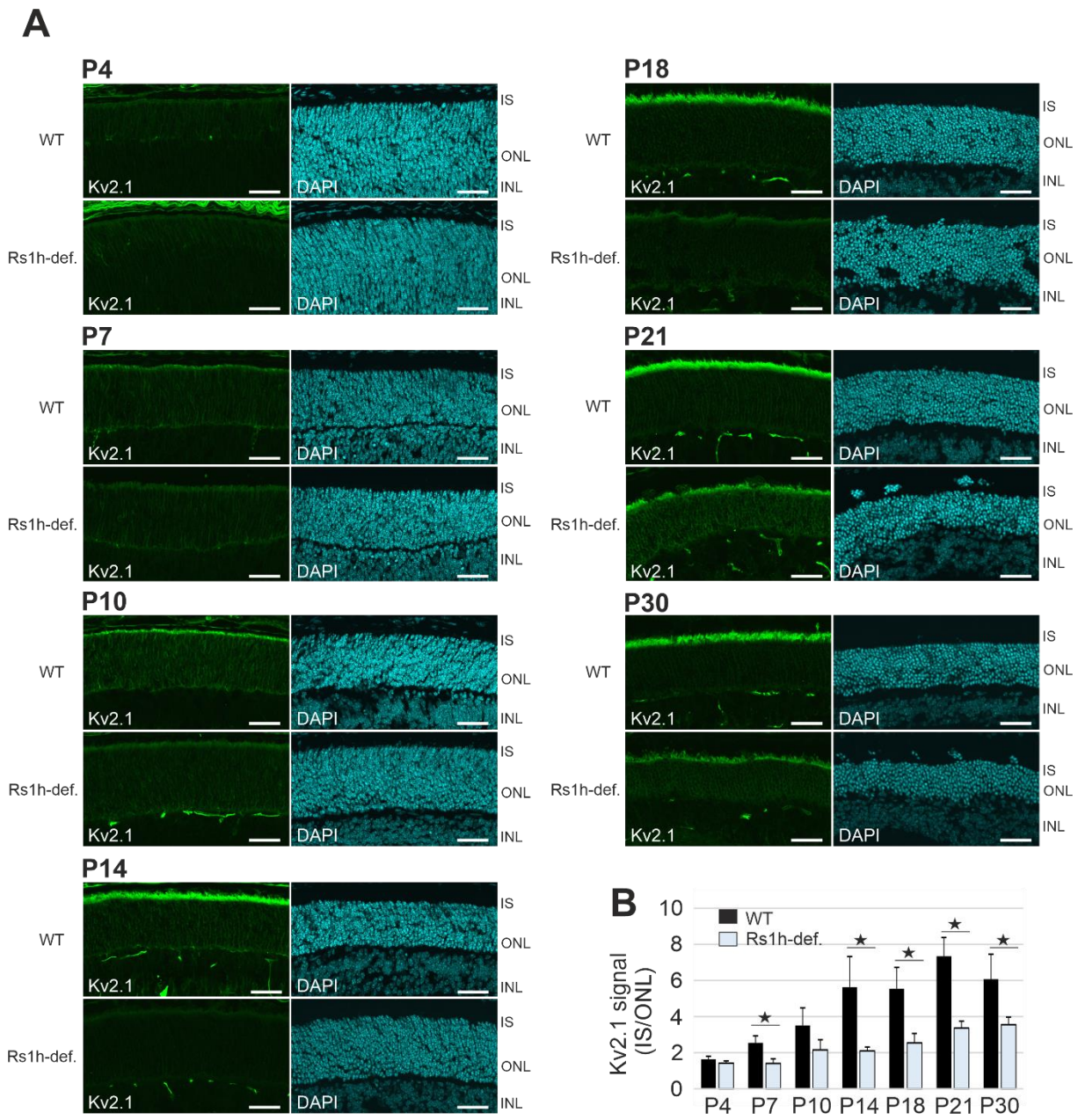

Figure 33: Localization of Kv2.1 in the retina of wildtype and retinoschisin-deficient mice of different postnatal stages.

A: Cryosections of eyes from wildtype (WT) and retinoschisin-deficient (Rs1h-def.) mice of different postnatal stages (P4, P7, P10, P14, P18, P21, and P30) were subjected to staining with antibodies against Kv2.1 (green), as well as DAPI staining (blue, depicting nuclei). Confocal microscopy was performed at 20x magnification. Scale bars: 40 µm; IS, inner segments; ONL, outer nuclear layer; INL, inner nuclear layer **B:** Kv2.1 signals in the inner segments and outer nuclear layer were measured using ImageJ. Data show the ratio of signal intensity from inner to outer segments r(IS/ONL), given as mean + SD of five biological replicates. Asterisks represent statistically significant differences (*P < 0.05; two-tailed Student's t-test). (Figure modified from Schmid et al. 2022)

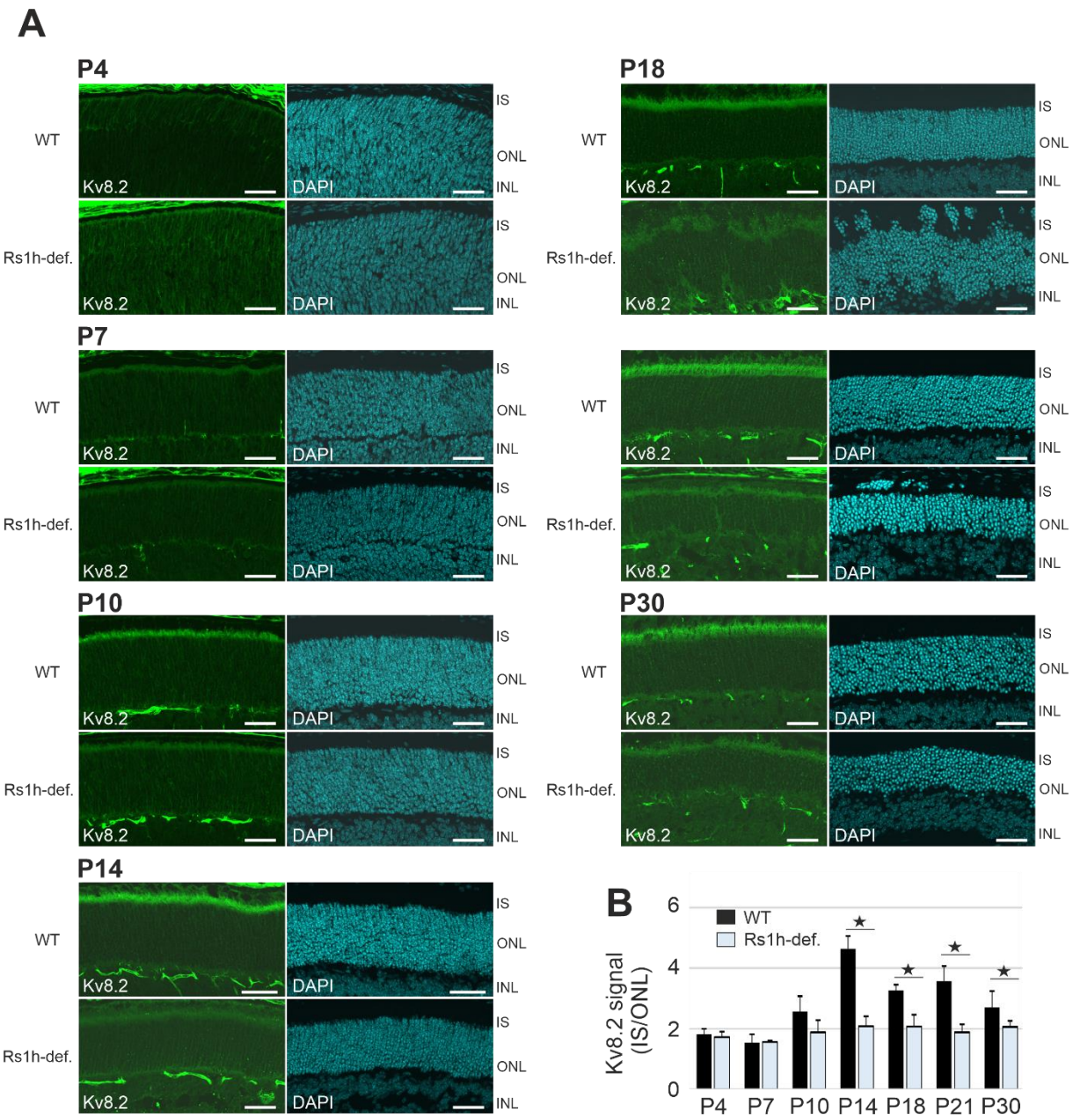

Figure 34: Localization of Kv8.2 in the retina of wildtype and retinoschisin-deficient mice of different postnatal stages.

A: Cryosections of eyes from wildtype (WT) and retinoschisin-deficient (Rs1h-def.) mice of different postnatal stages (P4, P7, P10, P14, P18, P21, and P30) were subjected to staining with antibodies against Kv8.2 (green), and to DAPI staining (blue, depicting nuclei). Confocal microscopy was performed at 20x magnification. Scale bars: 40 µm; IS, inner segments; ONL, outer nuclear layer; INL, inner nuclear layer **B:** Kv8.2 signals in the inner segments and outer nuclear layer were measured using ImageJ. Data show the ratio of signal intensity from inner to outer segments r(IS/ONL), given as mean + SD of five biological replicates. Asterisks represent statistically significant differences (*P < 0.05; two-tailed Student's t-test). (Figure modified from Schmid et al. 2022).

4.3.3.4 Effect of retinoschisin-deficiency on the protein level of Kv2.1 and Kv8.2 in the murine retina

As retinoschisin-deficiency was shown to differently affect localization of the retinal Na/K-ATPase and the Kv channels, the next assay addressed a putative effect of retinoschisin on the protein levels of the complex partners. Therefore, retinae of wildtype and retinoschisin-

deficient mice from P10, P14, P18, P21, and P30 were solubilized and subjected to western blot analysis.

In line with a previous analysis at the Institute of Human Genetics (Friedrich et al. 2011), no differences in the total protein amount of Atp1a3 and Atp1b2 were detected between retinal lysates from wildtype and retinoschisin-deficient mice at all developmental stages analyzed (**Figure 35A-C**). In contrast, retinoschisin-deficiency led to a statistically significant reduction ($p < 0.05$) of approximately 50% of Kv2.1 protein levels from P14 onward (**Figure 35A** and **D**) and to approximately 40% of Kv8.2 protein levels ($p < 0.05$) from P18 onward (**Figure 35A** and **E**).

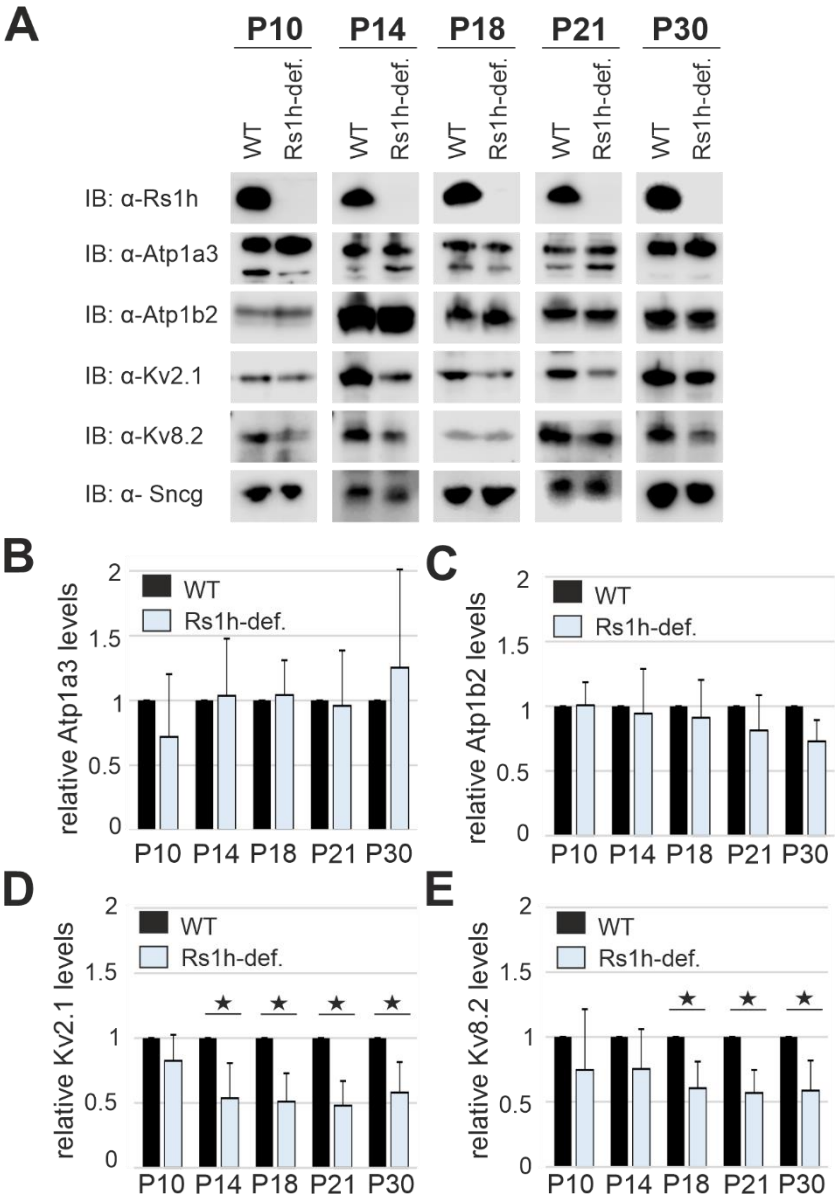

Figure 35: Total protein level of Atp1a3, Atp1b2, Kv2.1, and Kv8.2 in retinae from wildtype and retinoschisin-deficient mice of different postnatal stages

A: The total protein amount of Atp1a3, Atp1b2, Kv2.1 and Kv8.2 in retinal lysates of wildtype (WT) and retinoschisin-deficient (Rs1h-def.) mice of different postnatal stages (P10, P14, P18, P21, and P30) was evaluated by western blot analysis with antibodies against Atp1a3, Atp1b2, Kv2.1, and Kv8.2. Sncg staining served as loading control, retinoschisin (Rs1h) staining was used for genotype verification. **B-E**: Densitometric quantification of Atp1a3 (**B**), Atp1b2 (**C**), Kv2.1 (**D**), and Kv8.2 (**E**) signals. Signals were normalized to sncg and calibrated against the signals obtained in the wildtype retinae of the corresponding postnatal stage. Data show the mean + SD of five biological replicates. Asterisks represent statistically significant differences (*P < 0.05, Mann-Whitney U test). (Figure modified from Schmid et al. 2022).

4.3.3.5 Effect of retinoschisin-deficiency on gene expression of the identified complex components in murine retinae

To test whether the decreased protein expression observed for Kv2.1 and Kv8.2 in retinoschisin-deficient retinae from P14 on are caused by altered gene expression of *Kcnb1* (encoding for Kv2.1), and *Kcnv2* (encoding for Kv8.2), the transcription of *Atp1a3*, *Atp1b2*, *Kcnb1*, and *Kcnv2* in retinae of wildtype and retinoschisin-deficient mice were determined. Quantitative RT-PCR revealed no statistically significant differences in the mRNA levels of *Atp1a3, Atp1b2, Kcnb1*, and *Kcnv2* between wildtype and retinoschisin-deficient retinae form P14 to P21 (**Figure 36A-D**), excluding an effect of retinoschisin on the gene expression of these components. Only at P14, retinoschisin-deficiency induced a slight and statistically significant increase in the mRNA expression of *Atp1b2*. However, this effect was not reflected in the protein levels (**Figure 35A** and **C**).

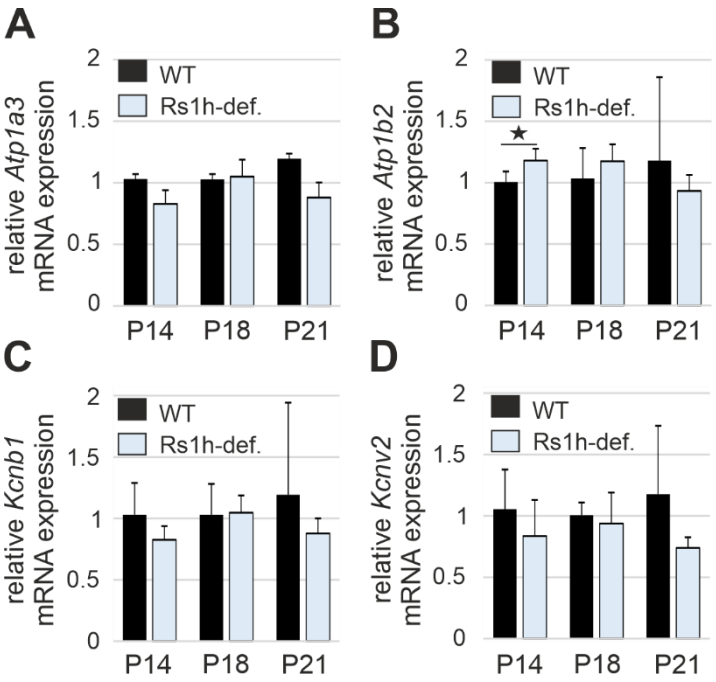

Figure 36: mRNA expression of *Atp1a3*, *Atp1b2*, *Kcnb1*, and *Kcnv2* in retinae of wildtype and retinoschisin-deficient mice of different postnatal stages

Atp1a3 (**A**), *Atp1b2* (**B**), *Kcnb1* (**C**), and *Kcnv2* (**D**) mRNA expression was determined in murine wildtype (WT) and retinoschisin-deficient (Rs1h-def.) retinae from different postnatal stages (P14, P18, P21) *via* qRT-PCR. Values were normalized to *sncg* transcript levels and calibrated against the wildtype. Data represent the mean + SD of six biological replicates, statistical evaluation was performed applying the Mann-Whitney U test. (Figure modified from Schmid et al. 2022).

4.3.3.6 Effect of retinoschisin-deficiency on Kv Channel mediated potassium ion currents

In mice, the permanent potassium outward current in photoreceptors arises from Kv2.1 and Kv8.2 as continuously active Kv channels (Gayet-Primo et al. 2018). To test whether retinoschisin modulates the potassium ion current mediated by Kv channels, patch-clamp analyses on Y-79 cells incubated with or without retinoschisin were performed. Y-79 cells were used for these analyses, as they endogenously express Kv2.1, Kv8.2 (**Figure 37A**), as well as ATP1A3 and ATP1B2, but not retinoschisin (**Figure 37A**) (Plössl et al. 2017a). All patch-clamp recordings were performed with a defined protocol: The holding potential was set to -60 mV

and voltage steps between -60 mV to 80 mV in 10 mV increments were applied (**Figure 37B**). The two parameters “Maximum” ion outflow (**Figure 37C**, indicated by a black rhombus) and “Mean End” (**Figure 37C**, indicated by a grey rhombus), the latter defined as the average calculated at the end of the measurement, were analyzed. Representative current traces of the different measurements are given in **Figure 37C**.

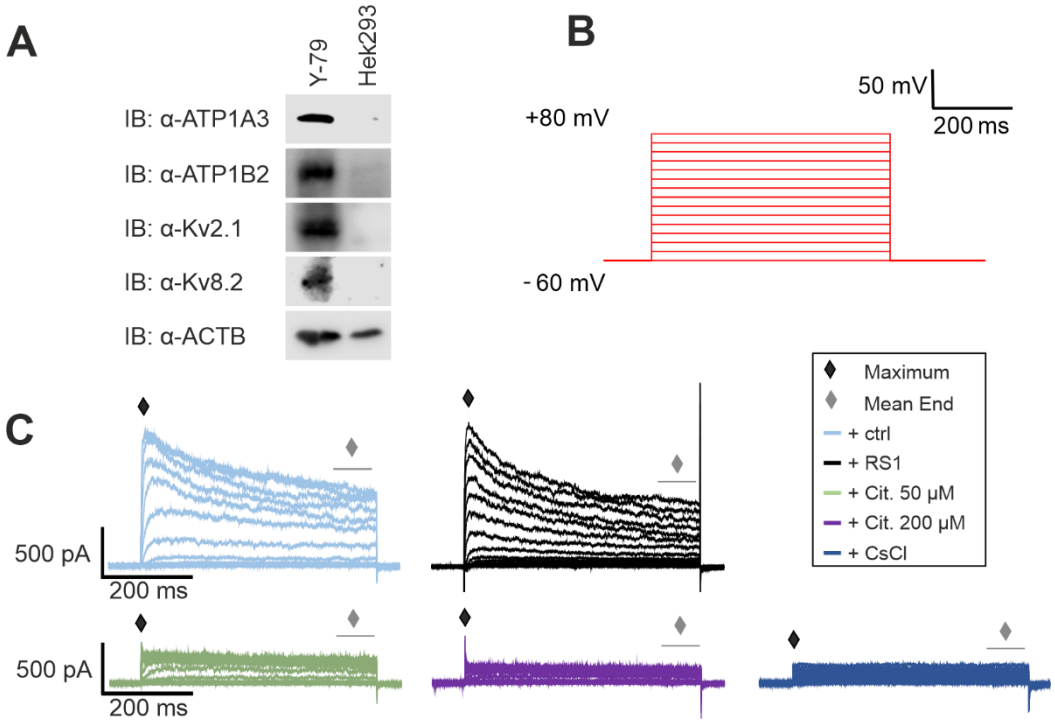

Figure 37: Expression analysis in Y-79 cells and representative current traces of patch-clamp analysis

A: Protein expression analysis of ATP1A3, ATP1B2, Kv2.1, and Kv8.2 in lysates of Y-79 and Hek293 cells *via* western blot analysis with antibodies against the specified proteins. ACTB staining served as loading control. **B**: Patch-clamp recording protocol of the performed analysis. The holding potential was set to -60 mV and voltage steps between -60 mV to 80 mV in 10 mV increments were applied. **C:** Representative current traces of Y-79 cells incubated with control eluate (+ ctrl, light blue), retinoschisin (+ RS1, black) or with the inhibitors citalopram (50 µM, green; 200 µM, purple) or CsCl (130 mM, dark blue) for 24 h. The two analyzed parameters “Maximum” (black rhombus) and “Mean End” (grey rhombus), the latter defined as the average calculated at the end of the measurement (grey line) are highlighted. (Figure modified from Schmid et al. 2022).

In a first step, patch-clamp recordings were performed in the presence of the potassium channel blocker cesium chloride (130 mM in the intracellular solution, replacing K^+) to test the specificity of this approach. As shown in **Figure 37C** (representative current traces) and **Figure 38A** and **B** no outward current was recorded, even at the highest potential of 80 mV. Furthermore, the specific Kv2 channel inhibitor citalopram (Gayet-Primo et al. 2018) was used for additional control experiments. Citalopram inhibited the recorded outward currents, in a dose-dependent manner, with 200 µM leading to a strong blocking of outward current (**Figure 37C** and **Figure 38A** and **B**).

Next, voltage-clamp recordings were conducted to investigate a possible effect of retinoschisin on the Kv mediated potassium ion current. Cells were incubated for 24 h (**Figure 38C** and **D**) or 48 h (**Figure 38E** and **F**) with or without purified recombinant retinoschisin before patch-

clamp recordings were started. After 24 h of incubation, retinoschisin did not affect the maximum outward current (**Figure 38C**) as well as the mean end (**Figure 38D**) in Y-79 cells. The curve progressions, showing an increasing ion current from an applied depolarization of -10 mV, were also similar for both conditions (**Figure 38C** and **D**). Similarly, after 48 h of incubation, no differences were observed in Y-79 cells incubated with retinoschisin or control eluate in the maximum outward current (**Figure 38E**), the mean end (**Figure 38F**), and the curve progressions (**Figure 38E** and **F**).

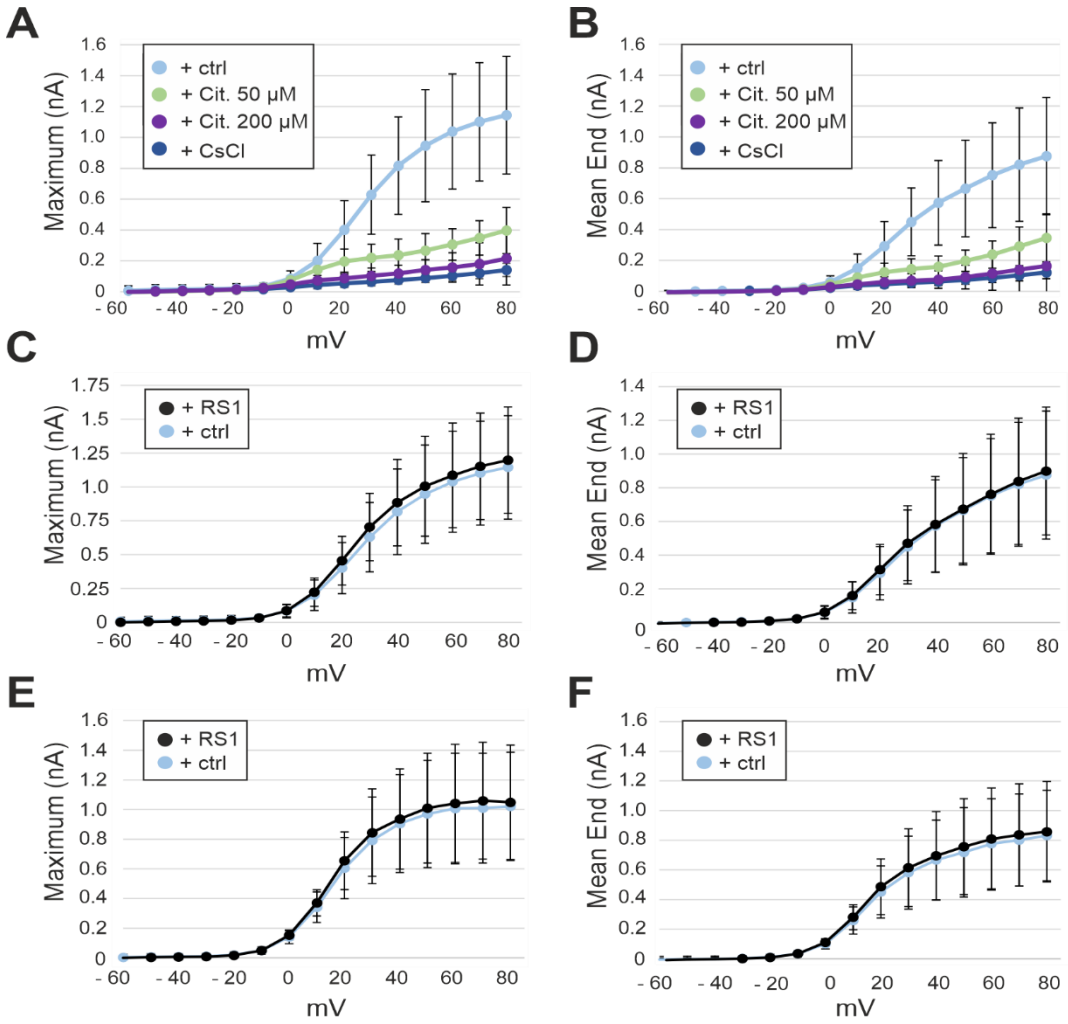

Figure 38: Patch-clamp analysis of Y-79 cells to analyze the effect of retinoschisin on Kv channel mediated potassium ion current

A; B: Effect of Kv channel inhibitors CsCl (+ CsCl, 130 mM, dark blue, n= 11) and citalopram (+ "Cit."50 µM, green, n = 10; 200 µM, purple, n = 6) Light blue circles indicate measurements without inhibitors (+ ctrl, n = 47). Average (± SD) voltage-gated Maximum currents (**A**) or Mean End (**B**) in response to voltage steps from a holding potential of -60 mV to 80 mV. (**C-F**): Effect of retinoschisin on Kv channel currents, after 24 h (**C** and **D**) and 48 h (**E** and **F**). Average (± SD) voltage-gated Maximum currents (**C** and **E**) or Mean End (**D** and **F**) in response to voltage steps from a holding potential of -60 mV to 80 mV. Light blue circles: cells incubated with control eluate (+ctrl, = 47 for 24 h, n = 26 for 48 h); Black circles: cells incubated with purified retinoschisin (+RS1, n = 53 for 24 h, n = 31 for 48 h). Statistical evaluation was performed applying the Mann-Whitney-U Test. (Figure modified from Schmid et al. 2022).

4.3.3.7 Effect of retinoschisin-deficiency on the intracellular calcium-level in Y-79 cells

Fortenbach and colleagues (2021) demonstrated that Kv2.1 channel activity also affects intracellular Ca^{2+}-levels in photoreceptors. Intracellular Ca^{2+}-levels were determined in Y-79 cells incubated with or without recombinant retinoschisin, measuring intracellular Ca^{2+} *via* Fura-2 staining. Fura-2 is a radio-metric dye, which changes its excitation spectra in response to Ca^{2+} binding. When intracellular Ca^{2+} binds to Fura-2/AM, the peak excitation wavelength switches from 380 to 340 nm, whereas the peak emission around 510 nm remains unaltered (Grynkiewicz et al. 1985). Thus, sequential excitation of Fura-2/AM at 340 and 380 nm were performed and the concentration of intracellular Ca^{2+} was calculated by the ratio of the emission signals for each excitation wavelength (340 nm and 380 nm). These ratios can be calibrated to a measurement of the corresponding intracellular calcium level by detecting the ratio of the fluorescence emission signal in the presence of known intracellular calcium concentrations (Tinning et al. 2018).

After the incubation of Y-79 cells for 24 h with purified retinoschisin or control eluate, no differences in the intracellular calcium levels were detected between the two differently treated groups (**Figure 39**).

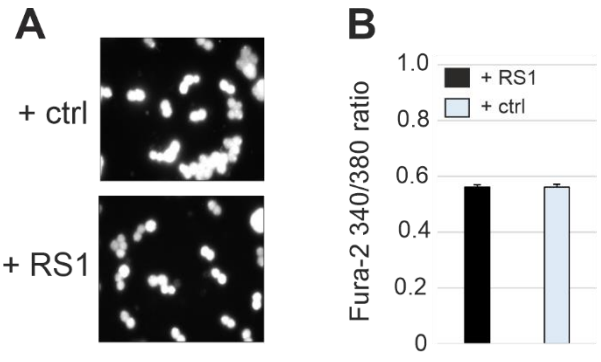

Figure 39: Intracellular Ca^{2+}-Imaging in Y-79 cells

A: Representative images of Y-79 cells, which were incubated for 24 h with purified retinoschisin (+ RS1) or the equal amount of control eluate (+ ctrl). After several washing steps, the medium was changed to ringer-solution containing 2 µM Fura-2/AM and Pluronic F1-2-7. Microscopic images were taken to measure the intracellular Ca^{2+} concentration at a wavelength of 340 nm (shown) and 380 nm. **B**: Intracellular Ca^{2+} was measured in Y-79 cells incubated with retinoschisin (n = 546) or control (n = 533) by calculating the fluorescence ratio at 510 nm after excitation at 340 and 380 nm using the ImageJ Plugin Fiji.

4.3.4 Studies on AnnexinA2 as a possible interaction partner of the retinoschisin-Na/K-ATPase complex

4.3.4.1 Analysis of Na/K-ATPase and AnnexinA2 interaction in murine and porcine retinae

To verify the interaction between the retinal Na/K-ATPase and ANXA2 observed in the undirected co-immunoprecipitation experiment targeting ATP1A3 in porcine lysates (**Table 32**), a further co-immunoprecipitation targeting Atp1a3 in murine retinal lysates was performed. AnxA2-precipitation was investigated *via* western blot analysis.

The direct Atp1a3 interaction partner Atp1b2 was strongly present in the precipitate of the co-immunoprecipitation targeting Atp1a3, whereas no Atp1b2 was observed in the control experiment using 6*His-tag antibodies. For AnxA2 (molecular weight = 36 kDa), two protein

species (both slightly divergent from that of AnxA2) were detected after staining with the AnxA2 antibodies in the Atp1a3 and 6*His-tag precipitate (**Figure 40A**).

In a second approach, co-immunoprecipitation was repeated with porcine retinal lysates. Comparable to previous analyses (**Figure 27**), ATP1B2 revealed a strong staining in the co-immunoprecipitate of ATP1A3, and a weak but slightly higher molecular weight staining in the precipitate of the 6*His-tag co-immunoprecipitation (likely due to an unspecific detection of the heavy chains of the used antibodies, as described in 4.3.1). ANXA2 was absent in both precipitates (co-immunoprecipitation of ATP1A3 and 6*His-tag) (**Figure 40B**). The LC-MS/MS results, suggesting an interaction of ATP1A3 and ANXA2, could thus not be reproduced in subsequent co-immunoprecipitation experiments.

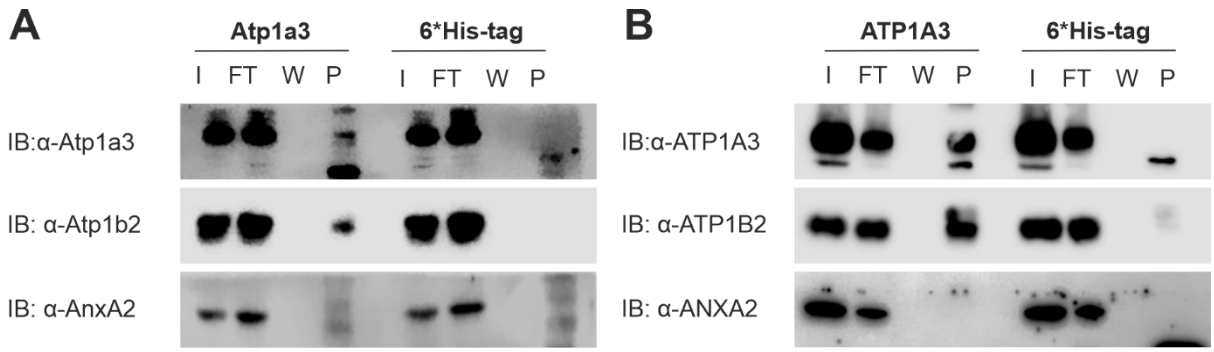

Figure 40: Co-Immunoprecipitation from murine and porcine retinal lysates to test the interaction between ANXA2 and the retinal Na/K-ATPase

Co-immunoprecipitations from murine (**A**) and porcine (**B**) retinal lysates were performed with antibodies against ATP1A3 and 6*His-tag as a control. Samples of input (I), flow through (FT), the last washing step (W) and precipitate (P, contains co-immunoprecipitated proteins) were stained with antibodies against the retinal Na/K-ATPase subunits ATP1A3 and ATP1B2, and ANXA2

4.3.4.2 Effect of retinoschisin-deficiency on the localization of AnnexinA2 in the murine retina

Despite the inconsistent results concerning an interaction between the retinal Na/K-ATPase and AnxA2, the effect of retinoschisin-deficiency on the localization of AnxA2 was further analyzed. Similar to the quantitative assessment of the AnkB (4.3.1.2) and Kv channel subunits Kv2.1 and Kv8.2 localization (4.3.3.3), the AnxA2 signal intensity in inner segments and outer nuclear layer was measured and the ratio from inner segments to outer nuclear layer, “r(IS/ONL)” was calculated in retinal cryosections of wildtype and retinoschisin-deficient mice at different postnatal stages from P4 to P30.

As illustrated in **Figure 41A,** immunolabeling of wildtype sections revealed strong AnxA2 signals in photoreceptor inner segments and weaker signals in the outer plexiform and inner nuclear layer. From P4 to P14, the distribution of AnxA2 in the inner segments and the outer nuclear layer was similar between wildtype and retinoschisin-deficient retinae, with an r(IS/ONL) of around 2 (**Figure 41A** and **B**). At P18, there was an enhanced accumulation of

AnxA2 in the inner segments from wildtype mice, but not from retinoschisin-deficient mice, (r(IS/ONL) = 3.28 + 0.81 in wildtype retinae compared to 1.68 + 0.18 in retinoschisin-deficient retinae, P < 0.05, **Figure 41B**). The r(IS/ONL) values for AnxA2 differed significantly in wildtype and retinoschisin-deficient retinae from P18 to P30. However, the strong accumulation of AnxA2 in inner segments observed in wildtype mice at P18 receded with ongoing age, leading to an r(IS/ONL) of 1.99 + 0.29 in wildtype retinae compared to 1.57 + 0.13 in retinoschisin-deficient retinae at P30 (P < 0.05, **Figure 41B**).

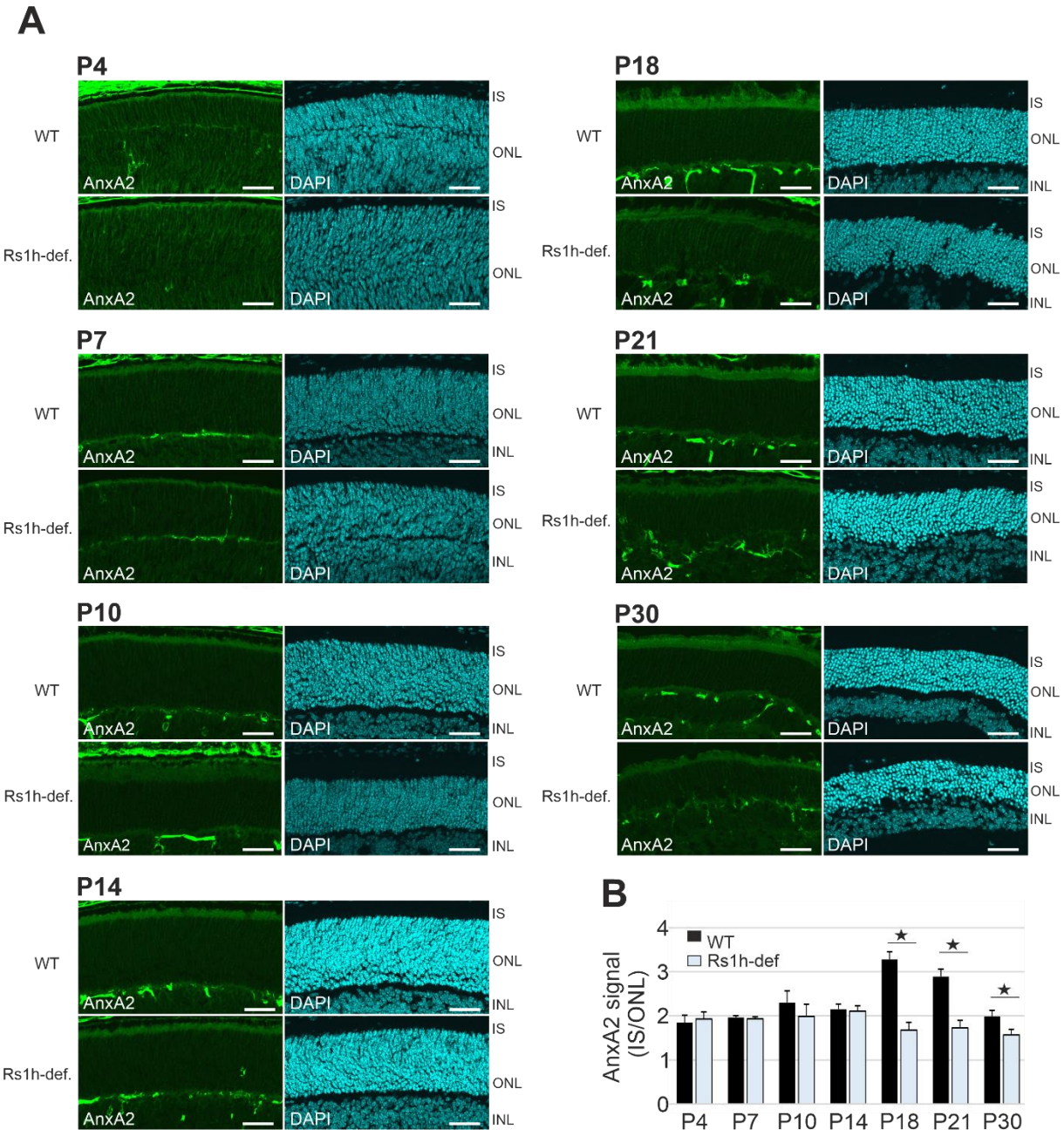

Figure 41: Localization of AnxA2 in the retina of wildtype and retinoschisin-deficient mice of different postnatal stages.

A: Cryosections of eyes of wildtype (WT) and retinoschisin-deficient (Rs1h-def.) mice of different postnatal stages (P4, P7, P10, P14, P18, P21, and P30) were subjected to staining with antibodies against AnxA2 (green), as well as DAPI staining (blue, depicting nuclei). Confocal microscopy was performed at 20x magnification. Scale bars: 40 µm; IS, inner segments; ONL, outer nuclear layer; INL, inner nuclear layer **B:** AnxA2 signals in the inner segments

and outer nuclear layer were measured using ImageJ. Data show the ratio of signal intensity from inner to outer segments r(IS/ONL), given as mean + SD of five biological replicates. Asterisks represent statistically significant differences (*P < 0.05; two-tailed Student's t-test)

4.3.5 Quantitative analysis of the effect of retinoschisin-deficiency on the localization of the retinal Na/K-ATPase in the murine retina

To compare the effects of retinoschisin-deficiency on the identified interaction partners, a quantitative analysis of altered localization of the retinal Na/K-ATPase was performed in wildtype and retinoschisin-deficient mice from P4 to P30 as well. Specifically, the signal intensities of Atp1a3 and Atp1b2 at the murine inner segments and outer nuclear layers were measured.

As seen in **Figure 42** (Atp1a3 localization) as well as **Figure 43** (Atp1b2 localization), the distribution of the retinal Na/K-ATPase subunits Atp1a3 and Atp1b2 in the inner segments and the outer nuclear layer appears similar in wildtype and retinoschisin-deficient retina from P4 to P10. The r(IS/ONL) of Atp1a3 and Atp1b2 was rather low at these stages, increasing from around 1 at P4 to around 2 at P10 in wildtype and retinoschisin-deficient retinae (**Figure 42B** and **Figure 43B**). From P14 onward, there is a strong accumulation of Atp1a3 and Atp1b2 in the inner segments from wildtype mice, but not from retinoschisin-deficient mice. The measured r(IS/ONL) values are statistically significant from P18 onward for Atp1a3 with an r(IS/ONL) of 4,78 + 1.14 in wildtype retinae compared to 1.82 + 0.21 in retinoschisin-deficient retinae at P18 ($P < 0.01$) (**Figure 42**) and for Atp1b2 with an r(IS/ONL) of 5.50 + 1.50 in wildtype retinae compared to 2.50 + 1.01 in retinoschisin-deficient retinae at P18 ($P < 0.05$) (**Figure 43**).

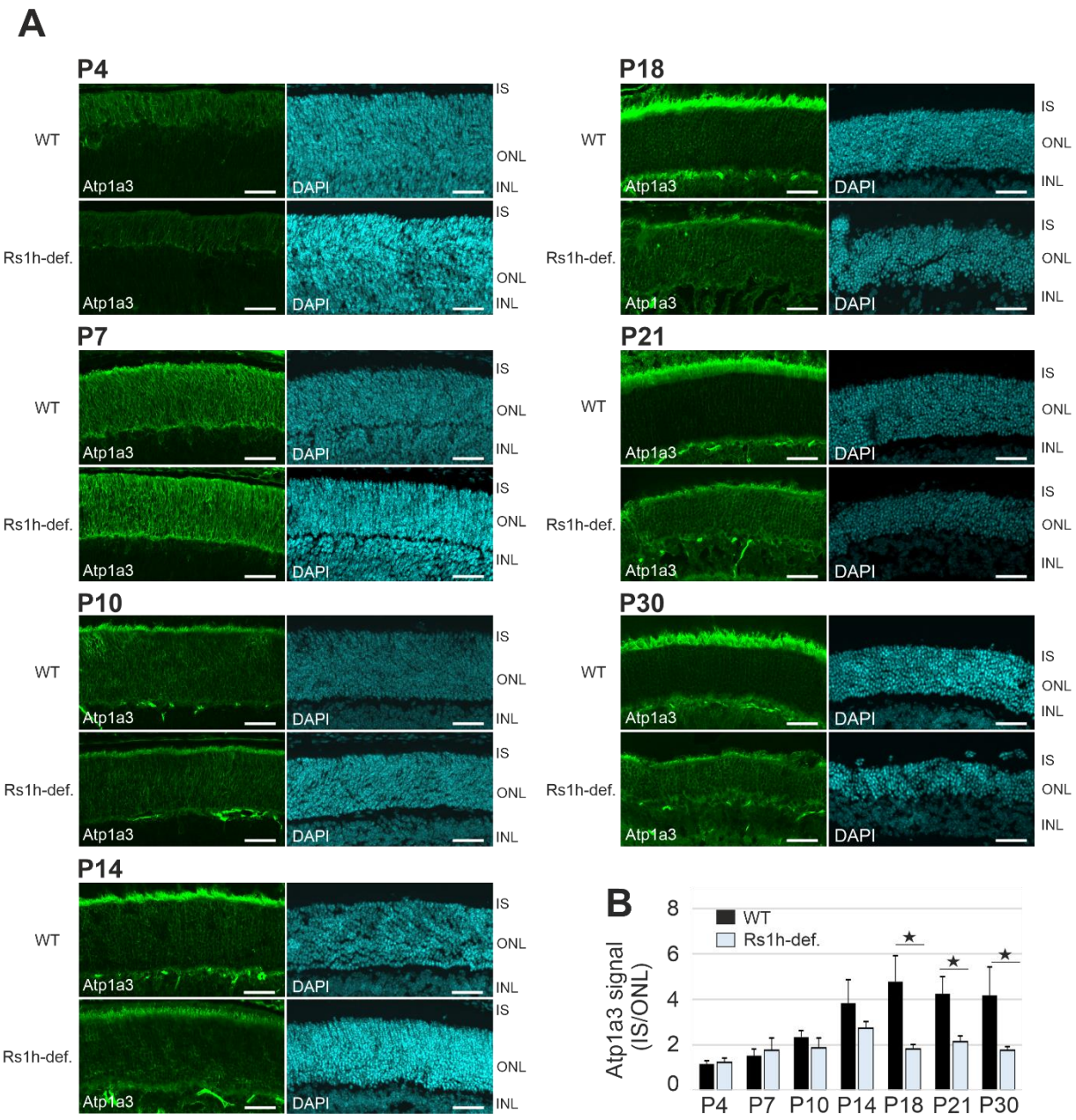

Figure 42: Localization of Atp1a3 in the retina of wildtype and retinoschisin-deficient mice of different postnatal stages

A: Cryosections of eyes from wildtype (WT) and retinoschisin-deficient (Rs1h-def.) mice of different postnatal stages (P4, P7, P10, P14, P18, P21, and P30) were subjected to staining with antibodies against Atp1a3 (green), as well as DAPI staining (blue, depicting nuclei). Confocal microscopy was performed at 20x magnification. Scale bars: 40 µm; IS, inner segments; ONL, outer nuclear layer; INL, inner nuclear layer **B:** Atp1a3 signals in the inner segments and outer nuclear layer were measured using ImageJ. Data show the ratio of signal intensity from inner to outer segments. r(IS/ONL), given as mean + SD of five biological replicates. Asterisks represent statistically significant differences (*P < 0.05; two-tailed Student's t-test). (Figure modified from Schmid et al. 2022).

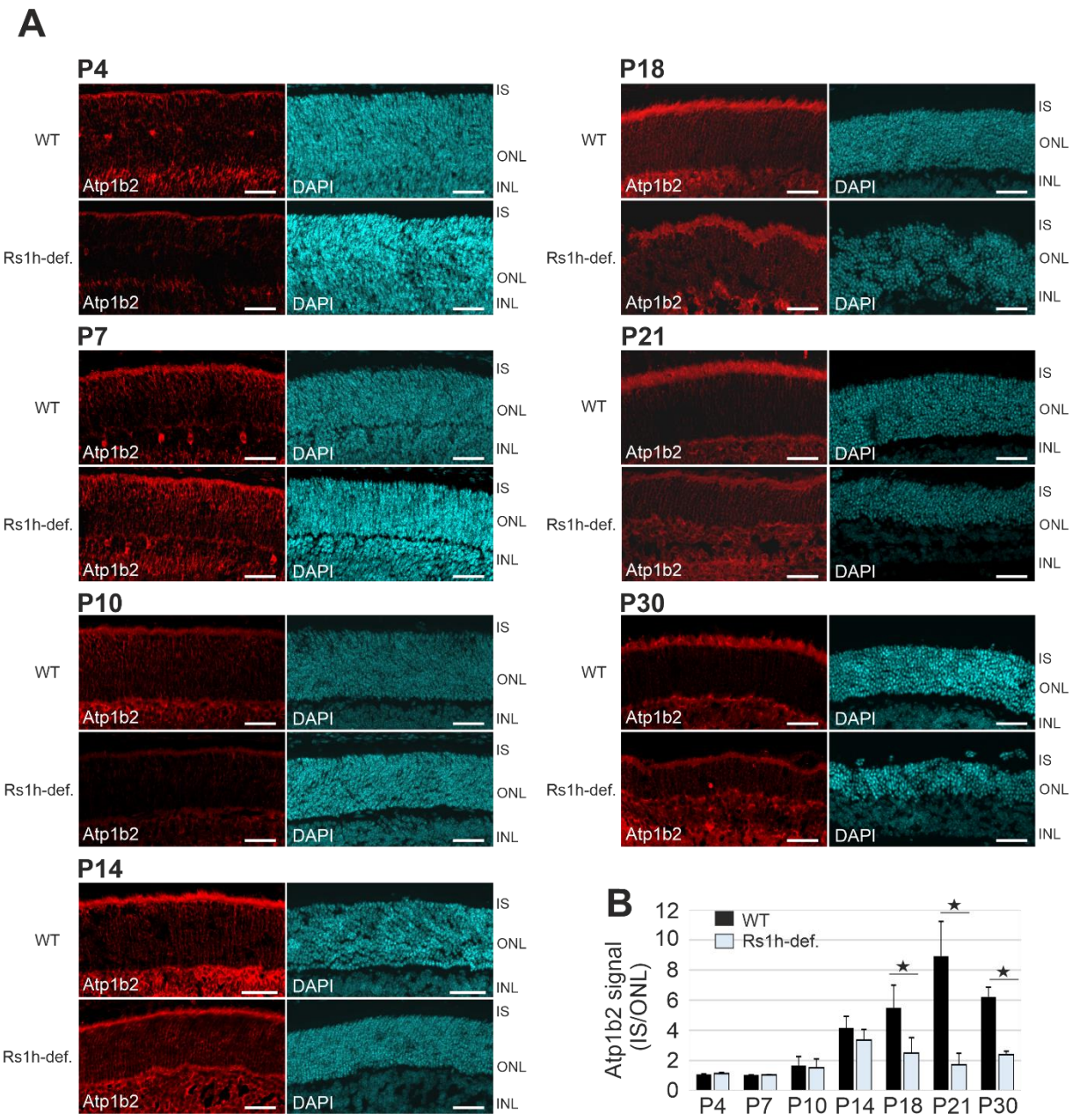

Figure 43: Localization of Atp1b2 in the retina of wildtype and retinoschisin-deficient mice of different postnatal stages

A: Cryosections of eyes from wildtype (WT) and retinoschisin-deficient (Rs1h-def.) mice of different postnatal stages (P4, P7, P10, P14, P18, P21, and P30) were subjected to staining with antibodies against Atp1b2 (red), as well as DAPI staining (blue, depicting nuclei). Confocal microscopy was performed at 20x magnification. Scale bars: 40 µm; IS, inner segments; ONL, outer nuclear layer; INL, inner nuclear layer **B:** Atp1b2 signals in the inner segments and outer nuclear layer were measured using ImageJ. Data show the ratio of signal intensity from inner to outer segments. r(IS/ONL), given as mean + SD of five biological replicates. Asterisks represent statistically significant differences (*P < 0.05; two-tailed Student's t-test). (Figure modified from Schmid et al. 2022).

5 Discussion

The present study focused on functional aspects of the retinoschisin-Na/K-ATPase complex at the mammalian photoreceptors to obtain insights into XLRS-associated disease processes. In a first project, details of the retinoschisin-Na/K-ATPase binding mechanism were addressed. It could be shown that the binding of retinoschisin to the ATP1B2 subunit of the retinal Na/K-ATPase is a direct interaction of retinoschisin with the ATP1B2 peptide moiety and not mediated by ATP1B2-attached glycoside chains. Specifically, the presence of a polar residue at aa 240 of ATP1B2 was identified to play a key role in the interaction with retinoschisin. The diffusion of membrane-bound proteins in the plasma membrane can be affected by the assembly into macromolecular complexes or by secreted proteins (Junghans et al. 2016, 2017; Pandya et al. 2018), thus the influence of retinoschisin on the lateral mobility of the Na/K-ATPase was investigated. Fluorescence correlation spectroscopy analysis revealed no effect of retinoschisin on the lateral diffusion of the Na/K-ATPase. In a second project, the crosstalk of retinoschisin and cardiac glycosides at the retinal Na/K-ATPase was investigated, as cardiac glycosides are also known Na/K-ATPase regulative binding partners (Schoner and Scheiner-Bobis 2007). The analysis revealed a displacement of retinoschisin from the Na/K-ATPase by the two tested cardiac glycosides ouabain and digoxin. In retinal explants of retinoschisin-deficient mice exposed to retinoschisin with or without preincubation of cardiac glycosides, their presence interfered with the capacity of retinoschisin to protect against photoreceptor apoptosis. The third project of the thesis aimed to identify interaction partners of the retinoschisin-Na/K-ATPase complex. Potential candidates were chosen from known interaction for the ATP1A1-containing Na/K-ATPase complex. None of these (SRC, RAS, PI3K, NCX, and PLC) were detected to interact with the retinal Na/K-ATPase. V*ia* co-immunoprecipitation targeting the Na/K-ATPase and subsequent mass spectrometric analysis, over 200 so far undescribed potential interaction partners of the retinal Na/K-ATPase were identified. Three of these, ANXA2, Kv2.1, and Kv8.2, were investigated in detail while a fourth candidate, ANKB, was already described as an interaction partner of the retinal Na/K-ATPase before (Kizhatil et al. 2009). In an independent approach, the direct interaction with the Kv channel subunits Kv2.1 and Kv8.2 was confirmed, whereas a direct interaction with ANXA2 could not be verified. Moreover, mislocalization of Kv2.1 and Kv8.2, AnxA2, and AnkB was observed in retinoschisin-deficient mice. Further analysis on Kv2.1 and Kv8.2 channel subunits revealed a reduction in their protein levels in retinoschisin-deficient mice, while their gene expression was unchanged. In Y-79 cells, retinoschisin exerted no effect on the potassium ion current mediated by Kv channels.

A previous study of the Institute of Human Genetics, University of Regensburg, demonstrated that retinoschisin binding requires the ATP1B2 subunit of the retinal Na/K-ATPase (Plössl et

al. 2017b), whereas the α-subunit is exchangeable. As the ATP1B2 subunit is highly glycosylated (Tokhtaeva et al. 2010) and retinoschisin exerts a high affinity to galactose-agarose beads (Dyka et al. 2008), it was hypothesized that the interaction between retinoschisin and the ATP1B2 subunit is mediated through the interaction with any of the glycoside side chains of ATP1B2 (Dyka et al. 2008). In retinoschisin binding assays, externally added galactose and glucose suppressed retinoschisin binding to the heterologously expressed retinal Na/K-ATPase, however only after applying very high (> 0.5 M) and thus rather unphysiological concentrations. In contrast, mannose revealed no significant effects on the retinoschisin binding capacity, which is in line with the analysis of Dyka and colleagues who identified only moderate binding of retinoschisin to mannose-agarose beads (Dyka et al. 2008). As different effects of glucose/galactose and mannose on retinoschisin binding were found, the decreased retinoschisin binding is probably not due to altered osmolality, but rather a consequence of specific interaction between retinoschisin and galactose or glucose. However, this binding could be a diffuse interaction with the sugars independent of the protein to which the chain is attached. Moreover, the extracellular domains of most cell membrane proteins are glycosylated, often at multiple sites (Chandler and Costello 2016) and thus the high specificity of retinoschisin for the retinal Na/K-ATPase in retinal membranes probably cannot be explained by a simple interaction with galactose or glucose. Consistent with this assumption, retinoschisin binding was observed to the fully deglycosylated Na/K-ATPase, suggesting an interaction with the ATP1B2 peptide moiety rather than with ATP1B2 glycoside side chains. This was also supported by the fact that retinoschisin mutant RS1_R141H, which showed a similar affinity to galactose-agarose beads as normal retinoschisin (Dyka et al. 2008), was not able to bind to the retinal Na/K-ATPase (normal or deglycosylated). Taken together, these data strongly exclude a specific binding of retinoschisin to the glycoside side chains of ATP1B2.

The question remains why sugars like galactose or glucose attenuate the interaction between ATP1B2 and retinoschisin. One explanation could be that ATP1B2 and these sugars compete for the same binding site in retinoschisin, which was assumed to be a substructure formed by the extruding retinoschisin spikes, specifically around arginine 141 in spike 3 (Plössl et al. 2018). The fundamental role of discoidin spikes to enable interaction with different ligands such as collagen (Leitinger 2003), phosphatidylserine (Fuentes-Prior et al. 2002), or galactose (Valencia et al. 1989) was also described for other discoidin domain containing proteins like discoidin domain receptor 1, blood coagulation factors V and VIII, and lectin discoidin 1 (Kiedzierska et al. 2007). An alternative explanation could be that galactose/glucose binding to a different retinoschisin region might induce structural alterations at retinoschisin, disrupting its Na/K-ATPase binding site, and thus attenuating the binding of retinoschisin to the retinal

Na/K-ATPase. Most proteins such as ion channels, kinases, or receptors are allosteric, allowing them to adopt two or more slightly different conformations, and a shift from one to another is caused by ligand binding (Alberts et al. 2002).

The high affinity of retinoschisin to galactose can be used for retinoschisin protein purification *via* galactose affinity chromatography (Dyka et al. 2008), still, there is no explanation for a physiological relevance of this interaction. The high galactose affinity of retinoschisin might be required for an interaction of retinoschisin with other glycosylated proteins like β2-laminin or αB-crystallin, both components of the interphotoreceptor matrix (Steiner-Champliaud et al. 2006). Following this logic, retinoschisin could be involved in stabilizing the structural and functional integrity of the retina by the interaction with the highly glycosylated interphotoreceptor matrix proteins surrounding the photoreceptor inner segments, a process which is disturbed in XLRS patients (Khan et al. 2001; Padrón-Pérez et al. 2018; Ambrosio et al. 2019). Alternatively, an interaction between retinoschisin and interphotoreceptor matrix proteins could contribute to stabilize the localization of the retinoschisin-Na/K-ATPase complex in the photoreceptor inner segments. Localization of this complex was significantly disturbed in retinoschisin-deficient mice (Plössl et al. 2017a, 2018). However, galactose binding might also simply represent a physiologically irrelevant, evolutionarily conserved property of discoidin domain containing proteins, as it is also observed in many other discoidin domain containing proteins including the blood coagulation Factor V and Factor VIII, milk fat globule protein, neuropilins, or neurexin IV (Baumgartner et al. 1998; Pratt et al. 1999; Kiedzierska et al. 2007; Dyka et al. 2008). For example, Dyka and colleagues also observed binding of galactose by blood coagulation Factor V, which was abolished by the presence of phosphatidylserine, the actual ligand for the blood coagulation Factor V (Dyka et al. 2008). Lastly, the binding of sugars by retinoschisin could represent a regulatory mechanism, regulating the affinity of retinoschisin to its interaction partners. For example, galactose was shown to reduce the affinity of the lac repressor for operator DNA (Barkley et al. 1975). As the glycoside side chains of the ATP1B2 subunit were excluded as the binding site for retinoschisin, further analyses were performed to identify the retinoschisin binding region of the retinal Na/K-ATPase.

As reported in Plössl et al. (2019), the hydrophobic patch at the extracellular domain of ATP1B2 around threonine 240 was identified as crucial for retinoschisin binding to ATP1B2. To better understand the role of aa 240 in retinoschisin binding, two novel ATP1B2 mutants were generated in the present thesis: ATP1B2_T240A, where threonine 240 was replaced by the non-bulky, chemically inert alanine, and ATP1B2_T240S, where threonine 240 was replaced by the chemically similar serine. Retinoschisin binding assays showed binding of retinoschisin to ATP1B2_T240S, but not to ATP1B2_T240A, indicating that a hydroxyl moiety

at aa 240 is essential for the interaction with retinoschisin. Notably, a similar finding showing the requirement of a hydroxyl moiety at a defined aa position for ligand binding was reported for the human prostaglandin EP_2 and EP_4 receptors (Stillman et al. 1998). Specifically, a threonine at position 185 and 168 of the EP_2 and EP_4 receptors, respectively, could be replaced by serine but not by alanine to still allow ligand binding by the receptors. Consistent with these findings, bioinformatics approaches to detect critical aa residues in protein-protein binding sites have found that, although the binding sites are hydrophobic overall, they have conserved polar residues at specific locations that serve as "hot spots" at the protein interfaces (Hu et al. 2000; Ma et al. 2003). Taken together, this analysis confirms an essential role of the hydrophobic patch around threonine 240 and suggests the necessity of a hydroxyl group at aa 240 to enable retinoschisin binding.

The next subproject of this study addressed the question, whether the binding of retinoschisin can influence the lateral mobility of the retinal Na/K-ATPase in the plasma membrane. According to the fluid mosaic model of Singer and Nicolson (Singer and Nicolson 1972), the biological membrane can be considered as a two-dimensional fluid in which transmembrane proteins can diffuse freely. However, the diffusion of membrane proteins is frequently affected or restricted by an assembly into large supramolecular complexes, leading to the formation of membrane subdomains (Junghans et al. 2016). Furthermore, the lateral diffusion can also be limited by secreted proteins binding to the extracellular domains of the transmembrane proteins (Pandya et al. 2018). Despite the formation of macromolecular complexes by Na/K-ATPases (Reinhard et al. 2013), fluorescence correlation spectrometry analyses by Junghans and colleagues (2016, 2017) demonstrated lateral diffusion of ATP1A2-containing Na/K-ATPases in the plasma membrane of Hek293 cells. Moreover, they demonstrated the presence of two different diffusion times for these Na/K-ATPase complexes. Comparable to these data, two diffusion times for the ATP1A3-containing Na/K-ATPase were observed in the present study, indicating the presence of two independent Na/K-ATPase populations with largely different mobility. The obtained diffusion coefficients obtained in this study (in average; D1: 4.0×10^{-11} $m^2 \cdot s^{-1}$ and D2: 1.8×10^{-13} $m^2 \cdot s^{-1}$) are in the same magnitude to those of the study by Junghans and colleagues (1.4×10^{-11} $m^2 \cdot s^{-1}$ and 1.1×10^{-13} $m^2 \cdot s^{-1}$, Junghans et al. 2017). Such multiple diffusion times are not uncommon for membrane proteins (Schwille et al 1999; Vukojevic et al. 2008; Chiantia et al. 2009) and reflect the complexity of the membrane environment (Junghans et al. 2017). For example, two diffusion times are also proposed for the μ-opioid receptor (MOP): One MOP population undergoes directed motion after expression and a second population showed increased mobility due to curvature coupling with plasma membrane lipids (Leitenberger et al. 2007) and/or plasma membrane surface fluctuations (Naji and Brown 2007; Vukojevic et al. 2008). However, in contrast to an observed effect of ANKB

and CAV1 on the lateral diffusion of ATP1A2-containing Na/K-ATPases (Junghans et al. 2017), correlation spectrometry analyses revealed no effect of retinoschisin binding on the lateral diffusion of the retinal ATP1A3-containing Na/K-ATPase. As previously reported, retinoschisin interacts with proteins of the interphotoreceptor matrix like β2-laminin and αB-crystallin (Steiner-Champliaud et al. 2006). This interaction could be required for the stabilization of the retinal Na/K-ATPase, which would lead to the observation that retinoschisin has no effect on lateral diffusion in the applied Hek293 expression system. This hypothesis would be supported by the fact that retinoschisin-deficiency leads to mislocalization of the Na/K-ATPase (Plössl et al. 2017b, 2018), which could be a consequence of the lack of stabilization of the retinal Na/K-ATPase complex by interphotoreceptor matrix bound retinoschisin. Finally, as also discussed by Junghans et al. (2017), it is also important to take into account that in fluorescence correlation spectrometry analysis all immobile fluorophores will be bleached; thus, completely fixed GFP-tagged retinal Na/K-ATPase molecules will not be recorded in the observed fluorescence fluctuation traces but will create inaccessible spaces that do not allow other molecules to enter (Junghans et al. 2017). In addition, the formation of signaling microdomains as it is seen for Na/K-ATPases could also influence the diffusion behavior, as it was reported that these proteins are trapped and cannot escape from certain microdomains (Xie and Cai 2003; Chiantia et al. 2009). It might thus be hypothesized that retinoschisin only binds to such Na/K-ATPase fractions, which are localized in microdomains and thus no effect on the lateral mobility would be observed after retinoschisin incubation.

Cardiac glycosides are also known to interact with and regulate Na/K-ATPases (Reinhard et al. 2013; Cui and Xie 2017). Cardiac glycosides can cross the blood–brain barrier and are highly enriched in the retina (Lissner et al. 1971; Binnion and Frazer 1980; Ritz et al. 1992; Fraunfelder et al. 2014). Cardiac glycosides are used as a treatment for patients with chronic heart failure and these patients often experience vision disturbances as a negative side effect (Haustein 1982; Lawrenson et al. 2002; Fraunfelder et al. 2014; Renard et al. 2015). This subproject of the dissertation aimed to analyze the interplay between retinoschisin and cardiac glycosides at the retinal Na/K-ATPase and its consequences on retinal integrity. Binding assays revealed a strong reduction in retinoschisin binding to the retinal Na/K-ATPase in the presence of the cardiac glycosides ouabain and digoxin. This effect was not accompanied by a decrease of retinoschisin in the input or by a decrease of the retinoschisin binding partner ATP1B2 in the cells. Moreover, cardiac glycosides did not impair retinoschisin binding to an ouabain-insensitive ATP1A3 mutant, thus a Na/K-ATPase-independent interaction between retinoschisin and cardiac glycosides can be excluded. In contrast, the binding of cardiac glycosides to the retinal Na/K-ATPase and their capacity to inhibit its pump function was not affected by retinoschisin. Such different effects of retinoschisin and cardiac glycosides on each

other's Na/K-ATPase binding capacities raise the question of how these two molecules bind to or interact at the Na/K-ATPase. The binding site of cardiac glycosides is formed by the TM 1 to 6 of the α-subunit (Yatime et al. 2011; Laursen et al. 2013), whereas retinoschisin binds to the ATP1B2 subunit, especially to a hydrophobic patch around threonine 240 (Plössl et al. 2017b; 2019). One explanation for the observed effect of cardiac glycosides on retinoschisin binding could lie in conformational changes of the Na/K-ATPase. During ion transport, the Na/K-ATPase switches between the E1 and E2 conformations (Post et al. 1972) and this conformational change affects the entire Na/K-ATPase, including distances between the α- and the β-subunits (Sánchez-Rodríguez et al. 2015). Cardiac glycoside binding induces the conformational switch from E1 to E2 (Silva and Soares-da-Silva 2012) and stabilizes the E2 conformation (Geibel et al. 2003). If retinoschisin has a higher affinity for E1, stabilization of E2 by cardiac glycosides could decrease retinoschisin binding to the Na/K-ATPase. Another explanation could be that bound cardiac glycosides might partially overlap with, and potentially block the binding region of retinoschisin. Interestingly, the identified retinoschisin binding patch on ATP1B2 lies in close proximity to the outer cardiac glycoside interface of the Na/K-ATPase. The study of Laursen et al. (2013) reported that the sugar moieties of bound cardiac glycosides are in a cavity enclosed by polar residues of the α- and the β-subunits (i.e., Gln84 of the ATP1B1-ectodomain). The homologous aa of Gln84 in ATP1B1 is Glu89 in ATP1B2, which is directly adjacent to the putative retinoschisin binding patch on ATP1B2. The patch is composed of four hydrophobic stretches, aa 83–88, 108–121, 181–184, and 240, which is the direct interphase of retinoschisin (Plössl et al. 2019). Consequently, the accessibility of the ATP1B2 binding patch by retinoschisin might be blocked by the protruding cardiac glycoside sugar moieties. As digoxin has three sugar moieties and is bulkier than ouabain, which has only one sugar residue, this could be a possible explanation for the stronger inhibitory effect of digoxin on retinoschisin binding compared to ouabain.

As mentioned before, retinoschisin has a protective effect on the survival of outer retinal cells (Gehrig et al. 2006; 2007), while cardiac glycosides show different effects depending on their concentration: Whereas low levels (10^{-11} to 10^{-13} M) of cardiac glycosides were reported to stimulate retinal explant growth (Lopatina et al. 2008), higher concentrations, which also showed retinoschisin displacement in this study, significantly disrupted retinal integrity and functionality (Kinoshita et al. 2014; Madreperla et al. 2015; Hinshaw et al. 2016). For example, in monkeys treated with digoxin, ERG analysis revealed a selective decrease in the maximum response parameter in the cone a-wave, which indicates dysfunction of cone photoreceptors (Kinoshita et al. 2014). In the present study, retinoschisin exerted a protective effect against photoreceptor degeneration in retinoschisin-deficient murine retinal explants, confirming previous analyses (Plössl et al. 2018), while high concentrations (10^{-5} M ouabain and 10^{-6} M

digoxin) of cardiac glycosides increased degeneration, also in line with previous analyses (Kinoshita et al. 2014; Madreperla et al. 2015; Hinshaw et al. 2016). The simultaneous presence of cardiac glycosides strongly reduced the capacity of retinoschisin to protect against photoreceptor degeneration. This effect might be explained by the observed displacement of retinoschisin from the Na/K-ATPase by cardiac glycosides. However, it could also be a simple consequence of the strong negative effect of highly concentrated cardiac glycosides on retinal integrity (Kinoshita et al. 2014; Madreperla et al. 2015; Hinshaw et al. 2016), which superimposes the protective effect of retinoschisin. Taken together, the findings of this subproject demonstrate opposing effects of retinoschisin and cardiac glycosides on retinal Na/K-ATPase binding and retinal integrity, suggesting that a fine-tuned interplay between both components is required to maintain retinal homeostasis.

Na/K-ATPases formed by isoforms ATP1A1 or ATP1A2 were reported to assemble in a membrane-bound macromolecular protein complex with intracellular signal transducers, ion channels, transporters, or scaffolding proteins (Mohler et al. 2005; Reinhard et al. 2013; Cui and Xie 2017). Thus, the Na/K-ATPase is also referred to as a protein-docking station for a fast-growing number of protein interaction partners (Mohler et al. 2005; Reinhard et al. 2013 Cui and Xie 2017). In contrast, there are only a few interaction partners known for ATP1A3-containing Na/K-ATPases: Specifically, in the brain, an interaction with the Proline Rich Transmembrane protein 2 (Sterlini et al. 2021), the Neuronal Glycine Transporter GlyT2 (de Juan-Sanz et al. 2013) GLAST, and GLT-1 (Rose et al. 2009) were described and in the retina, interaction with ANKB was reported (Kizhatil et al. 2009). This subproject aimed to investigate interaction partners of the retinal Na/K-ATPase to assess its function as a putative protein-docking station, similar to ATP1A1 or ATP1A2-containing Na/K-ATPases.

In co-immunoprecipitation analyses from porcine retinal lysates targeting ATP1A3, the ATP1A1-containing Na/K-ATPase complex associated interaction partners SRC, PI3K, RAS, NCX, and PLC were not detected in the precipitate of ATP1A3 *via* western blot analyses. In a control co-immunoprecipitation targeting ATP1A1, all these proteins except RAS were verified in the ATP1A1 precipitate. RAS is part of the ATP1A1-associated Na/K-ATPase complex but shows no direct binding to ATP1A1. Instead, it binds to the ATP1A1 interacting epidermal growth factor receptor (EGFR) (Cui and Xie 2017). EGFR could not be detected in murine or human photoreceptors (Chen et al. 2007). The missing detection of RAS after co-immunoprecipitation targeting ATP1A1 from porcine retinal lysates might thus be a consequence of the absence of EGFR in mammalian photoreceptors. The successful precipitation of SRC, PI3K, NCX, and PLC in the control co-immunoprecipitations targeting ATP1A1 documents the applicability of this approach to detect an existing interaction between

Na/K-ATPases and these proteins. Together with the results from co-immunoprecipitation analyses targeting ATP1A3, this suggests that there is indeed no interaction between ATP1A3 and SRC, PI3K, NCX, and PLC.

As already mentioned, AnkB was described to form a complex with the retinal Na/K-ATPase in photoreceptor inner segments in mice (Kizhatil et al. 2009). Furthermore, AnkB was shown to be required for the coordinated expression of the retinal Na/K-ATPase (Kizhatil et al. 2009). Therefore, another subproject of this thesis investigated whether retinoschisin-deficiency could lead to a maldistribution of AnkB within the retinal layers, similar to the maldistribution observed for the retinal Na/K-ATPase (Friedrich et al. 2011). Immunolabeling of murine retinal cryosections revealed a significant difference in the distribution of AnkB between wildtype and retinoschisin-deficient mice from P18 onward. This finding is in line with the retinoschisin-deficiency induced Na/K-ATPase mislocalization, which is also seen from P18 on, supporting a complex formation between AnkB and the retinoschisin-Na/K-ATPase complex. As these significant changes occur from P18 onward, the mislocalization could be a consequence of apoptotic photoreceptor degeneration starting around P14 (Gehrig et al. 2006; Friedrich et al. 2011). The observed effect of retinoschisin-deficiency on AnkB localization could also have severe effects on the structuring of other plasma membrane components, for which ANKB was postulated to have an important organizing role. In cardiomyocytes, ANKB organizes a macromolecular complex between the Na/K-ATPase, NCX, and the IP3 receptor (Mohler et al. 2005; Skogestad et al. 2020). Additionally, it seems that ANKB provides the molecular basis for the Na/K-ATPase and NCX interaction (Mohler et al. 2005). Interestingly, it was reported that Na/K-ATPase binding to ANKB in cardiomyocytes controls the ion homeostasis *via* regulating the NCX activity in a local domain. Disruption of this interaction resulted in increased calcium sparks and waves, a possible mechanism for arrhythmogenesis in the ANKB syndrome (Skogestad et al. 2020). Similar to the Ca^{2+}-dysregulation in cardiomyocytes, it can be assumed that a mislocalization of the AnkB-Na/K-ATPase complex in murine photoreceptors could also result in misregulation of ion homeostasis, which can be seen in the XRLS pathology (Gehrig et al. 2006). In addition, the observed altered distribution of AnkB could affect the localization of AnkB-structured proteins in photoreceptors. The loss of cellular organization might contribute to the XLRS pathology, comparable to the negative effect of mislocalized protein complexes in the pathology of other diseases like distinct late-onset neurogenerative diseases such as Huntington's disease or Alzheimer's disease (Labbadia and Morimoto 2015). Similarly, the mislocalization of many membrane-bound proteins like E-cadherin, β-catenin, or the EGFR, which have oncogenic, tumor suppressive, or other functions, are associated with tumorigenesis (Wang and Li 2014).

As the targeted approach focusing on known protein partners of the ATP1A1-containing Na/K-ATPase complex revealed no new interaction partners for the ATP1A3-containing retinoschisin-Na/K-ATPase complex, a second undirected approach was conducted. A co-immunoprecipitation from porcine retinal lysates targeting ATPA3 was performed, followed by LC-MS/MS analysis of the precipitate. Besides the known complex partner ATP1B2 and retinoschisin, over 200 proteins were detected only in the precipitate of ATP1A3. Notably, ANKB (220 kDa) was not detected among these > 200 proteins. This might be explained by the fact, that the detection of ANKB in LC-MS/MS analysis is rather difficult: Except for one study (Liu et al. 2007), proteomic approaches have failed to identify ankyrin family members in photoreceptors (Matsumoto and Komori 2000; Morel et al. 2000; Kwok et al. 2008), while immunohistochemical analyses clearly stained AnkB in murine photoreceptors (Kizhatil et al. 2009). Several studies suggest a high sensitivity of the ankyrin proteins to proteases (Bennett and Stenbuck 1979; Kizhatil et al. 2009). Furthermore, ANKB is a very large protein and thus detection was not possible in this approach.

After prioritizing over 200 identified proteins, ANXA2, Kv2.1, and Kv8.2 were selected for further analyses. Co-immunoprecipitation analysis with murine or porcine retinal lysates could not confirm the direct interaction between ATP1A3 and ANXA2. One explanation for this result could be an insufficient sensitivity of the antibody to detect putatively low levels of precipitated ANXA2. Another possibility could be that ANXA2 was a false-positive LC-MS/MS result and that there actually is no direct interaction between ANXA2 and ATP1A3, although the high Mascot-score and the high number of detected peptides in the LC-MS/MS analysis would argue against this. Finally, the contradictory results might be a consequence of methodological challenges connected to ANXA2 biology: Annexins are cytosolic proteins, with a soluble and a stable form, which reversibly interacts with components of the cell membrane (Mirsaeidi et al. 2016). In addition, co-immunoprecipitation of membrane complexes is challenging due to the inherent properties of membrane proteins: E.g.; they present limited solubility due to the requirement of a hydrophobic environment, and they are often heavily glycosylated which makes the access of proteases difficult (Prados-Rosales et al. 2019).

The localization analysis of AnxA2 in murine retinal cryosections revealed significant differences in the distribution of AnxA2 between wildtype and retinoschisin-deficient mice. As for the retinal Na/K-ATPase, mislocalization of AnxA2 was detectable from P18 onward, which might suggest an interaction between AnxA2 and Atp1a3. As also discussed for AnkB, this effect occurs after photoreceptor apoptosis and schisis formation and thus might be a direct consequence of photoreceptor degeneration. ANXA2, a Ca^{2+}-regulated, phospholipid-binding protein, is present in the cytoplasm and on cell surfaces, with location specific functionality: On

the cell surface, it regulates processes like plasmin generation and fibrin homeostasis. Intracellularly, ANXA2 fulfills many functions, including organization of specialized membrane microdomains, signal transduction, and regulation of additional membrane dynamic events (Dallacasagrande and Hajjar 2020; Jiang and Xu 2019; Moss and Morgan 2004). Mislocalization of AnxA2 under retinoschisin-deficiency could thus induce disorganization of membrane microdomains and altered signal transduction, all processes, which have been established in XLRS pathogenesis.

The present analysis strongly confirmed the physical interaction of the Kv channel subunits Kv2.1 and Kv8.2 with the retinoschisin-Na/K-ATPase complex. Immunolabeling of retinal cryosections revealed an increasing mislocalization of the retinal Na/K-ATPase and the Kv channel subunits Kv2.1 and Kv8.2 during postnatal retinal development of the XLRS mouse retina. Notably, in contrast to the retinal Na/K-ATPase, AnkB and AnxA2, an even earlier starting point of mislocalization at P7 was detected for Kv2.1. Consequently, it can be hypothesized, that this effect is not a consequence of photoreceptor degeneration starting at P14. Instead, it could be explained by an instability of the Na/K-ATPase-Kv channel complex due to retinoschisin-deficiency. A Na/K-ATPase stabilized localization of Kv2.1 and Kv8.2 is supported by immunohistochemical analyses in Atp1b2-deficient mice, revealing an altered distribution of Kv2.1 and Kv8.2 under Na/K-ATPase deficiency. In addition to the observed mislocalization of Kv2.1 and Kv8.2 under retinoschisin-deficiency, altered protein expression levels of these two proteins were also observed before P14, whereas no effect on the protein expression of the retinal Na/K-ATPase was detected at all other stages investigated. In contrast, RT-PCR analysis revealed no changes in *Kcnb1* and *Kcnv2* (as well as in *Atp1a3* and *Atp1b2*) mRNA transcript levels in retinoschisin-deficient retinae, which largely excludes altered gene expression as the cause for altered protein levels of Kv2.1 and Kv8.2. The mRNA expression data are in line with a previous untargeted study by Vijayasarathy and colleagues (2021), who used microarray-based genome-wide expression profiling and observed no mRNA expression differences for *Kcnb1* and *Kcnv2* as well as for *Atp1a*3 and *Atp1b2* in wildtype and retinoschisin-deficient retinae of P12 and P21 old mice. Accordingly, the effect of retinoschisin-deficiency on Kv2.1 and Kv8.2 protein levels should be attributed to a posttranslational process. One possibility might be a reduced stability of the Kv channel-Na/K-ATPase macromolecular complex due to the absence of retinoschisin. The integrity of a macromolecular complex is determined by its composition, i.e. the presence of specific ligands/protein binding partners (Kamerzell and Middaugh 2008). The stability of the individual complex constituents is also strongly dependent on protein-protein interactions (Marquis-Omer et al. 1991; Volkin et al. 1993; Kamerzell and Middaugh 2008). Retinoschisin-deficiency could also impair other processes like protein internalization, as the binding of extracellular ligands

to membrane-bound proteins like the G-protein-coupled receptors regulates its internalization and this can also have severe effects on signal transduction mechanisms (Yin et al. 2014). Furthermore, the loss of retinoschisin at the plasma membrane could also affect photoreceptor integrity and thus lead to impaired functional compartmentalization, which may occur before photoreceptor degeneration at P14. Taken together, the absence of the Na/K-ATPase ligand retinoschisin could negatively affect the integrity of the Na/K-ATPase and its complex partners like Kv2.1 and Kv8.2.

The effect of retinoschisin on the Kv channel-mediated potassium ion current was also tested using Y-79 cells as a model system. The analyses revealed no effect of retinoschisin on the ion current mediated by the Kv channels Kv2.1 and Kv8.2. As altered Kv channel activity also affects intracellular calcium levels in photoreceptors (Fortenbach et al. 2021), a putative effect of retinoschisin on intracellular calcium levels was also measured in Y-79 cells. Again, no effect of retinoschisin was observed. These two consistent results might simply be explained by the fact, that binding of retinoschisin to the retinal Na/K-ATPase has no effect on the Kv channel mediated ion current. Alternatively, as already discussed for the measurement of lateral diffusion before, the applied Y-79 cell model system might not be appropriate to detect specific effects of retinoschisin on the retinal Na/K-ATPase and its complex partners, as essential photoreceptor-specific components, like specific interphotoreceptor matrix proteins, are missing. Another finding might also explain the absent effect of retinoschisin on Kv channel activity: Previous studies showed that there are two populations of Kv2.1 channels in Hek293 cells and hippocampal neurons, whereas the non-conducting clustered population is able to form microdomains and is involved in membrane trafficking (Deutsch et al. 2012), the whole-cell Kv2.1 current in patch-clamp analysis is likely derived from conducting non-clustered Kv2.1 channels (O'Connell et al. 2010). Hence, it can be speculated that the Na/K-ATPase bound Kv channel subunits Kv2.1 and Kv8.2 are non-conducting (due to their presence in a macromolecular protein complex). Following such a speculation, the binding of retinoschisin to the retinal Na/K-ATPase would not affect Kv channel activity, which simply would only arise from freely diffusing Kv channels.

Kv2.1 and Kv8.2 were shown to be highly expressed in photoreceptor inner segments, but absent or poorly expressed in other retinal layers (Gayet-Primo et al. 2018). Furthermore, Kv channels together with the Na/K-ATPase play a major role in generating the outward dark current during phototransduction keeping the photoreceptors depolarized and driving the release of glutamate neurotransmitters (Heidelberger et al. 2005; Fortenbach et al. 2021). In addition, Kv2.1 has a structural function as it mediates spatial and functional coupling of LTCCs and ryanodine receptors in mammalian neurons (Vierra et al. 2019). Finally, Kv2.1 was also

reported to modulate intracellular signaling (Wang et al. 2006; Vierra et al. 2019). Aberrant phototransduction, structural integrity of photoreceptors, and intracellular signaling are associated with the pathology of XLRS (summarized in Vijayasarathy et al. (2021)). Mislocalization and reduced protein amount of Kv2.1 and Kv8.2 could lead to a disturbance of specific or all of these processes and thus contribute to the molecular pathogenesis of XLRS. Aberrant functionality of Kv channels has been implicated in various pathological events before, i.e. pathogenic mutations in *KCNB1* encoding the Kv2.1 subunit have been identified in patients with different neurodevelopmental disorders like epilepsy or autism (Jędrychowska and Korzh 2019). Further, Kv2.1-knockout mice manifest neuronal and behavioral hyperexcitability (Jacobson et al. 2007), as well as retinal dysfunction. Fortenbach and colleagues (2021) could show that the loss of Kv2.1 in mice causes elevated intracellular Ca^{2+} levels in rod photoreceptors due to elevated Ca^{2+} influx through cone cyclic nucleotide-gated channels which ultimately causes rod degeneration. In the brain, the defective formation of an integrin-α5-Kv2.1 macromolecular complex was connected to epilepsy through mechanisms such as abnormal neuronal development (Yu et al. 2019). Finally, mutations in *KCNV2,* encoding Kv8.2, cause the retinal condition cone dystrophy with supernormal rod response (Wu et al. 2006). Similar to retinoschisin-deficient mice (Weber et al. 2002; Gehrig et al. 2006; Takada et al. 2008), Kv8.2-knockout mice reveal a significantly higher apoptotic cell count, a thinner retina, and increased microglia occurrence in the subretinal space (Inamdar et al. 2021; Jiang et al. 2021). Further, it was shown that the localization of Kv2.1 is unaffected in Kv8.2-knockout mice (Inamdar et al. 2021). Thus, it can be speculated that the observed mislocalization of Kv2.1 in retinoschisin-deficient mice is not a consequence of retinal degeneration in general, since retinal degeneration also occurs in Kv8.2-knockout mice. Together, these examples emphasize a possible involvement of aberrantly regulated Kv channels in the pathology of XLRS.

In conclusion, the present findings on interaction partners of the retinal Na/K-ATPase suggest that the retinal Na/K-ATPase interacts with many different proteins and thus may form a macromolecular complex at the inner segments of the mammalian photoreceptors, similar to ATP1A1 and ATP1A2-containing Na/K-ATPases in other cell types like cardiomyocytes or kidney cells (Cui and Xie 2017). Retinoschisin might be a crucial component of the retinal Na/K-ATPase complex by regulating the distribution and stability of the complex and its individual partners.

6 Outlook

In this study, various aspects of retinoschisin interaction with the retinal Na/K-ATPase were addressed. Furthermore, the interplay of retinoschisin with cardiac glycosides at the retinal Na/K-ATPase was dissected and first evidence was given that the retinoschisin-Na/K-ATPase complex forms a macromolecular complex with numerous proteins at the photoreceptor inner segments, regulating their localization, protein expression, and thus probably functionality in the retina.

Data obtained on the ATP1B2 interphase to retinoschisin might contribute to further developments of new therapeutic options for the treatment of XLRS. One option could be an application of artificially generated peptides that simulate the retinoschisin binding site. The advantage in contrast to retinoschisin would be that these peptides are smaller than the double octamer retinoschisin and might therefore be easier to solve, stabilize and apply to the site of pathology (Lee et al. 2019). In general, generation of peptides that mimic the respective protein-binding site are becoming more relevant as drug candidates (Fosgerau and Hoffmann 2015), due to their potential for highly specific binding, combined with low immunogenicity (Groß et al. 2016).

Data on the interplay of retinoschisin and cardiac glycosides at the retinal Na/K-ATPase provide new contemplations for patients administered cardiac glycosides due to cardiac disease and consequently suffer as a side effect from visual disturbances (e.g., Haustein 1982). To reduce pathological effects in the retina after cardiac glycoside treatment, the direct effects of cardiac glycosides on the Na/K-ATPase (regulation of pump activity and intracellular signaling, Aperia et al. (2016)), but also the displacement of retinoschisin and effects on retinal integrity should be considered. It could be plausible to apply externally additional retinoschisin or in general to develop treatments for secondary effects of retinoschisin-deficiency.

Finally, as LC-MS/MS analysis revealed a large number of possible ATP1A3 interaction partners, further verification of other components of the macromolecular complex and the effect of retinoschisin-deficiency on their function is of utmost importance. In addition, it is essential to analyze the interaction with Kv channels in more detail. Like in other studies (Gayet-Primo et al. 2018; Fortenbach et al. 2021), patch-clamp recordings should be carried out in photoreceptors of retinal slices or intact retinal whole mounts of wildtype and retinoschisin-deficient mice to exclude an effect of retinoschisin on the Kv channel mediated ion flow. Based on these results, possible pathological changes in the action potential firing could be treated using Kv channel therapeutics, which may improve symptoms of XLRS pathology. Interestingly, there are pre- and clinical trials for pharmacological modulators of Kv

channels for example to reduce atrial fibrillation or as a possible treatment for epilepsy and multiple sclerosis (Wulff et al. 2009). In addition, further analysis of the interaction partners of ATP1A3 could reveal possible initial signal transducers, which in turn could provide a therapeutic approach by using corresponding inhibitors. In cancer therapy there are many FDA-approved drugs, which can inhibit SRC-mediated signaling (Belli et al. 2020).

Taken together, these new data provide a basis for further studies to elucidate the underlying causes of XLRS and to develop novel targeted therapeutic options.

7 References

Albers, RW. 1967. “Biochemical Aspects of Active Transport.” *Annual Review of Biochemistry* 36:727–56. doi: 10.1146/ANNUREV.BI.36.070167.003455.

Alberts, B., A. Johnson, and J. Lewis. 2002. *Protein Function - Molecular Biology of the Cell*.

Alexander, KR., GA. Fishman, CS. Barnes, and S. Grover. 2001. “ON-Response Deficit in the Electroretinogram of the Cone System in X-Linked Retinoschisis.” *Investigative Ophthalmology and Visual Science* 42(2):453–59.

Ambrosio, L., R. Hansen, R. Kimia, and A. Fulton. 2019. “Retinal Function in X-Linked Juvenile Retinoschisis.” *Investigative Ophthalmology and Visual Science* 60(14):4872–81. doi: 10.1167/iovs.19-27897.

Aperia, A., EE Akkuratov, JM Fontana, and H. Brismar. 2016. “Na+-K+-ATPase, a New Class of Plasma Membrane Receptors.” *American Journal of Physiology. Cell Physiology* 310(7):C491–95. doi: 10.1152/AJPCELL.00359.2015.

Apushkin, MA., GA. Fishman, and AS. Rajagopalan. 2005. “Fundus Findings and Longitudinal Study of Visual Acuity Loss in Patients with X-Linked Retinoschisis.” *Retina (Philadelphia, Pa.)* 25(5):612–18. doi: 10.1097/00006982-200507000-00012.

Bagrov, AlY, OV. Fedorova, RI. Dmitrieva, WN. Howald, AP. Hunter, EA. Kuznetsova, and VlM. Shpen. 1998. “Characterization of a Urinary Bufodienolide Na+,K+-ATPase Inhibitor in Patients after Acute Myocardial Infarction.” *Hypertension (Dallas, Tex. : 1979)* 31(5):1097–1103. doi: 10.1161/01.HYP.31.5.1097.

Barkley, MD., A. Jobe, S. Bourgeois, and AD. Riggs. 1975. “Interaction of Effecting Ligands with Lac Repressor and Repressor-Operator Complex.” *Biochemistry* 14(8):1700–1712. doi: 10.1021/BI00679A024.

Barnes, S., and MEM. Kelly. 2002. “Calcium Channels at the Photoreceptor Synapse.” *Advances in Experimental Medicine and Biology* 514:465–76. doi: 10.1007/978-1-4615-0121-3_28.

Baumgartner, S., K. Hofmann, R. Chiquet-Ehrismann, and P. Bucher. 1998. “The Discoidin Domain Family Revisited: New Members from Prokaryotes and a Homology-Based Fold Prediction.” *Protein Science : A Publication of the Protein Society* 7(7):1626–31. doi: 10.1002/PRO.5560070717.

Belli, S., D. Esposito, A. Servetto, A. Pesapane, L. Formisano, and R. Bianco. 2020. “C-Src and EGFR Inhibition in Molecular Cancer Therapy: What Else Can We Improve?” *Cancers* 12(6):1–16. doi: 10.3390/CANCERS12061489.

Bennett, V., and P. J. Stenbuck. 1979. “Identification and Partial Purification of Ankyrin, the High Affinity Membrane Attachment Site for Human Erythrocyte Spectrin.” *Journal of Biological Chemistry* 254(7):2533–41. doi: 10.1016/s0021-9258(17)30254-5.

Binnion, PF, and G. Frazer. 1980. “[3H]Digoxin in the Optic Tract in Digoxin Intoxication.” *Journal of Cardiovascular Pharmacology* 2(5):699–706. doi: 10.1097/00005344-198009000-00018.

Bush, M., D. Setiaputra, CK. Yip, and RS. Molday. 2016. “Cog-Wheel Octameric Structure of RS1, the Discoidin Domain Containing Retinal Protein Associated with X-Linked Retinoschisis.” *PloS One* 11(1):e0147653. doi: 10.1371/JOURNAL.PONE.0147653.

Chandler, KB, and CE Costello. 2016. “Glycomics and Glycoproteomics of Membrane Proteins and Cell-Surface Receptors: Present Trends and Future Opportunities.” *Electrophoresis* 37(11):1407–19. doi: 10.1002/ELPS.201500552.

Chen, D., T. Xu, M. Tu, J. Xu, C. Zhou, L. Cheng, R. Yang, T. Yang, W. Zheng, X. He, R. Deng, X. Ge, J. Li, Z. Song, J. Zhao, and F. Gu. 2018. “Recapitulating X-Linked Juvenile Retinoschisis in Mouse Model by Knock-In Patient-Specific Novel Mutation.” *Frontiers in Molecular Neuroscience* 10:453. doi: 10.3389/FNMOL.2017.00453.

Chen, H., B. Liu, and AH Neufeld. 2007. “Epidermal Growth Factor Receptor in Adult Retinal Neurons of Rat, Mouse, and Human.” *The Journal of Comparative Neurology* 500(2):299–310. doi: 10.1002/CNE.21161.

Chiantia, S., J. Ries, and P. Schwille. 2009. “Fluorescence Correlation Spectroscopy in Membrane Structure Elucidation.” *Biochimica et Biophysica Acta (BBA) - Biomembranes* 1788(1):225–33. doi: 10.1016/J.BBAMEM.2008.08.013.

Le Clainche, C., SP. Dwivedi, D. Didry, and MF. Carlier. 2010. “Vinculin Is a Dually Regulated Actin Filament Barbed End-Capping and Side-Binding Protein.” *The Journal of Biological Chemistry* 285(30):23420–32. doi: 10.1074/JBC.M110.102830.

Clausen, MV., F. Hilbers, and H. Poulsen. 2017. “The Structure and Function of the Na,K-ATPase Isoforms in

Health and Disease." *Frontiers in Physiology* 8(jun 6):371.

Cui, X., and Z. Xie. 2017. "Protein Interaction and Na/K-ATPase-Mediated Signal Transduction." *Molecules* 22(6):990. doi: 10.3390/MOLECULES22060990.

Dai, J., Q. Zhou, J. Chen, ML. Rexius-Hall, J. Rehman, and G. Zhou. 2018. "Alpha-Enolase Regulates the Malignant Phenotype of Pulmonary Artery Smooth Muscle Cells via the AMPK-Akt Pathway." *Nature Communications* 9(1):3850. doi: 10.1038/S41467-018-06376-X.

Dallacasagrande, V., and KA. Hajjar. 2020. "Annexin A2 in Inflammation and Host Defense." *Cells* 9(6):1499. doi: 10.3390/CELLS9061499.

Dempski, Robert E., T. Friedrich, and E. Bamberg. 2005. "The β Subunit of the Na+/K+-ATPase Follows the Conformational State of the Holoenzyme." *The Journal of General Physiology* 125(5):505. doi: 10.1085/JGP.200409186.

Deutsch, E., AV. Weigel, EJ. Akin, P: Fox, G: Hansen, CJ. Haberkorn, R. Loftus, D: Krapf, and MM. Tamkun. 2012. "Kv2.1 Cell Surface Clusters Are Insertion Platforms for Ion Channel Delivery to the Plasma Membrane." *Molecular Biology of the Cell* 23(15):2917–29. doi: 10.1091/MBC.E12-01-0047/ASSET/IMAGES/LARGE/2917FIG10.JPEG.

Duncker, G. 1981. "Ocular Side Effects of Digitalis." *Klinische Monatsblatter Fur Augenheilkunde* 178(5):397–98. doi: 10.1055/S-2008-1057231.

Dyka, F., WW. Wu, TA. Pfeifer, LL. Molday, TA. Grigliatti, and RS. Molday. 2008. "Characterization and Purification of the Discoidin Domain-Containing Protein Retinoschisin and Its Interaction with Galactose." *Biochemistry* 47(35):9098–9106. doi: 10.1021/BI800938G.

Fahim, AT., N. Ali, T. Blachley, and M. Michaelides. 2017. "Peripheral Fundus Findings in X-Linked Retinoschisis." *British Journal of Ophthalmology* 101(11):1555–59. doi: 10.1136/BJOPHTHALMOL-2016-310110.

Forsius, H., U. Krause, J. Helve, V. Vuopala, E. Mustonen, B. Vainio-Mattila, J. Fellman, and A. W. Eriksson. 1973. "Visual Acuity in 183 Cases of X-Chromosomal Retinoschisis." *Canadian Journal of Ophthalmology. Journal Canadien d'ophtalmologie* 8(3):385–93.

Fortenbach, C., GP. Allina, CM. Shores, SJ. Karlen, EB. Miller, H. Bishop, JS. Trimmer, ME. Burns, and EN. Pugh. 2021. "Loss of the K+ Channel Kv2.1 Greatly Reduces Outward Dark Current and Causes Ionic Dysregulation and Degeneration in Rod Photoreceptors." *The Journal of General Physiology* 153(2):e202012687. doi: 10.1085/JGP.202012687.

Fosgerau, K., and T. Hoffmann. 2015. "Peptide Therapeutics: Current Status and Future Directions." *Drug Discovery Today* 20(1):122–28. doi: 10.1016/J.DRUDIS.2014.10.003.

Fraunfelder, FT, and FW Fraunfelder. 2014. *Drug-Induced Ocular Side Effects*.

Friedrich, U., H. Stöhr, D. Hilfinger, T. Loenhardt, M. Schachner, T. Langmann, and BHF. Weber. 2011. "The Na/K-ATPase Is Obligatory for Membrane Anchorage of Retinoschisin, the Protein Involved in the Pathogenesis of X-Linked Juvenile Retinoschisis." *Human Molecular Genetics* 20(6):1132–42. doi: 10.1093/HMG/DDQ557.

Fuentes-Prior, P., K. Fujikawa, and K. P. Pratt. 2002. "New Insights into Binding Interfaces of Coagulation Factors V and VIII and Their Homologues Lessons from High Resolution Crystal Structures." *Current Protein & Peptide Science* 3(3):313–39. doi: 10.2174/1389203023380639.

Gaborit, N., A. Varro, S. Le Bouter, V. Szuts, D. Escande, S. Nattel, and S. Demolombe. 2010. "Gender-Related Differences in Ion-Channel and Transporter Subunit Expression in Non-Diseased Human Hearts." *Journal of Molecular and Cellular Cardiology* 49(4):639–46. doi: 10.1016/J.YJMCC.2010.06.005.

Gayet-Primo, J., DB. Yaeger, RA. Khanjian, and T. Puthussery. 2018. "Heteromeric K V 2/K V 8.2 Channels Mediate Delayed Rectifier Potassium Currents in Primate Photoreceptors." *The Journal of Neuroscience : The Official Journal of the Society for Neuroscience* 38(14):3414–27. doi: 10.1523/JNEUROSCI.2440-17.2018.

Geering, K. 2006. "FXYD Proteins: New Regulators of Na-K-ATPase." *American Journal of Physiology. Renal Physiology* 290(2):F241-50. doi: 10.1152/AJPRENAL.00126.2005.

Geering, K. 2008. "Functional Roles of Na,K-ATPase Subunits." *Current Opinion in Nephrology and Hypertension* 17(5):526–32. doi: 10.1097/MNH.0B013E3283036CBF.

Gegelashvili, M., A. Rodriguez-Kern, L. Sung, K. Shimamoto, and G. Gegelashvili. 2007. "Glutamate Transporter GLAST/EAAT1 Directs Cell Surface Expression of FXYD2/Gamma Subunit of Na, K-ATPase in Human Fetal Astrocytes." *Neurochemistry International* 50(7–8):916–20. doi: 10.1016/J.NEUINT.2006.12.015.

Gehrig, A., A. Janssen, F. Horling, C. Grimm, and B. H. F. Weber. 2006. "The Role of Caspases in Photoreceptor Cell Death of the Retinoschisin-Deficient Mouse." *Cytogenetic and Genome Research* 115(1):35–44. doi:

10.1159/000094799.

Gehrig, A., T. Langmann, F. Horling, A. Janssen, M. Bonin, M. Walter, S. Poths, and B. H. F. Weber. 2007. “Genome-Wide Expression Profiling of the Retinoschisin-Deficient Retina in Early Postnatal Mouse Development.” *Investigative Ophthalmology and Visual Science* 48(2):891–900. doi: 10.1167/IOVS.06-0641.

Geibel, S., D. Zimmermann, G. Zifarelli, A. Becker, JB. Koenderink, YK Hu, JH. Kaplan, T. Friedrich, and E. Bamberg. 2003. “Conformational Dynamics of Na+/K+- and H+/K+-ATPase Probed by Voltage Clamp Fluorometry.” *Annals of the New York Academy of Sciences* 986:31–38. doi: 10.1111/J.1749-6632.2003.TB07136.X.

George, N. D. L., J. R. W. Yates, and A. T. Moore. 1995. “X Linked Retinoschisis.” *The British Journal of Ophthalmology* 79(7):697. doi: 10.1136/BJO.79.7.697.

George, N. D. L., J. R. W. Yates, and A. T. Moore. 1996. “Clinical Features in Affected Males with X-Linked Retinoschisis.” *Archives of Ophthalmology (Chicago, Ill.: 1960)* 114(3):274–80. doi: 10.1001/ARCHOPHT.1996.01100130270007.

Gerth, C., RJ. Zawadzki, JS. Werner, and E. Héon. 2008. “Retinal Morphological Changes of Patients with X-Linked Retinoschisis Evaluated by Fourier-Domain Optical Coherence Tomography.” *Archives of Ophthalmology (Chicago, Ill. : 1960)* 126(6):807–11. doi: 10.1001/ARCHOPHT.126.6.807.

Gloor, S., H. Antonicek, K. J. Sweadner, S. Pagliusi, R. Frank, M. Moos, and M. Schachner. 1990. “The Adhesion Molecule on Glia (AMOG) Is a Homologue of the Beta Subunit of the Na,K-ATPase.” *The Journal of Cell Biology* 110(1):165. doi: 10.1083/JCB.110.1.165.

Goto, A., T. Ishiguro, K. Yamada, M. Ishii, M. Yoshioka, C. Eguchi, M. Shimora, and T. Sugimoto. 1990. “Isolation of a Urinary Digitalis-like Factor Indistinguishable from Digoxin.” *Biochemical and Biophysical Research Communications* 173(3):1093–1101. doi: 10.1016/S0006-291X(05)80898-8.

Graven, KK., LH. Zimmerman, EW. Dickson, GL. Weinhouse, and HW. Farber. 1993. “Endothelial Cell Hypoxia Associated Proteins Are Cell and Stress Specific.” *Journal of Cellular Physiology* 157(3):544–54. doi: 10.1002/JCP.1041570314.

Grayson, C., SNM. Reid, JA. Ellis, A. Rutherford, JC. Sowden, JRW. Yates, DB. Farber, and D. Trump. 2000. “Retinoschisin, the X-Linked Retinoschisis Protein, Is a Secreted Photoreceptor Protein, and Is Expressed and Released by Weri-Rb1 Cells.” *Human Molecular Genetics* 9(12):1873–79. doi: 10.1093/HMG/9.12.1873.

Groß, A., C. Hashimoto, H. Sticht, and J. Eichler. 2016. “Synthetic Peptides as Protein Mimics.” *Frontiers in Bioengineering and Biotechnology* 3:211. doi: 10.3389/FBIOE.2015.00211.

Grynkiewicz, G., M. Poenie, and R. Y. Tsien. 1985. “A New Generation of Ca2+ Indicators with Greatly Improved Fluorescence Properties.” *Journal of Biological Chemistry* 260(6):3440–50.

Haas, J. 1898. “Ueber Das Zusammenvorkommen von Veranderungen Der Retina Und Choroidea.” *Arch Augenheilkd* 37:343–48.

Hamlyn, J. M., M. P. Blaustein, S. Bova, D. W. Ducharme, D. W. Harris, F. Mandel, W. R. Mathews, and J. H. Ludens. 1991. “Identification and Characterization of a Ouabain-like Compound from Human Plasma.” *Proceedings of the National Academy of Sciences of the United States of America* 88(14):6259–63. doi: 10.1073/PNAS.88.14.6259.

Hanson, SM., WM. Cleghorn, DJ. Francis, SA. Vishnivetskiy, D. Raman, X. Song, KS Nair, VZ. Slepak, CS. Klug, and VV. Gurevich. 2007. “Arrestin Mobilizes Signaling Proteins to the Cytoskeleton and Redirects Their Activity.” *Journal of Molecular Biology* 368(2):375. doi: 10.1016/J.JMB.2007.02.053.

Hasler, D., R. Meduri, M. Bąk, G. Lehmann, L. Heizinger, X. Wang, Z. Li, FM. Sement, A. Bruckmann, AC Dock-Bregeon, R. Merkl, R. Kalb, E. Grauer, E. Kunstmann, M. Zavolan, MF Liu, U. Fischer, and G. Meister. 2020. “The Alazami Syndrome-Associated Protein LARP7 Guides U6 Small Nuclear RNA Modification and Contributes to Splicing Robustness.” *Molecular Cell* 77(5):1014-1031.e13. doi: 10.1016/J.MOLCEL.2020.01.001.

Haustein, K. O. 1982. “Digitalis.” *Pharmacology & Therapeutics* 18(1):1–89. doi: 10.1016/0163-7258(82)90026-2.

Heidelberger, R., WB. Thoreson, and P. Witkovsky. 2005. “Synaptic Transmission at Retinal Ribbon Synapses.” *Progress in Retinal and Eye Research* 24(6):682–720. doi: 10.1016/J.PRETEYERES.2005.04.002.

Heymann, JB, C. Vijayasarathy, RK. Huang, AD. Dearborn, PA. Sieving, and AC. Steven. 2019. “Cryo-EM of Retinoschisin Branched Networks Suggests an Intercellular Adhesive Scaffold in the Retina.” *Journal of Cell Biology* 218(3):1027–38. doi: 10.1083/jcb.201806148.

Hinshaw, SJH., O. Ogbeifun, WS. Wandu, C. Lyu, G. Shi, Y. Li, H. Qian, and I. Gery. 2016. “Digoxin Inhibits Induction of Experimental Autoimmune Uveitis in Mice, but Causes Severe Retinal Degeneration.”

Investigative Ophthalmology & Visual Science 57(3):1441–47. doi: 10.1167/IOVS.15-19040.

Howard, JL., and SM. Ridley. 1990. “Acetyl-CoA Carboxylase: A Rapid Novel Assay Procedure Used in Conjunction with the Preparation of Enzyme from Maize Leaves.” *FEBS Letters* 261(2):261–64. doi: 10.1016/0014-5793(90)80567-3.

Hu, Z., B. Ma, H. Wolfson, and R. Nussinov. 2000. “Conservation of Polar Residues as Hot Spots at Protein Interfaces.” *Proteins: Structure, Function and Genetics* 39(4):331–42. doi: 10.1002/(SICI)1097-0134(20000601)39:4<331::AID-PROT60>3.0.CO;2-A.

Illarionova, N. B., E. Gunnarson, Y. Li, H. Brismar, A. Bondar, S. Zelenin, and A. Aperia. 2010. “Functional and Molecular Interactions between Aquaporins and Na,K-ATPase.” *Neuroscience* 168(4):915–25. doi: 10.1016/J.NEUROSCIENCE.2009.11.062.

Inamdar, SM., CK. Lankford, D. Poria, JG. Laird, E. Solessio, VJ. Kefalov, and SA. Baker. 2021. “Differential Impact of Kv8.2 Loss on Rod and Cone Signaling and Degeneration.” *Human Molecular Genetics* Oct(15):ddab301. doi: 10.1093/HMG/DDAB301.

Jablonski, M. M., C. Dalke, X. F. Wang, L. Lu, K. F. Manly, W. Pretsch, J. Favor, M. T. Pardue, E. M. Rinchik, R. W. Williams, D. Goldowitz, and J. Graw. 2005. “An ENU-Induced Mutation in Rs1h Causes Disruption of Retinal Structure and Function.” *Molecular Vision* 11:569–81.

Jacobson, DA., A. Kuznetsov, JP. Lopez, S. Kash, CE. Ämmälä, and LHH. Philipson. 2007. “Kv2.1 Ablation Alters Glucose-Induced Islet Electrical Activity, Enhancing Insulin Secretion.” *Cell Metabolism* 6(3):229–35. doi: 10.1016/J.CMET.2007.07.010.

Jędrychowska, J., and V. Korzh. 2019. “Kv2.1 Voltage-Gated Potassium Channels in Developmental Perspective.” *Developmental Dynamics : An Official Publication of the American Association of Anatomists* 248(12):1180–94. doi: 10.1002/DVDY.114.

Jiang, S., and Y. Xu. 2019. “Annexin A2 Upregulation Protects Human Retinal Endothelial Cells from Oxygen-glucose Deprivation Injury by Activating Autophagy.” *Experimental and Therapeutic Medicine* 18(4):2901–8. doi: 10.3892/ETM.2019.7909.

Jiang, X., R. Rashwan, V. Voigt, J. Nerbonne, DM. Hunt, and LS. Carvalho. 2021. “Molecular, Cellular and Functional Changes in the Retinas of Young Adult Mice Lacking the Voltage-Gated K+ Channel Subunits Kv8.2 and K2.1.” *International Journal of Molecular Sciences* 22(9):4877. doi: 10.3390/IJMS22094877.

Jones, TY Li, Arystarkhova; E, KJ Barr, RK Wetzel, K. Markham, KJ Sweadner, GH Fong, and GM Kidder. 2005. “Na,K-ATPase from Mice Lacking the Gamma Subunit (FXYD2) Exhibits Altered Na+ Affinity and Decreased Thermal Stability.” *The Journal of Biological Chemistry* 280(19):19003–11. doi: 10.1074/JBC.M500697200.

de Juan-Sanz, J., E. Núñez, L. Villarejo-López, D. Pérez-Hernández, AEF Rodriguez, B. López-Corcuera, J. Vázquez, and C. Aragón. 2013. “Na+/K+-ATPase Is a New Interacting Partner for the Neuronal Glycine Transporter GlyT2 That Downregulates Its Expression In Vitro and In Vivo.” *Journal of Neuroscience* 33(35):14269–81. doi: 10.1523/JNEUROSCI.1532-13.2013.

Junghans, C., FJ. Schmitt, V. Vukojević, and T. Friedrich. 2016. “Monitoring the Diffusion Behavior of Na,K-ATPase by Fluorescence Correlation Spectroscopy (FCS) upon Fluorescence Labelling with EGFP or Dreiklang.” *Optofluidics, Microfluidics and Nanofluidics* 2(1):1–14. doi: 10.1515/OPTOF-2015-0001/PDF.

Junghans, C., V. Vukojević, NN. Tavraz, EG. Maksimov, W. Zuschratter, FJ. Schmitt, and T. Friedrich. 2017. “Disruption of Ankyrin B and Caveolin-1 Interaction Sites Alters Na +,K +-ATPase Membrane Diffusion.” *Biophysical Journal* 113(10):2249–60. doi: 10.1016/J.BPJ.2017.08.053.

Kamerzell, TJ., and CR Middaugh. 2008. “The Complex Inter-Relationships between Protein Flexibility and Stability.” *Journal of Pharmaceutical Sciences* 97(9):3494–3517. doi: 10.1002/JPS.21269.

Kanner, BI. 2006. “Structure and Function of Sodium-Coupled GABA and Glutamate Transporters.” *The Journal of Membrane Biology* 213(2):89–100. doi: 10.1007/S00232-006-0877-5.

Kawamura, A., J. Guo, Y. Itagaki, C. Bell, Y. Wang, GT. Haupert, S. Magil, RT. Gallagher, N. Berova, and K. Nakanishi. 1999. “On the Structure of Endogenous Ouabain.” *Proceedings of the National Academy of Sciences of the United States of America* 96(12):6654–59. doi: 10.1073/PNAS.96.12.6654.

Keller, A., J. Peltzer, G. Carpentier, I. Horváth, J. Oláh, A. Duchesnay, F. Orosz, and J. Ovádi. 2007. “Interactions of Enolase Isoforms with Tubulin and Microtubules during Myogenesis.” *Biochimica et Biophysica Acta* 1770(6):919–26. doi: 10.1016/J.BBAGEN.2007.01.015.

Khan, NW., JA. Jamison, JA. Kemp, and PA. Sieving. 2001. “Analysis of Photoreceptor Function and Inner Retinal Activity in Juvenile X-Linked Retinoschisis.” *Vision Research* 41(28):3931–42. doi: 10.1016/S0042-6989(01)00188-2.

Kiedzierska, A., K. Smietana, H. Czepczynska, and J. Otlewski. 2007. “Structural Similarities and Functional Diversity of Eukaryotic Discoidin-like Domains.” *Biochimica et Biophysica Acta* 1774(9):1069–78. doi: 10.1016/J.BBAPAP.2007.07.007.

Kinoshita, J., N. Iwata, T. Kimotsuki, and M. Yasuda. 2014. “Digoxin-Induced Reversible Dysfunction of the Cone Photoreceptors in Monkeys.” *Investigative Ophthalmology & Visual Science* 55(2):881–92. doi: 10.1167/IOVS.13-13296.

Kizhatil, K., NK. Sandhu, NS. Peachey, and V. Bennett. 2009. “Ankyrin-B Is Required for Coordinated Expression of Beta-2-Spectrin, the Na/K-ATPase and the Na/Ca Exchanger in the Inner Segment of Rod Photoreceptors.” *Experimental Eye Research* 88(1):57–64. doi: 10.1016/J.EXER.2008.09.022.

Kotova, S., C. Vijayasarathy, EK. Dimitriadis, L. Ikonomou, H. Jaffe, and PA. Sieving. 2010. “Retinoschisin (RS1) Interacts with Negatively Charged Lipid Bilayers in the Presence of Ca2+: An Atomic Force Microscopy Study.” *Biochemistry* 49(33):7023–32. doi: 10.1021/BI1007029.

Krupinski, T., and GJ. Beitel. 2009. “Unexpected Roles of the Na-K-ATPase and Other Ion Transporters in Cell Junctions and Tubulogenesis.” *Physiology (Bethesda, Md.)* 24(3):192–201. doi: 10.1152/PHYSIOL.00008.2009.

Kwok, MCM., JM. Holopainen, LL. Molday, LJ. Fosteer, and RS. Molday. 2008. “Proteomics of Photoreceptor Outer Segments Identifies a Subset of SNARE and Rab Proteins Implicated in Membrane Vesicle Trafficking and Fusion.” *Molecular & Cellular Proteomics : MCP* 7(6):1053–66. doi: 10.1074/MCP.M700571-MCP200.

Labbadia, J., and RI. Morimoto. 2015. “The Biology of Proteostasis in Aging and Disease.” *Annual Review of Biochemistry* 84:435–64. doi: 10.1146/ANNUREV-BIOCHEM-060614-033955.

Laurita, KR., and DS. Rosenbaum. 2008. “Mechanisms and Potential Therapeutic Targets for Ventricular Arrhythmias Associated with Impaired Cardiac Calcium Cycling.” *Journal of Molecular and Cellular Cardiology* 44(1):31–43. doi: 10.1016/J.YJMCC.2007.10.012.

Laursen, M., L. Yatime, P. Nissen, and NU. Fedosova. 2013. “Crystal Structure of the High-Affinity Na+,K+-ATPase–Ouabain Complex with Mg2+ Bound in the Cation Binding Site.” *Proceedings of the National Academy of Sciences of the United States of America* 110(27):10958. doi: 10.1073/PNAS.1222308110.

Lawrenson, J. G., C. Kelly, A. L. Lawrenson, and J. Birch. 2002. “Acquired Colour Vision Deficiency in Patients Receiving Digoxin Maintenance Therapy.” *The British Journal of Ophthalmology* 86(11):1259–61. doi: 10.1136/BJO.86.11.1259.

Lee, ACL., JL. Harris, KK. Khanna, and JH. Hong. 2019. “A Comprehensive Review on Current Advances in Peptide Drug Development and Design.” *International Journal of Molecular Sciences* 20(10). doi: 10.3390/IJMS20102383.

Lee, JJ., JH. Kim, SY. Kim, SS. Park, and YS. Yu. 2009. “Infantile Vitreous Hemorrhage as the Initial Presentation of X-Linked Juvenile Retinoschisis.” *Korean Journal of Ophthalmology : KJO* 23(2):118. doi: 10.3341/KJO.2009.23.2.118.

Léger, H., E. Santana, WA. Beltran, and FC. Luca. 2019. “Preparation of Mouse Retinal Cryo-Sections for Immunohistochemistry.” *Journal of Visualized Experiments : JoVE* 2019(149). doi: 10.3791/59683.

Leitenberger, SM., E. Reister-Gottfried, and U. Seifert. 2008. “Curvature Coupling Dependence of Membrane Protein Diffusion Coefficients.” *Langmuir* 24(4):1254–61. doi: 10.1021/la702319q.

Leitinger, B. 2003. “Molecular Analysis of Collagen Binding by the Human Discoidin Domain Receptors, DDR1 and DDR2. Identification of Collagen Binding Sites in DDR2.” *The Journal of Biological Chemistry* 278(19):16761–69. doi: 10.1074/JBC.M301370200.

Lissner, W., JE. Greenlee, JD. Cameron, and SB. Goren. 1971. “Localization of Tritiated Digoxin in the Rat Eye.” *American Journal of Ophthalmology* 72(3):608–14. doi: 10.1016/0002-9394(71)90860-9.

Liu, G., N. Volpe, and S. Galetta. 2019. *Liu, Volpe, and Galetta’s Neuro-Ophthalmology*. Elsevier.

Liu, Pin W., and Bruce P. Bean. 2014. “Kv2 Channel Regulation of Action Potential Repolarization and Firing Patterns in Superior Cervical Ganglion Neurons and Hippocampal CA1 Pyramidal Neurons.” *The Journal of Neuroscience : The Official Journal of the Society for Neuroscience* 34(14):4786–4800. doi: 10.1523/JNEUROSCI.1925-13.2014.

Liu, Q., G. Tan, N. Levenkova, T. Li, EN. Pugh, JJ. Rux, DW. Speichers, and EA. Pierce. 2007. “The Proteome of the Mouse Photoreceptor Sensory Cilium Complex.” *Molecular & Cellular Proteomics : MCP* 6(8):1299–1317. doi: 10.1074/MCP.M700054-MCP200.

Liu, Y., J. Kinoshita, E. Ivanova, D. Sun, H. Li, T. Liao, J. Cao, BA. Bell, JM. Wang, and Y. Tang. 2019. “Mouse Models of X-Linked Juvenile Retinoschisis Have an Early Onset Phenotype, the Severity of Which Varies with

Genotype." *Human Molecular Genetics* 28(18):3072–90. doi: 10.1093/HMG/DDZ122.

Livak, KJ., and TD. Schmittgen. 2001. "Analysis of Relative Gene Expression Data Using Real-Time Quantitative PCR and the 2(-Delta Delta C(T)) Method." *Methods (San Diego, Calif.)* 25(4):402–8. doi: 10.1006/METH.2001.1262.

Lopatina, E. V., AV. Karetsky, VA. Penniyaynen, and TV Vinogradova. 2008. "Role of Cardiac Glycosides in Regulation of the Growth of Retinal Tissue Explants." *Bulletin of Experimental Biology and Medicine* 146(6):744–46. doi: 10.1007/S10517-009-0384-7.

Lubarski, I., K. Pihakaski-Maunsbach, SJD. Karlish, AB. Maunsbach, and H. Garty. 2005. "Interaction with the Na,K-ATPase and Tissue Distribution of FXYD5 (Related to Ion Channel)." *The Journal of Biological Chemistry* 280(45):37717–24. doi: 10.1074/JBC.M506397200.

Ma, B., T. Elkayam, H. Wolfson, and R. Nussinov. 2003. "Protein-Protein Interactions: Structurally Conserved Residues Distinguish between Binding Sites and Exposed Protein Surfaces." *Proceedings of the National Academy of Sciences of the United States of America* 100(10):5772–77. doi: 10.1073/PNAS.1030237100.

Madan, N., Y. Xu, Q. Duan, M. Banerjee, I. Larre, SV. Pierre, and Z. Xie. 2017. "Src-Independent ERK Signaling through the Rat A3 Isoform of Na/K-ATPase." *American Journal of Physiology. Cell Physiology* 312(3):C222–32. doi: 10.1152/AJPCELL.00199.2016.

Madreperla, SA., M Johnson, and K. Nakatani. 1994. "Electrophysiologic and Electroretinographic Evidence for Photoreceptor Dysfunction as a Toxic Effect of Digoxin." *Archives of Ophthalmology (Chicago, Ill. : 1960)* 112(6):807–12. doi: 10.1001/ARCHOPHT.1994.01090180105044.

Marquis-Omer, D., G. Sanyal, DB. Volkin, AI. Marcy, HK Chan, JA. Ryan, and CR Middaugh. 1991. "Stabilization of the FK506 Binding Protein by Ligand Binding." *Biochemical and Biophysical Research Communications* 179(2):741–48. doi: 10.1016/0006-291X(91)91879-H.

Mathews, WR, DW. DuCharme, JM. Hamlyn, DW. Harris, F. Mandel, MA. Clark, and JH. Ludens. 1991. "Mass Spectral Characterization of an Endogenous Digitalislike Factor from Human Plasma." *Hypertension (Dallas, Tex. : 1979)* 17(6 Pt 2):930–35. doi: 10.1161/01.HYP.17.6.930.

Matsumoto, H., and N. Komori. 2000. "Ocular Proteomics: Cataloging Photoreceptor Proteins by Two-Dimensional Gel Electrophoresis and Mass Spectrometry." *Methods in Enzymology* 316:492–511. doi: 10.1016/S0076-6879(00)16745-X.

Mirsaeidi, M., S. Gidfar, A. Vu, and D. Schraufnagel. 2016. "Annexins Family: Insights into Their Functions and Potential Role in Pathogenesis of Sarcoidosis." *Journal of Translational Medicine* 14(1):14:89. doi: 10.1186/S12967-016-0843-7.

Mohler, PJ., JQ. Davis, and V. Bennett. 2005. "Ankyrin-B Coordinates the Na/K ATPase, Na/Ca Exchanger, and InsP3 Receptor in a Cardiac T-Tubule/SR Microdomain." *PLoS Biology* 3(12):1–10. doi: 10.1371/JOURNAL.PBIO.0030423.

Molday, L. L., D. Hicks, C. G. Sauer, B. H. F. Weber, and R. S. Molday. 2001. "Expression of X-Linked Retinoschisis Protein RS1 in Photoreceptor and Bipolar Cells." *Investigative Ophthalmology & Visual Science* 42(3):816–25.

Molday, RS, WW Wu, and LL Molday. 2007. "Retinoschisin (RS1), the Protein Encoded by the X-Linked Retinoschisis Gene, Is Anchored to the Surface of Retinal Photoreceptor and Bipolar Cells through Its Interactions with a Na/K ATPase-SARM1 Complex." *The Journal of Biological Chemistry* 282(45):32792–801. doi: 10.1074/JBC.M706321200.

Morel, V., R. Poschet, V. Traverso, and D. Deretic. 2000. "Towards the Proteome of the Rhodopsin-Bearing Post-Golgi Compartment of Retinal Photoreceptor Cells." Pp. 3460–69 in *Electrophoresis*. Vol. 21.

Morgans, CW., PR. Bayley, NW. Oesch, G. Ren, L. Akileswaran, and WR Taylor. 2005. "Photoreceptor Calcium Channels: Insight from Night Blindness." *Visual Neuroscience* 22(5):561–68. doi: 10.1017/S0952523805225038.

Moss, SE., and RO. Morgan. 2004. "The Annexins." *Genome Biology* 5(4). doi: 10.1186/GB-2004-5-4-219.

Naji, A., and FLH Brown. 2007. "Diffusion on Ruffled Membrane Surfaces." *The Journal of Chemical Physics* 126(23):235103. doi: 10.1063/1.2739526.

Nam, JS, S. Hirohashi, and LM. Wakefield. 2007. "Dysadherin: A New Player in Cancer Progression." *Cancer Letters* 255(2):161–69. doi: 10.1016/J.CANLET.2007.02.018.

Nishi, A., G. Fisone, GL. Snyder, I. Dulubova, A. Aperia, AC. Nairn, and P. Greengard. 1999. "Regulation of Na+, K+-ATPase Isoforms in Rat Neostriatum by Dopamine and Protein Kinase C." *Journal of Neurochemistry* 73(4):1492–1501. doi: 10.1046/J.1471-4159.1999.0731492.X.

Nishimura, N., M. Munakata, T. Mori, K. Okuda, N. Nishino, S. Hirose, C. Kosaka, M. Masuda, and H. Takahashi. 2001. “Identification of Endogenous Ouabain in Culture Supernatant of PC12 Cells.” *Journal of Hypertension* 19(2):229–36. doi: 10.1097/00004872-200102000-00009.

O’Connell, KMS, R. Loftus, and MM. Tamkun. 2010. “Localization-Dependent Activity of the Kv2.1 Delayed-Rectifier K + Channel.” *Proceedings of the National Academy of Sciences of the United States of America* 107(27):12351–56. doi: 10.1073/PNAS.1003028107/-/DCSUPPLEMENTAL/PNAS.201003028SI.PDF.

Padrón-Pérez, N., J. Català-Mora, J. Díaz, L. Arias, J. Prat, and J. M. Caminal. 2018. “Swept-Source and Optical Coherence Tomography Angiography in Patients with X-Linked Retinoschisis.” *Eye (London, England)* 32(4):707–15. doi: 10.1038/EYE.2017.281.

Pagenstecher, H. E. 1913. “Ueber Eine Unter Dem Bilde Der Netzhauterblosung Verlaufende, Erbliche Erkrankung Der Retina.” *Graefes Arch Ophthalmol* 86:457–62.

Pandya, NJ., C. Seeger, N. Babai, MA. Gonzalez-Lozano, V. Mack, JC. Lodder, Y. Gouwenberg, HD. Mansvelder, U. H. Danielson, KW Li, M. Heine, S. Spijker, R. Frischknecht, and AB. Smit. 2018. “Noelin1 Affects Lateral Mobility of Synaptic AMPA Receptors.” *Cell Reports* 24(5):1218–30. doi: 10.1016/J.CELREP.2018.06.102.

Patel, S. 2016. “Plant-Derived Cardiac Glycosides: Role in Heart Ailments and Cancer Management.” *Biomedicine & Pharmacotherapy = Biomedecine & Pharmacotherapie* 84:1036–41. doi: 10.1016/J.BIOPHA.2016.10.030.

Pfeffer, SR., AB. Dirac-Svejstrup, and T. Soldati. 1995. “Rab GDP Dissociation Inhibitor: Putting Rab GTPases in the Right Place.” *The Journal of Biological Chemistry* 270(29):17057–59. doi: 10.1074/JBC.270.29.17057.

Piesse, C., S. Cadel, C. Gouzy-Darmon, JC Jeanny, V. Carrière, D. Goidin, L. Jonet, D. Gourdji, P. Cohen, and Thierry Foulon. 2004. “Expression of Aminopeptidase B in the Developing and Adult Rat Retina.” *Experimental Eye Research* 79(5):639–48. doi: 10.1016/J.EXER.2004.06.030.

Del Pilar Gomez, M., G. Waloga, and E. Nasi. 1993. “Electrical Properties of Y-79 Cells, a Multipotent Line of Human Retinoblastoma.” *Journal of Neurophysiology* 70(4):1476–86. doi: 10.1152/JN.1993.70.4.1476.

Plössl, K., M. Royer, S. Bernklau, NN. Tavraz, T. Friedrich, J. Wild, BHF Weber, and U. Friedrich. 2017. “Retinoschisin Is Linked to Retinal Na/K-ATPase Signaling and Localization.” *Molecular Biology of the Cell* 28(16):2178–89. doi: 10.1091/MBC.E17-01-0064. (b)

Plössl, K., V. Schmid, K. Straub, C. Schmid, M. Ammon, R. Merkl, B H F Weber, and U. Friedrich. 2018. “Pathomechanism of Mutated and Secreted Retinoschisin in X-Linked Juvenile Retinoschisis.” *Experimental Eye Research* 177:23–34. doi: 10.1016/J.EXER.2018.07.021.

Plössl, K., B. H. F. Weber, and U. Friedrich. 2017. “The X-Linked Juvenile Retinoschisis Protein Retinoschisin Is a Novel Regulator of Mitogen-Activated Protein Kinase Signalling and Apoptosis in the Retina.” *Journal of Cellular and Molecular Medicine* 21(4):768–80. doi: 10.1111/JCMM.13019. (a)

Plössl, K. Straub, V. Schmid, F. Strunz, J. Wild, R. Merkl, BHF Weber, and U. Friedrich. 2019. “Identification of the Retinoschisin-Binding Site on the Retinal Na/K-ATPase.” *PloS One* 14(5):e0216320. doi: 10.1371/JOURNAL.PONE.0216320.

Post, R. L., C. Hegyvary, and S. Kume. 1972. “Activation by Adenosine Triphosphate in the Phosphorylation Kinetics of Sodium and Potassium Ion Transport Adenosine Triphosphatase.” *The Journal of Biological Chemistry* 247(20):6530–40. doi: 10.1016/s0021-9258(19)44725-x.

Post, R. L., S. Kume, T. Tobin, B. Orcutt, and A. K. Sen. 1969. “Flexibility of an Active Center in Sodium-plus-Potassium Adenosine Triphosphatase.” *The Journal of General Physiology* 54(1):306–26. doi: 10.1085/JGP.54.1.306.

Prados-Rosales, RC., G. Aragoneses-Cazorla, H. Estevez, E. Garcia-Calvo, A. Machuca, and JL. Luque-Garcia. 2019. “Strategies for Membrane Protein Analysis by Mass Spectrometry.” *Advances in Experimental Medicine and Biology* 1140:289–98. doi: 10.1007/978-3-030-15950-4_16.

Prasad, A., R. Wagner, and N. Bhagat. 2006. “Vitreous Hemorrhage as the Initial Manifestation of X-Linked Retinoschisis in a 9-Month-Old Infant.” *Journal of Pediatric Ophthalmology and Strabismus* 43(1):56–58. doi: 10.3928/01913913-20060101-12.

Prassas, I., and EP. Diamandis. 2008. “Novel Therapeutic Applications of Cardiac Glycosides.” *Nature Reviews. Drug Discovery* 7(11):926–35. doi: 10.1038/NRD2682.

Pratt, KP., BW. Shen, K. Takeshima, EW. Davie, K. Fujikawat, and BL. Stoddard. 1999. “Structure of the C2 Domain of Human Factor VIII at 1.5 A Resolution.” *Nature* 402(6760):439–42. doi: 10.1038/46601.

Price, EM., and JB. Lingrel. 2002. “Structure-Function Relationships in the Sodium-Potassium ATPase .Alpha. Subunit: Site-Directed Mutagenesis of Glutamine-111 to Arginine and Asparagine-122 to Aspartic Acid Generates a Ouabain-Resistant Enzyme.” *Biochemistry* 27(22):8400–8408. doi: 10.1021/BI00422A016.

Ramsay, EP., RF. Collins, TW. Owens, C. Alistair Siebert, RPO. Jones, T. Wang, AM. Roseman, and C. Baldock. 2016. “Structural Analysis of X-Linked Retinoschisis Mutations Reveals Distinct Classes Which Differentially Effect Retinoschisin Function.” *Human Molecular Genetics* 25(24):5311–20. doi: 10.1093/HMG/DDW345.

Razafsky, D., C. Ward, C. Potter, W. Zhu, Y. Xue, VlJ. Kefalov, LG. Fong, SG. Young, and D. Hodzic. 2016. “Lamin B1 and Lamin B2 Are Long-Lived Proteins with Distinct Functions in Retinal Development.” *Molecular Biology of the Cell* 27(12):1928–37. doi: 10.1091/MBC.E16-03-0143.

Reid, SNM., C. Yamashita, and DB Farber. 2003. “Retinoschisin, a Photoreceptor-Secreted Protein, and Its Interaction with Bipolar and Muller Cells.” *The Journal of Neuroscience : The Official Journal of the Society for Neuroscience* 23(14):6030–40. doi: 10.1523/JNEUROSCI.23-14-06030.2003.

Reinhard, L., H. Tidow, MJ. Clausen, and P. Nissen. 2013. “Na(+),K (+)-ATPase as a Docking Station: Protein-Protein Complexes of the Na(+),K (+)-ATPase.” *Cellular and Molecular Life Sciences : CMLS* 70(2):205–22. doi: 10.1007/S00018-012-1039-9.

Renard, D., E. Rubli, N. Voide, F. X. Borruat, and L. E. Rothuizen. 2015. “Spectrum of Digoxin-Induced Ocular Toxicity: A Case Report and Literature Review.” *BMC Research Notes* 8(1):8:368. doi: 10.1186/S13104-015-1367-6.

de Rezende Corrêa, G., VHP Soares, L. de Araújo-Martins, AA dos Santos, and E. Giestal-de-Araujo. 2015. “Ouabain and BDNF Crosstalk on Ganglion Cell Survival in Mixed Retinal Cell Cultures.” *Cellular and Molecular Neurobiology* 35(5):651–60. doi: 10.1007/S10571-015-0160-3.

Ritz, S., P. Harding, W. Martz, HW. Schütz, and HJ. Kaatsch. 1992. “Measurement of Digitalis-Glycoside Levels in Ocular Tissues: A Way to Improve Postmortem Diagnosis of Lethal Digitalis-Glycoside Poisoning? I. Digoxin.” *International Journal of Legal Medicine* 105(3):149–54. doi: 10.1007/BF01625167.

Roesch, MT, CC Ewing, AE Gibson, and BHF Weber. 1998. “The Natural History of X-Linked Retinoschisis.” *Canadian Journal of Ophthalmology. Journal Canadien d’ophtalmologie* 33(3):149–58.

Rose, E., JCP. Koo, JE. Antflick, SM. Ahmed, S. Angers, and DR. Hampson. 2009. “Glutamate Transporter Coupling to Na,K-ATPase.” *The Journal of Neuroscience : The Official Journal of the Society for Neuroscience* 29(25):8143–55. doi: 10.1523/JNEUROSCI.1081-09.2009.

Saleheen, D., A. Ali, S. Khanum, MZ. Ozair, M. Zaidi, MJ. Sethi, N. Khan, and P. Frossard. 2008. “Molecular Analysis of the XLRS1 Gene in 4 Females Affected with X-Linked Juvenile Retinoschisis.” *Canadian Journal of Ophthalmology. Journal Canadien d’ophtalmologie* 43(5):596–99. doi: 10.3129/I08-143.

Sánchez-Rodríguez, J. E., F. Khalili-Araghi, P. Miranda, B. Roux, M. Holmgren, and F. Bezanilla. 2015. “A Structural Rearrangement of the Na+/K+-ATPase Traps Ouabain within the External Ion Permeation Pathway.” *Journal of Molecular Biology* 427(6 Pt B):1335–44. doi: 10.1016/J.JMB.2015.01.011.

Sauer, CG., A. Gehrig, R. Warneke-Wittstock, A. Marquardt, CC. Ewing, A. Gibson, B. Lorenz, B. Jurklies, and BHF Weber. 1997. “Positional Cloning of the Gene Associated with X-Linked Juvenile Retinoschisis.” *Nature Genetics* 17(2):164–70. doi: 10.1038/NG1097-164.

Schmid, V., K. Plössl, C. Schmid, S. Bernklau, BHF Weber, and U. Friedrich. 2020. “Retinoschisin and Cardiac Glycoside Crosstalk at the Retinal Na/K-ATPase.” *Investigative Ophthalmology & Visual Science* 61(5):1. doi: 10.1167/iovs.61.5.1.

Schmid V., A. Wurzel, CH. Wetzel, K. Plössl, A Bruckmann, BHF Weber, and U Friedrich. 2022 “Retinoschisin and novel Na/K-ATPase interaction partners Kv2.1 and Kv8.2 define a growing protein complex at the inner segments of mammalian photoreceptors” *Cellular and Molecular Life Sciences 25;79(8):448..doi: 10.1007/s00018-022-04409-9*

Schneider, BG., and E. Kraig. 1990. “Na+, K(+)-ATPase of the Photoreceptor: Selective Expression of Alpha 3 and Beta 2 Isoforms.” *Experimental Eye Research* 51(5):553–64. doi: 10.1016/0014-4835(90)90086-A.

Schneider, R., V. Wray, M. Nimtz, WD Lehmann, U. Kirch, R. Antolovic, and W. Schoner. 1998. “Bovine Adrenals Contain, in Addition to Ouabain, a Second Inhibitor of the Sodium Pump.” *The Journal of Biological Chemistry* 273(2):784–92. doi: 10.1074/JBC.273.2.784.

Schoner, W., and G. Scheiner-Bobis. 2007. “Endogenous and Exogenous Cardiac Glycosides and Their Mechanisms of Action.” *American Journal of Cardiovascular Drugs : Drugs, Devices, and Other Interventions* 7(3):173–89. doi: 10.2165/00129784-200707030-00004.

Schwille, P., J. Korlach, and WW. Webb. 1999. “Fluorescence Correlation Spectroscopy with Single-Molecule Sensitivity on Cell and Model Membranes.” *Cytometry* 36(3):176–82. doi: 10.1002/(SICI)1097-0320(19990701)36:3<176::AID-CYTO5>3.0.CO;2-F.

Shamraj, OI, and JB. Lingrel. 1994. “A Putative Fourth Na+,K(+)-ATPase Alpha-Subunit Gene Is Expressed in

Testis." *Proceedings of the National Academy of Sciences of the United States of America* 91(26):12952–56. doi: 10.1073/PNAS.91.26.12952.

Shi, L., K. Jian, ML. Ko, D. Trump, and GYP. Ko. 2009. "Retinoschisin, a New Binding Partner for L-Type Voltage-Gated Calcium Channels in the Retina." *The Journal of Biological Chemistry* 284(6):3966–75. doi: 10.1074/JBC.M806333200.

Shi, L., ML. Ko, and GYP. Ko. 2017. "Retinoschisin Facilitates the Function of L-Type Voltage-Gated Calcium Channels." *Frontiers in Cellular Neuroscience* 11(8):232. doi: 10.3389/FNCEL.2017.00232.

Silva, E., and P. Soares-da-Silva. 2012. "New Insights into the Regulation of Na+,K+-ATPase by Ouabain." *International Review of Cell and Molecular Biology* 294:99–132. doi: 10.1016/B978-0-12-394305-7.00002-1.

Singer, S., and GL. Nicolson. 1972. "The Fluid Mosaic Model of the Structure of Cell Membranes." *Science (New York, N.Y.)* 175(4023):720–31. doi: 10.1126/SCIENCE.175.4023.720.

Skogestad, J., JM Aronsen, N. Tovsrud, P. Wanichawan, K. Hougen, MK Stokke, CR Carlson, I. Sjaastad, OM Sejersted, and F. Swift. 2020. "Coupling of the Na+/K+-ATPase to Ankyrin B Controls Na+/Ca2+ Exchanger Activity in Cardiomyocytes." *Cardiovascular Research* 116(1):78–90. doi: 10.1093/CVR/CVZ087.

Skou, JC, and JF. Hoffman. 1998. "The Influence of Some Cations on an Adenosine Triphosphatase from Peripheral Nerves." *Journal of the American Society of Nephrology : JASN* 9(11):2170–77. doi: 10.1681/ASN.V9112170.

Staffieri, SE., L. Rose, A. Chang, JN. De Roach, TL. Mclaren, DA. Mackey, AW. Hewitt, and TM. Lamey. 2015. "Clinical and Molecular Characterization of Females Affected by X-Linked Retinoschisis." *Clinical & Experimental Ophthalmology* 43(7):643–47. doi: 10.1111/CEO.12541.

Steiner-Champliaud, MF, J. Sahel, and D. Hicks. 2006. "Retinoschisin Forms a Multimolecular Complex with Extracellular Matrix and Cytoplasmic Proteins: Interactions with B2 Laminin and AB-Crystallin." *Molecular Vision* 12:892–901.

Sterlini, B., A. Romei, C. Parodi, D. Aprile, M. Oneto, A. Aperia, P. Valente, F. Valtorta, A. Fassio, P. Baldelli, F. Benfenati, and A. Corradi. 2021. "An Interaction between PRRT2 and Na+/K+ ATPase Contributes to the Control of Neuronal Excitability." *Cell Death & Disease 2021 12:4* 12(4):1–18. doi: 10.1038/s41419-021-03569-z.

Stillman, BA., L. Audoly, and RM. Breyer. 1998. "A Conserved Threonine in the Second Extracellular Loop of the Human EP2 and EP4 Receptors Is Required for Ligand Binding." *European Journal of Pharmacology* 357(1):73–82. doi: 10.1016/S0014-2999(98)00522-6.

Takada, Y., R. N. Fariss, M. Müller, R. A. Bush, E. J. Rushing, and P. A. Sieving. 2006. "Retinoschisin Expression and Localization in Rodent and Human Pineal and Consequences of Mouse RS1 Gene Knockout." *Molecular Vision* 12:1108–16.

Takada, Y., C. Vijayasarathy, Y. Zeng, S. Kjellstrom, RA. Bush, and PA. Sieving. 2008. "Synaptic Pathology in Retinoschisis Knockout (Rs1-/y) Mouse Retina and Modification by RAAV-Rs1 Gene Delivery." *Investigative Ophthalmology & Visual Science* 49(8):3677–86. doi: 10.1167/IOVS.07-1071.

Tantri, A., T. R. Vrabec, A. Cu-Unjieng, A. Frost, W. H. Annesley, and L. A. Donoso. 2004. "X-Linked Retinoschisis: A Clinical and Molecular Genetic Review." *Survey of Ophthalmology* 49(2):214–30. doi: 10.1016/J.SURVOPHTHAL.2003.12.007.

Therien, A. G., and R. Blostein. 2000. "Mechanisms of Sodium Pump Regulation." *American Journal of Physiology - Cell Physiology* 279(3):541–66. doi: 10.1152/ajpcell.2000.279.3.c541.

Tidow, H., A. Aperia, and P. Nissen. 2010. "How Are Ion Pumps and Agrin Signaling Integrated?" *Trends in Biochemical Sciences* 35(12):653–59. doi: 10.1016/J.TIBS.2010.05.004.

Tinning, PW., AJPM. Franssen, SU. Hridi, TJ. Bushell, and G. Mcconnell. 2018. "A 340/380 Nm Light-Emitting Diode Illuminator for Fura-2 AM Ratiometric Ca 2+ Imaging of Live Cells with Better than 5 NM Precision." *Journal of Microscopy* 269(3):212–20. doi: 10.1111/JMI.12616.

Tokhtaeva, E., K. Munson, G. Sachs, and O. Vagin. 2010. "N-Glycan-Dependent Quality Control of the Na,K-ATPase Beta(2) Subunit." *Biochemistry* 49(14):3116–28. doi: 10.1021/BI100115A.

Tolun, G., C. Vijayasarathy, R. Huang, Y. Zeng, Y. Li, AC. Steven, PA. Sieving, and JB Heymann. 2016. "Paired Octamer Rings of Retinoschisin Suggest a Junctional Model for Cell-Cell Adhesion in the Retina." *Proceedings of the National Academy of Sciences of the United States of America* 113(19):5287–92. doi: 10.1073/PNAS.1519048113.

Toyoshima, C., R. Kanai, and F. Cornelius. 2011. "First Crystal Structures of Na+,K+-ATPase: New Light on the Oldest Ion Pump." *Structure (London, England : 1993)* 19(12):1732–38. doi: 10.1016/J.STR.2011.10.016.

Valencia, Al, A. Pestaña, and A. Cano. 1989. “Spectroscopical Studies on the Structural Organization of the Lectin Discoidin I: Analysis of Sugar- and Calcium-Binding Activities.” *Biochimica et Biophysica Acta (BBA) - General Subjects* 990(1):93–97. doi: 10.1016/S0304-4165(89)80017-0.

Vierra, NC., M. Kirmiz, D. van der List, LF Santana, and JS. Trimmer. 2019. “Kv2.1 Mediates Spatial and Functional Coupling of L-Type Calcium Channels and Ryanodine Receptors in Mammalian Neurons.” *ELife* 8:e49953. doi: 10.7554/ELIFE.49953.

Vijayasarathy, C., SPB Sardar Pasha, and PA. Sieving. 2021. “Of Men and Mice: Human X-Linked Retinoschisis and Fidelity in Mouse Modeling.” *Progress in Retinal and Eye Research* (11):100999. doi: 10.1016/J.PRETEYERES.2021.100999.

Villoutreix, BO., and MA. Miteva. 2016. “Discoidin Domains as Emerging Therapeutic Targets.” *Trends in Pharmacological Sciences* 37(8):641–59. doi: 10.1016/J.TIPS.2016.06.003.

Volkin, DB., AM. Verticelli, KE. Marfia, CJ. Burke, H. Mach, and CR Middaugh. 1993. “Sucralfate and Soluble Sucrose Octasulfate Bind and Stabilize Acidic Fibroblast Growth Factor.” *Biochimica et Biophysica Acta* 1203(1):18–26. doi: 10.1016/0167-4838(93)90031-L.

Vukojevic, V., Y. Ming, C. D’Addario, M. Hansen, Ü. Langel, R. Schulz, B. Johansson, R. Rigler, and L. Terenius. 2008. “Mu-Opioid Receptor Activation in Live Cells.” *FASEB Journal : Official Publication of the Federation of American Societies for Experimental Biology* 22(10):3537–48. doi: 10.1096/FJ.08-108894.

Wang, T., Caroline T. Waters, Alex M. K. Rothman, Tracy J. Jankins, Karin Römisch, and Dorothy Trump. 2002. “Intracellular Retention of Mutant Retinoschisin Is the Pathological Mechanism Underlying X-Linked Retinoschisis.” *Human Molecular Genetics* 11(24):3097–3105. doi: 10.1093/HMG/11.24.3097.

Wang, T., A. Zhou, C. T. Waters, E. O’Connor, R. J. Read, and Dorothy Trump. 2006. “Molecular Pathology of X Linked Retinoschisis: Mutations Interfere with Retinoschisin Secretion and Oligomerisation.” *The British Journal of Ophthalmology* 90(1):81–86. doi: 10.1136/BJO.2005.078048.

Wang, X., and S. Li. 2014. “Protein Mislocalization: Mechanisms, Functions and Clinical Applications in Cancer.” *Biochimica et Biophysica Acta* 1846(1):13–25. doi: 10.1016/J.BBCAN.2014.03.006.

Weber, BHF, H. Schrewe, LL Molday, A. Gehrig, KL White, MW Seeliger, GB Jaissle, C. Friedburg, E. Tamm, and RS Molday. 2002. “Inactivation of the Murine X-Linked Juvenile Retinoschisis Gene, Rs1h, Suggests a Role of Retinoschisin in Retinal Cell Layer Organization and Synaptic Structure.” *Proceedings of the National Academy of Sciences of the United States of America* 99(9):6222–27.

Wetzel, RK, E. Arystarkhova, and KJ Sweadner. 1999. “Cellular and Subcellular Specification of Na,K-ATPase Alpha and Beta Isoforms in the Postnatal Development of Mouse Retina.” *The Journal of Neuroscience : The Official Journal of the Society for Neuroscience* 19(22):9878–89. doi: 10.1523/JNEUROSCI.19-22-09878.1999.

Wieacker, P., TF. Wienker, B. Dallapiccola, K. Bender, KE. Davies, and HH Ropers. 1983. “Linkage Relationships between Retinoschisis, Xg, and a Cloned DNA Sequence from the Distal Short Arm of the X Chromosome.” *Human Genetics* 64(2):143–45. doi: 10.1007/BF00327111.

Wikimedia, https://commons.wikimedia.org/wiki/Category:Digoxin

Wold, F., and CE. Ballou. 1957. “Studies on the Enzyme Enolase. I. Equilibrium Studies.” *The Journal of Biological Chemistry* 227(1):301–12. doi: 10.1016/S0021-9258(18)70816-8.

Wood, EH., I. Lertjirachai, BK. Ghiam, N. Koulisis, SN. Moysidis, A. Dirani, KA. Drenser, A. Capone, and MT. Trese. 2019. “The Natural History of Congenital X-Linked Retinoschisis and Conversion between Phenotypes over Time.” *Ophthalmology. Retina* 3(1):77–82. doi: 10.1016/J.ORET.2018.08.006.

Wu, H., JA. Cowing, Mi Michaelides, SE. Wilkie, G. Jeffery, SA. Jenkins, V. Mester, AC. Bird, AG. Robson, GE. Holder, AT. Moore, DM. Hunt, and AR. Webster. 2006. “Mutations in the Gene KCNV2 Encoding a Voltage-Gated Potassium Channel Subunit Cause ‘Cone Dystrophy with Supernormal Rod Electroretinogram’ in Humans.” *American Journal of Human Genetics* 79(3):574–79. doi: 10.1086/507568.

Wu, WW, and RS. Molday. 2003. “Defective Discoidin Domain Structure, Subunit Assembly, and Endoplasmic Reticulum Processing of Retinoschisin Are Primary Mechanisms Responsible for X-Linked Retinoschisis.” *The Journal of Biological Chemistry* 278(30):28139–46. doi: 10.1074/JBC.M302464200.

Wu, WW, JP. Wong, J. Kast, and RS. Molday. 2005. “RS1, a Discoidin Domain-Containing Retinal Cell Adhesion Protein Associated with X-Linked Retinoschisis, Exists as a Novel Disulfide-Linked Octamer.” *The Journal of Biological Chemistry* 280(11):10721–30. doi: 10.1074/JBC.M413117200.

Wulff, H., NA. Castle, and LA. Pardo. 2009. “Voltage-Gated Potassium Channels as Therapeutic Targets.” *Nature Reviews. Drug Discovery* 8(12):982–1001. doi: 10.1038/NRD2983.

Xie, J., Q. Ye, X. Cui, N. Madan, Q. Yi, SV. Pierre, and Z. Xie. 2015. “Expression of Rat Na-K-ATPase A2 Enables Ion Pumping but Not Ouabain-Induced Signaling in A1-Deficient Porcine Renal Epithelial Cells.” *American Journal of Physiology. Cell Physiology* 309(6):C373–82. doi: 10.1152/AJPCELL.00103.2015.

Xie, Z., and T. Cai. 2003. “Na+-K+--ATPase-Mediated Signal Transduction: From Protein Interaction to Cellular Function.” *Molecular Interventions* 3(3):157–68. doi: 10.1124/MI.3.3.157.

Yap, JQ., J. Seflova, R. Sweazey, P. Artigas, and SL. Robia. 2021. “FXYD Proteins and Sodium Pump Regulatory Mechanisms.” *The Journal of General Physiology* 153(4). doi: 10.1085/JGP.202012633.

Yatime, L., M. Laursen, JP Morth, M. Esmann, P. Nissen, and NU. Fedosova. 2011. “Structural Insights into the High Affinity Binding of Cardiotonic Steroids to the Na+,K+-ATPase.” *Journal of Structural Biology* 174(2):296–306. doi: 10.1016/J.JSB.2010.12.004.

Yin, W., H. Liu, Z. Peng, D. Chen, J Li, and JD Li. 2014. “Mechanisms That Underlie the Internalization and Extracellular Signal Regulated Kinase 1/2 Activation by PKR2 Receptor.” *Cellular Signalling* 26(5):1118–24. doi: 10.1016/J.CELLSIG.2014.01.031.

Yu, J., Y. Ni, PA. Keane, C. Jiang, W. Wang, and G. Xu. 2010. “Foveomacular Schisis in Juvenile X-Linked Retinoschisis: An Optical Coherence Tomography Study.” *American Journal of Ophthalmology* 149(6):973-978.e2. doi: 10.1016/J.AJO.2010.01.031.

Yu, W., MR Shin, and F. Sesti. 2019. “Complexes Formed with Integrin-A5 and KCNB1 Potassium Channel Wild Type or Epilepsy-Susceptibility Variants Modulate Cellular Plasticity via Ras and Akt Signaling.” *FASEB Journal : Official Publication of the Federation of American Societies for Experimental Biology* 33(12):14680–89. doi: 10.1096/FJ.201901792R.

Zeng, Y., Y. Takada, S. Kjellstrom, K. Hiriyanna, A. Tanikawa, E. Wawrousek, N. Smaoui, R. Caruso, RA. Bush, and PA. Sieving. 2004. “RS-1 Gene Delivery to an Adult Rs1h Knockout Mouse Model Restores ERG b-Wave with Reversal of the Electronegative Waveform of X-Linked Retinoschisis.” *Investigative Ophthalmology & Visual Science* 45(9):3279–85. doi: 10.1167/IOVS.04-0576.

Zhang, D., Q. Hou, M. Wang, A. Lin, L. Jarzylo, A. Navis, A. Raissi, F. Liu, and HY Man. 2009. “Na,K-ATPase Activity Regulates AMPA Receptor Turnover through Proteasome-Mediated Proteolysis.” *The Journal of Neuroscience : The Official Journal of the Society for Neuroscience* 29(14):4498–4511. doi: 10.1523/JNEUROSCI.6094-08.2009.

Zhang, W., B. Baban, M. Rojas, S. Tofigh, SK. Virmani, C. Patel, MA Behzadian, MJ. Romero, RW. Caldwell, and RB. Caldwell. 2009. “Arginase Activity Mediates Retinal Inflammation in Endotoxin-Induced Uveitis.” *The American Journal of Pathology* 175(2):891–902. doi: 10.2353/AJPATH.2009.081115.

List of abbreviations

Abbreviation	Meaning	Abbreviation	Meaning
µ	micro	LB	Lysogeny Broth
µl	microliter	LC-MS/MS	Liquid Chromatography-tandem Mass Spectrometry
µM	micromolar	LTCC	L-type voltage-gated calcium channel
µm	micrometer	m	milli
aa	Amino acid	M	Molar
AMOG	Adhesion Molecule on Glia	MAP	Mitogen-Activated Protein
ANKB	AnkyrinB	MFI	Mean Fluorescence Intensity
APS	Ammoniumpersulfate	min	Minute
ATP	Adenosine triphosphate	MM	Mastermix
ATP1A3-OI	Ouabain-Insensitive ATP1A3 mutant	MOP	µ-Opioid Receptor
BF	Brightfield	mRNA	Messenger Ribonucleic Acid
bp	Basepair	nA	Nanoampere
BSA	Bovine Serum Albumin	Na/K-ATPase	Sodium Potassium ATPase
CAV1	Caveolin1	NCX	Na^{+}/Ca^{2+} exchanger
cDNA	Complementary DNA	nm	nanometer
DAPI	4'.6'-Diamidin-2-phenylindol	OCT	Optic Coherence Tomography
DMEM	Dulbecco's Modified Eagle Medium	ONL	Outer Nuclear Layer
DMSO	Dimethylsulfoxide	OPL	Outer Plexiform Layer
DNA	Desoxyribonucleicacid	P	Postnatal day
dNTP	Desoxynucleotidephosphate	P/S	Penicillin/Streptomycin
E. Coli	*Escherichia Coli*	PB	Phosphate Buffer
ECL	Enhanced Chemiluminescence	PBS	Phosphate Buffered Saline
EGFR	Epidermal Growth Factor Receptor	PCR	Polymerase Chain Reaction
ER	Endoplasmic Reticulum	PFA	Paraformaldehyde
ERG	Electroretinography	PI3K	Phosphatidylinositol 3-kinase
ERK	Extracellular-signal Regulated Kinase	PLC	Phospholipase C
Et al.	Et aliter (and others)	PVDF	Polyvinylidenfluorid
FACS	Fluorescence Activated Cell Sorting	rpm	Rounds per minute
FCS	Fetal Calf Serum	RPMI	Roswell Park Memorial Institute
FXYD	Phe-X-Tyr-Asp protein	RS1	Retinoschisin
G	Gram	RT-PCR	Real-Time Polymerase Chain Reaction
G-418	Geneticin	s	second
GLAST	Glutamate Aspartate Transporter	SDS	Sodium Dodecyl Sulfate
GLT-1	Glutamate Transporter	SDS-PAGE	SDS-polyacrylamide gel electrophoresis
h	hour	SRP	Signal Recognition Particle
Hek	Human embryonic kidney	TBE	Tris Borat EDTA
HRP	Horse Radish Peroxidase	TBS	Tris-buffered Saline
IB	Immunoblot	TEMED	Tetramethylethylendiamine
ICC	Immunocytochemistry	TM	Transmembrane
IHC	Immunohistochemistry	Tris	Tris(hydroxymethyl-)aminomethane
INL	Inner Nuclear Layer	TUNEL	TdT-mediated dUTP-biotin nick end labeling
IP3	Inositol 1,4,5-trisphosphate	V	Volt
IPL	Inner Plexiform Layer	WB	Western Blot
kb	kilobase	XLRS	X-linked juvenile Retinoschisis
kDA	kilodalton		
Kv	Voltage-gated potassium channel		
l	liter		

List of figures

List of tables

Acknowledgments

I would like to express my deepest gratitude to my PhD supervisor Prof. Dr. Bernhard Weber for giving me the opportunity to do my PhD project at the Institute of Human Genetics and for supporting me in all aspects of my thesis. I really appreciated the discussions about new ideas, the feedback on publications or labmeetings or also his immense knowledge and experience.

I also would like to thank my mentors Prof. Dr. Dr. Barbara Braunger and Prof. Dr. Wolf Hayo Castrop for their helpful advice and their feedback in my progress reports and for taking over the position of the second examiner and of the third party auditor of my thesis.

I would like to say a special thank you to Dr. Ulrike Friedrich for her incredibly valuable support throughout my whole doctoral thesis. Thank you for the help in planning new projects, data evaluation, or writing and designing manuscripts. Thank you for just always being there for me.

I am deeply grateful to Prof. Dr. Wetzel for helping me to realize my ideas regarding electrophysiology. Thank you for teaching me the patch-clamp method, evaluating the data and giving me valuable advice.

Many thanks to Prof. Thomas Friedrich, Dr. Neslihan Tavraz and Albert Prause at the Technical University of Berlin for your help in performing the fluorescence correlation spectrometry analysis, in evaluating the data, and interpreting the results.

I would like to thank Dr. Vladimir Milenkovic for introducing me the intracellular Calcium Imaging Method.

I wish to show my gratitude to Dr. Astrid Bruckmann for support in LC-MS/MS analysis and data interpretation.

Thanks a lot, Martina Esser, for excellent technical assistance and perfect support with lab work.

I would also like to thank Denise Schmied for helping with and teaching me a lot about mouse work involved in this project.

Very special thank you to all my colleagues at the Institute of Human Genetics for a cherished time spent together in the lab, and for the fruitful discussions about methods or data interpretation. In particular I would like to thank Fabiola Biasella, Martina Esser and Karolina Plössl for their advice both scientifically and personally.

Finally, I would like to express my gratitude to my boyfriend Lukas, my parents, and my friends. Without their tremendous understanding and encouragement in the past few years, it would be impossible for me to complete my study.